Constant Orbital Momentum Equilibrium Trajectories of a Gyrostat-Satellite

Matthew Clark VanDyke

Dissertation submitted to the Faculty of the
Virginia Polytechnic Institute and State University
in partial fulfillment of the requirements for the degree of

Doctor of Philosophy
in
Aerospace Engineering

Christopher Hall, Chair
Craig Woolsey, Co-Chair
Cornel Sultan
Gregory Earle
Yigang Fan

December 10, 2013
Blacksburg, Virginia

Keywords: Gyrostat-Satellite, Relative Equilibrium, Spacecraft Dynamics, Attitude Control, Attitude Guidance, Gravitational Torque, Attitude Maneuvers

Constant Orbital Momentum Equilibrium Trajectories of a Gyrostat-Satellite

Matthew Clark VanDyke

(ABSTRACT)

This dissertation investigates attitude transition maneuvers of a gyrosat-satellite between relative equilibria. The primary challenge in transitioning between relative equilibria is the proper adjustment of the system angular momentum so that upon completing the transition maneuver the gyrostat-satellite will satisfy all the requirements for a relative equilibrium. The system angular momentum is a function of the attitude trajectory taken during the transition maneuver. A new concept, the constant orbital momentum equilibrium trajectory or COMET, is introduced as a means to a straight-forward solution to a subset of the possible transitions between relative equilbria. COMETs are a class of paths in SO(3) that a gyrostat-satellite may travel along that maintain a constant system angular momentum. The primary contributions of this dissertation are the introduction and analysis of COMETs and their application to the problem of transitioning a gyrostat-satellite between two relative equilibria.

The current work introduces, defines, and analyzes COMETs in detail. The requirements for a path in SO(3) to be a COMET are defined. It is shown via example that COMETs are closed-curves in SO(3). Visualizations of families of COMETs are presented and discussed in detail. A subset of COMETs are shown to contain critical points that represent isolated relative equilibrium attitudes or furcations of the COMET.

The problem of transitioning between two relative equilibria is split into the sub-problems of transitioning between relative equilibria on the same COMET and transitioning between relative equilibria on different COMETs. For transitions between relative equilibria on the same COMET, an open-loop control law is developed that drives a gyrostat-satellite along the COMET until the target relative equilibrium is reached. For transitions between relative equilibria on different COMETs, an open-loop control law is developed that transfers a gyrostat-satellite from the initial relative equilibrium to a relative equilibrium that resides on the same COMET as the target relative equilbrium. Acquisition of the target relative equilibrium is then accomplished via the application of the open-loop control law for transitions between relative equilibria on the same COMET. The results of numeric simulations of gyrostat-satellites executing these transitions are presented.

Dedication & Acknowledgments

This dissertation is dedicated to my exceedingly wonderful wife, Melissa, and our two beautiful daughters, Lilly and Madeline. I will endeavor to make up for the evenings and weekends of my delightful company that they sacrificed (whether they like it or not).

I would like to thank the extraordinarily patient chair of my advisory committee, Dr. Christopher Hall, without whom this dissertation may have never been completed. I would also like to thank the other members of my advisory committee (Dr. Craig Woolsey, Dr. Cornel Sultan, Dr. Gregory Earle, and Dr. Yigang Fan) and the Aerospace and Ocean Engineering Department's unfailingly helpful Graduate Program Coordinator, Rachel Hall Smith.

I would like to acknowledge the funding I received (via tuition reimbursement) from Orbital Sciences Corporation, where I have had the pleasure of working during the course of my dissertation research. And finally, I would like to thank my many colleagues at Orbital Sciences Corporation for the support, advice, and understanding they provided over the years it took to complete my studies.

Contents

List of Figures

List of Tables

List of Algorithms

Chapter 1

Introduction

Artificial satellites have become a critical component of modern life. Communication satellites connect billions of people all over the world in near real-time. The Global Positioning System (GPS) satellite constellation provides accurate real-time navigation that enables a multitude of commercial, scientific, and military applications. Remote sensing satellites provide a wealth of information that serves to progress many scientific fields of research. These are just a few of the many contributions made by artificial satellites.

The successful operation of an artificial satellite requires that its attitude be stabilized or controlled. Communications between an artificial satellite and a ground station (or other satellites) may require the use of directed antennas, which must be pointed (with varying accuracies) at intended targets. Solar cells (either body-mounted or on a solar array) must be pointed at the Sun to generate sufficient power for mission operations. Thermal control of an artificial satellite often requires pointing radiators away from the Sun or preventing constant Sun exposure on a given portion of the satellite. Most satellite payloads, whether for communication, science, or other use, are required to be pointed at an intended target to accomplish mission objectives.

Attitude control and stabilization methodologies used by artificial satellites may be split into three general categories: passive stabilization, semi-passive stabilization, and active control. Some early satellites employed passive attitude stabilization. These satellites used high-spin rates (spin-stabilization) to generate gyroscopic stabilizing torques or long booms to generate stabilizing gravitational torques (gravity-gradient stabilization) to maintain spacecraft pointing within mission constraints. Some later satellites employed semi-passive attitude stabilization. These satellites represent the early dual-spin* satellites and used internal or external rotors to generate a momentum bias that resulted in gyric stabilization of two axes inertially and three axes in an orbit-referenced frame. Modern satellites typically employ active three-axis attitude control. The attitude determination and control subsystem (ADCS

* Dual-spin refers to the fact that the spacecraft consists of two primary bodies that are rotating with respect to one another.

or ADACS) of an active three-axis attitude controlled satellite monitors attitude sensor data and issues commands to torque actuators to correct attitude deviations. These satellites typically utilize a complement of reaction wheels, CMGs, thrusters, and/or magnetic torquers to apply torque to the satellite.

The motivating engineering problem explored by this dissertation is the attitude control of an artificial satellite equipped with reaction wheels. Many modern satellites use reaction wheels as the primary torque actuators. A reaction wheel is a mechanism that consists of a rotor (or flywheel), motor, housing, and associated electronics for command and data handling.* Reaction wheels are relatively simple mechanisms (when compared to control moment gyros) that provide precise, propellant-less internal torque actuation. Alternative simple torque actuators are not able to couple precision with propellant-less operation. Magnetic torque actuators are imprecise. Thrusters are imprecise and require the expenditure of propellant. However, a reaction wheel attitude control system must be coupled with either magnetic torque actuators or thrusters to unload any secular accumulation of angular momentum.†

The subsequent sections of this chapter introduce important concepts related to the current work, present the thesis of the dissertation, and provide an overview of the dissertation.

1.1 Important Concepts

The current work focuses on two important concepts: the gyrostat-satellite and relative equilibria of a gyrostat-satellite.

The gyrostat-satellite is a useful mathematical abstraction for the attitude dynamics of an artificial satellite equipped with reaction wheels. A gyrostat-satellite is a gyrostat that is in orbit about a massive body.[22] A gyrostat ($\mathcal{G}$) is a mechanical system consisting of a rigid body‡ ($\mathcal{P}$) with one or more symmetrical rotors ($\mathcal{R}_i$) whose spin axes are fixed in the rigid body, and which are allowed to rotate about their axes of symmetry.[11]

$$\mathcal{G} \;=\; \mathcal{P} \cup \bigcup_{i=1}^{n} \mathcal{R}_i \tag{1.1}$$

The gyrostat does not model a number of (sometimes important) effects including flexible structures, liquid slosh, bearing friction, and dynamic and static imbalance. These effects are often analyzed using extensions of the gyrostat model.

* The literature interchangeably uses the terms "reaction wheel" and "momentum wheel". Some authors distinguish "momentum wheels" as nominally operating at a high rotor speeds, whereas "reaction wheels" nominally operate at rotor speeds near zero. The term "reaction wheel" is used throughout this dissertation.
† In Low Earth Orbits (LEOs), reaction wheels are coupled with magnetic torquing devices to unload accumulated momentum. In higher Earth orbits (where the magnetic field is significantly weaker), thrusters are used to unload the secular accumulation of momentum. ‡ Sometimes called the platform

Relative equilibria of a gyrostat-satellite are equilibria in which the platform of a gyrostat rotates about the normal vector of the gyrostat-satellite's orbital plane at the orbital rate.[11] A gyrostat-satellite in relative equilibrium would appear to be motionless with respect to an observer in an orbit-fixed reference frame. Many modern satellites (including some communication and remote sensing satellites) use orbit-fixed attitudes to meet mission pointing requirements. The sum of the disturbance torques for a gyrostat-satellite in a relative equilibrium is zero, thus eliminating secular angular momentum accumulation. Unloading angular momentum may require an artificial satellite to expend propellant possibly resulting in a reduction in mission life.

1.2 Thesis of the Dissertation

This dissertation investigates the dynamics and control of an artificial satellite equipped with reaction wheels. In particular, semi-passive attitude stabilization techniques (mostly from the 1960s through the 1980s) are extended and their application to active three-axis attitude controlled satellites is investigated.

The majority of the existing open literature on relative equilibria of a gyrostat-satellite focused on the determination of relative equilibrium attitudes and necessary and sufficient conditions for the stability of those relative equilibria. Only two authors discussed the possibility of utilizing internal torques (i.e. due to a reaction wheel) to perform transitions between relative equilibria. And, only one author has investigated these types of maneuvers in any detail. The current work focuses on a special set of attitude trajectories, called constant orbital momentum equilibrium trajectories or COMETs, that may be used to perform transitions between relative equilibria via internal torque actuation.

A COMET is a closed-curve in SO(3) that represents a continuous connection of relative equilibrium attitudes. A gyrostat-satellite starting at a relative equilibrium may travel along the COMET, on which the starting relative equilibrium resides, and, at any point along the COMET, apply internal torques to null its rate with respect to an orbit-fixed reference frame, and be at another relative equilibrium. This type of maneuver along a COMET represents a simple, "free" transition that eliminates or minimizes propellant expenditure, which may result in an extended mission life.

The current work introduces and provides a rigorous mathematical definition of COMETs of a gyrostat-satellite. Attitude and momentum guidance algorithms that exploit the existence of COMETs are presented and discussed in detail. The results of several numeric simulations are presented to verify the efficacy of the algorithms and the concept of COMETs.

1.3 Dissertation Overview

Chapters 2 through 3 are background material and provide context for the reader on the new contributions presented in later chapters. Chapter 2 presents a review of the literature related to relative equlibria of a gyrostat-satellite. The chapter summarizes the published literature, identifies a gap in the literature, and discusses how the current work addresses that gap. Chapter 3 contains a development of the equations of motion for a gyrostat-satellite. The chapter also sets the assumptions, nomenclature, and conventions used throughout the dissertation.

Chapter 4 introduces and defines the concept of relative equilibria for a gyrostat-satellite. This chapter derives the necessary and sufficient condition that a given attitude can be a relative equilibrium attitude, presents a three-variable parameterization of all possible relative equilibrium attitudes, and provides some discussion on the stability of relative equilibria. Chapter 4 also includes a detailed discussion of the directions of the basis vectors of the orbital and principal reference frames that admit relative equilibrium attitudes, which represents a new contribution to the field.

Chapters 5 and 6 contain the bulk of the new contributions offered by the current work. Chapter 5 introduces and defines the concept of a COMET for a gyrostat-satellite. The chapter derives the necessary conditions for a trajectory to be a COMET, discusses the existence of critical points of a small subset of COMETs, and presents numeric simulation results of gyrostat-satellites on COMETs. Chapter 6 investigates transitions between relative equilibria with specific emphasis on the use of COMETs to execute those transitions. The chapter splits the investigation into transitions between relative equilibria that reside on the same COMET, and transitions between different COMETs.

Chapter 7 summarizes the dissertation and discusses recommendations for further study.

Chapter 2

Literature Review

Investigations into the dynamics and control of a gyrostat-satellite have been extensively documented in the published literature. The purpose of this chapter is to provide a review of the portion of the literature that documents investigations pertinant to the current work. The reviewed literature is catagorized into three topics. Section 2.1 covers literature pertaining to the determination of the relative equilibrium attitudes of a gyrostat-satellite and studies into the stability characteristics of those relative equilibria. This section represents the bulk of the work from prior authors. Section 2.2 reviews a small set of papers that investigate the use of gravitational torques to unload accumulated angular momentum. Section 2.3 presents all work found in the literature related to gyrostat-satellites performing transitions between relative equilibria. Section 2.4 summarizes the findings of the literature review and discusses how the contributions of the current work intersect with those findings.

2.1 Relative Equilibria and Their Stability

The literature reviewed in this section investigates the determination of relative equilibrium attitudes of a gyrostat-satellite and the stability characteristics of the corresponding equilibria. There are two primary contributions of this literature. The first contribution is the determination of relative equilibrium attitudes of a gyrostat-satellite. The second contribution is the conditions on the inertia and relative angular momentum of the gyrostat-satellite that must be satisfied to ensure that the relative equilibria are stable.

The literature divides the relative equilibria of a gyrostat-satellite into four cases: cylindrical, conical, hyperbolic, and offset hyperbolic. The cases are distinguished by the alignment of the relative angular momentum vector with respect to the orbital reference frame.[11] The cylindrical, conical, and hyperbolic cases are sometimes lumped together under the term elementary cases.[11] The relative angular momentum vector lies in a plane perpendicular to one of the orbital reference frame basis axes in the elementary cases.[25]

2.1.1 Relative Equilibrium Attitudes

The earliest reviewed work that investigated the existence of relative equilibria of a gyrostat-satellite is Roberson and Hooker.[27] In this conference paper, and most subsequent work on the topic, the gyrostat-satellite is assumed to be in a circular orbit. Analytic expressions for the relative equilibrium attitudes are developed for the configuration in which the relative angular momentum vector is perpendicular to a principal axis of the gyrostat-satellite. This configuration corresponds to the cylindrical, conical, and hyperbolic cases. The authors also develop a set of equations that can be solved simultaneously to determine the relative equilibrium attitudes of the most general configuration.

Longman and Roberson[20] extend the results of Roberson and Hooker.[27] The authors derive a simple necessary and sufficient condition for the existence a relative angular momentum vector that will make an attitude a relative equilibrium. It is determined that there exists a two-parameter family of orientations which can be made to be relative equilibria by the proper choice of the relative angular momentum vector. The authors develop analytic equations for the relative equilibrium attitudes for the offset hyperbolic case. Another contribution of the article is the investigation of the unrestricted case. The unrestricted case refers to the removal of the assumption that the rotational motion of the gyrostat-satellite does not effect its translational motion. This assumption is made implicitly in the equations of motion used in prior work. The primary result is that the relative equilibrium attitudes found for the "restricted case" are still valid for the "unrestricted case" with slight modifications to the relative angular momentum vector. The required modifications are defined. These results are also presented in Longman,[15] which is a RAND Corporation memorandum.

Longman[18] determines the relative equilibria that exist when the direction of the relative angular momentum vector is constrained to lie in a principal plane. A principal plane is defined as any plane perpendicular to a principal axis. Several interesting figures depicting the surfaces defined by the principal axis directions of the relative equilibrium attitudes for a given relative angular momentum direction while varying the magnitude of the relative angular momentum vector are included.

Pascal and Stepanov[23] provide solutions to what they term the the "semi-inverse" problem. The "semi-inverse" problem involves determining all of the possible relative equilibria (attitude and corresponding relative angular momentum vector) given a constrained set of attitudes. Pascal and Stepanov[23] constrain the relative equilibrium attitudes such that a given vector expressed in a body-fixed reference frame must be aligned with a given vector expressed in the orbital reference frame. The new solutions presented restrict the vector expressed in an orbit reference frame to lie in one of the planes formed by the orbital basis vectors. Sarychev and Mirer[29] present a new analytic solution to the problem of determining all equilibria of a gyrostat satellite when the internal angular momentum is aligned with a principal axis of inertia.

2.1.2 Stability of Relative Equilibria

Kane and Mingori[12] is one of the earliest works to investigate the stability of relative equilibrium of a gyrostat-satellite. The authors devise a procedure using Floquet theory to analyze the stability characteristics of the cylindrical relative equilibria. Their primary finding is that very light, low-speed rotors in this configuration can act to stabilize or destabilize the attitude dynamics of the gyrostat-satellite. Stepanov[32] investigates the stability of the cylindrical relative equilibria in both the "restricted" and "unrestricted" cases. It is determined that the differences in the stability criteria are on the order of l^2/R^2, where l is the characteristic length of the gyrostat-satellite and R is the distance from the center of the celestial primary. Crespo da Silva[3] states that some of the stable configurations determined using the procedure in Kane and Mingori[12] result in resonant rotational motion of the gyrostat-satellite. Crespo da Silva[3] defines three parameters that determine the stability of the equilibrium. The parameters are functions of the principal moments of inertia of the gyrostat-satellite and the magnitude of the relative angular momentum vector. The conditions on these parameters to guarantee local stability are determined using both linear and Liapunov stability theory. Like Crespo da Silva,[3] Yu[37] examines the infinitesimal stability of the cylindrical relative equilibrium using the linearized equations of motion. Sufficient conditions on the principal moments of inertia and the relative angular momentum vector for stability are stated in the form of inequalities. The author also investigates the effect of the addition of two different damping mechanisms on the stability of the equilibrium. The first damping mechanism uses the relative motion of a much smaller body constrained to move in a plane. An example of such as device provided by the author is a small ball moving in a toroid-shaped pipe filled with gas. The second damping mechanism uses a thin metal coil that interacts with an external magnetic or electrical field to generate an eddy-current torque for damping.

Roberson[26] investigates the stability of the relative equilibria of all the elementary cases. The investigation is prompted by two previous analyses that either omitted an elementary case or arrived at unnecessarily restrictive sufficient conditions for stability. The stability analysis is performed using three methods: Chetaevs method, dynamic energy potential method, and application of Thomson-Tait-Chetaev theorem. The author shows that the three methods provide the same results, and states that the application of Thomson-Tait-Chetaev theorem is the least laborious of the three methods given the classical formulation of the rotational equations of motion. Longman[18] also analyzes the stability of the relative equilibria of the elementary cases. Sufficient conditions for stability on the principal moments of inertia and relative angular momentum vector are determined using the Hamiltonian as a Liapunov testing function.

The stability of the two-parameter family of all possible relative equilibrium attitudes presented in Longman and Roberson[20] is investigated by Longman.[16] A parameter space is defined that includes the principal moments of inertia of the gyrostat-satellite, the two parameters defining the relative equilibrium attitude, and the component of the angular

momentum along the orbit normal. The boundaries of the parameter space along which the nature of the stability behavior changes are determined using a quadratic approximation of the dynamic potential with Poincare's theory of bifurcation. The region of parameter space that admits Liapunov stable relative equlibria is defined. Longman, Hagedorn, and Beck[19] investigate the stability of the elementary cases as a generalization of the classical problem of the gravitational stabilization of a rigid body. In particular, the effect of the magnitude of the relative angular momentum vector on the boundaries of the Lagrange, Beletskii-Delp, and instability regions in the parameter space is identified. Hughes[10] presents a detailed investigation of the stability of conical relative equilibrium, and provides many diagrams showing parameter effects on stability.

Ge and Chen[5] determine sufficient conditions for the global stability of the cylindrical relative equilibria using Liapunov's direct method. The authors compare their new results with existing results published in the literature. Ge and Chen[5] also investigate the stability of steady spins with respect to the orbital reference frame. Sarychev, Mirer, and Degtyarev[30] investigate the relative equilibria and stability for the case when the relative angular momentum vector has one zero-component in the principal reference frame. The authors determine parameter dependencies of the stability results, and bifurcation values of the parameters are determined.

2.1.3 Other Analyses

Perhaps one of the most interesting findings in the literature, is the existence of continua of relative equilibria for certain configurations. Roberson[25] is the earliest reviewed paper to mention that when the relative angular momentum vector is aligned with a principal axis there is a critical value of the relative angular momentum magnitude that results in a continuum of relative equilibrium attitudes instead of the usual isolated equilibrium points. Longman[15] is earliest reviewed paper to describe the continuum of relative equilibria in detail.

Longman[17] presents a stability analysis of the continua of relative equilibrium presented in Longman.[15] The topology of the dynamic potential surface expressed in the parameter space is investigated to determine stability. The primary result is that if the relative angular momentum vector is aligned with the minor principal axis a stable tumbling motion results. The author also shows that the critical spin rate is a point of bifurcation in the stability behavior of many of the isolated relative equilibria.

Crespo da Silva[4] investigates nonlinear coupling between finite motions that leads to energy exchanges which may excite nonlinear resonances. The author determines that the nonlinear resonances can cause roll-yaw motion to increase significantly beyond its initial state to an amplitude independent of initial conditions. Liu[14] looks at how small eccentricities can excite librational motions about a relative equilibrium.

Optimal feedback control laws utilizing internal torques are devised by Krementulo[13] and Saakian.[28] Krementulo[13] develops an optimal feedback control law for an axial symmetric gyrostat-satellite near a cylindrical relative equilibrium. Saakian[28] extends the work of Krementulo[13] by developing an optimal feedback control law for a tri-inertial gyrostat-satellite.

A relatively recent subset of the literature have used a noncanonical Hamiltonian approach to study the dynamics of a gyrostat-satellite. The earliest reviewed work to use this approach is Wang, Lian, and Chen.[35] The authors investigate the "unrestricted" case for the 24 "great-circle" (cylindrical) relative equilibria and their stability. Hall and Beck,[8] Hall,[6] and Hall and Beck[9] are a series of papers that present an algorithm for computing the relative equilibria of a gyrostat-satellite that also directly provides stability information. As an example, the authors apply the algorithm to the problem of determining cylindrical relative equilibrium. Molina and Mondejar[21] use a noncanonical Hamiltonian approach to determine sufficient conditions for the nonlinear stability in the case when the relative angular momentum vector is aligned with a principal axis.

2.2 Momentum Unloading via Gravitational Torques

Several authors investigate the use of gravitational torques to unload accumulated angular momentum in satellites equipped with momentum-exchange actuators for attitude stabilization and control. The authors investigate attitude deviation profiles that result in the application of gravitational torques on the satellite in such a way to allow the unloading of accumulated momentum. The primary benefit of this method is the elimination or minimization of thruster firing and therefore of propellant expenditure. Powell[24] discusses the development of a momentum management system for a satellite that is nominally inertially-orientated. The author defines theoretical limits for regions of controllable angular momentum. Powell's[24] momentum management system uses one or two large angle slew maneuvers to perform the bulk of the "unloading" and trim maneuvers for finer corrections. Tong[33] also investigates unloading angular momentum via controlled attitude deviations from nominal mission attitude profile to use gravity-gradient torques. The author demonstrates feasibility via a case study of an asymmetric satellite equipped with CMGs in an elliptical orbit. Yamada, Yoshikawa, Kashiwase, and Matsue[36] analyze a control method using gravitational torques to unload angular momentum, and determine the method's momentum unloading capability.

2.3 Transitions between Relative Equilibria

The literature on gyrostat-satellite dynamics and control contains only a few works that discuss transitioning between relative equilibrium. Roberson[25] is the earliest work. Roberson[25] states (almost as an aside) that the reorientation of the gyrostat from one relative equilibria

to another may be accomplished by "simply turning on a certain rotor." The only technical investigation into transitions of a gyrostat-satellite between relative equilibria in the reviewed literature is Anchev.[1] The author describes open-loop control strategies for the transition from a cylindrical relative attitude equilibrium to another relative equilibrium. Specifically, re-orientations about the orbit normal, nadir, and the velocity vector are investigated. Hall and Beck[9] and Hall[6] have also noted that Anchev[1] is the only work documented in the literature to investigate transitions between relative equilibria.

2.4 Summary & Conclusions

A significant amount of work is documented in the literature on the dynamics and control of gyrostat-satellites. The vast majority of the work has focused on the application of relative equilibria for semi-passive stabilization of the attitude of an artificial satellite. The problem of determining the relative equilibrium attitudes of a gyrostat-satellite has been solved.[11,25,27,20,18,23,29] The stability of the relative attitude equilibria has been investigated in detail.[12,32,3,37,26,16,19,10,5,30]

Although much work has been done in the field, there is a significant gap in the literature. Roberson[25] and Anchev[1] are the only works to mention the possibility of using internal torque actuation to transition between relative equilibria. Roberson[25] briefly discusses reorienting a gyrostat-satellite from one relative attitude equilibrium to another by "simply turning on a certain rotor." Anchev[1] is the only author to investigate (in any detail) these types of transitions between relative equilibria in the reviewed literature.

The current work starts to address the significant gap that has been identified in the literature. The primary new contribution is the definition of COMETs and an investigation into their utilization for performing transitions between the relative equilibria of a gyrostat-satellite.

Chapter 3

Gyrostat-Satellite Dynamics

The equations of motion for a gyrostat-satellite are derived in this chapter. The literature contains many presentations of the derivation of the equations of motion for a gyrostat-satellite. The reader is referred to Hughes,[11] Hall,[7] and Schaub and Junkins[31] as good examples. The presentation given here loosely follows that of Hughes,[11] but has been tailored to the problem of interest and introduces the notation used throughout the rest of the dissertation. The equations of motion form the foundation for the results presented in later chapters.

First, the linear momentum and moment of momentum for a gyrostat are derived in Sections 3.1 and 3.2, respectively. The gravitational force and torque experienced by a gyrostat-satellite are then derived in Section 3.3. The translational and rotational equations of motion for a gyrostat-satellite are determined via application of Newton's and Euler's second laws, respectively, in Section 3.4. Section 3.5 summarizes the important points from the chapter.

3.1 Linear Momentum

The equations defining the linear momentum of a gyrostat are derived in this section. First, equations are derived for the linear momentum of the platform, Section 3.1.1, and a single rotor, Section 3.1.2. The linear momenta are summed to arrive at the equation of linear momentum for a gyrostat in Section 3.1.3.

3.1.1 Platform ($\mathcal{P}$)

The linear momentum of the gyrostat platform, $\vec{p}_p$, is

$$\vec{p}_p = \int_{\mathcal{P}} \vec{v}_o + \vec{\omega} \times \vec{r}_p \, dm \tag{3.1}$$

where $\vec{v}_o$ is the velocity with respect to inertial space of the point o fixed in the platform, $\vec{\omega}$ is the angular velocity of the platform with respect to inertial space, and $\vec{r}_p$ is a vector directed from the point o to the infinitesimal mass element dm. The values of $\vec{v}_o$ and $\vec{\omega}$ do not vary over the platform, and may therefore be moved outside of the integral over the platform $\mathcal{P}$.

$$\vec{p}_p = \int_{\mathcal{P}} dm\ \vec{v}_o + \vec{\omega} \times \int_{\mathcal{P}} \vec{r}_p\ dm \tag{3.2}$$

The first term is equal to the total mass of the gyrostat platform, m_p. The integral in the second term in Eq. 3.2 is equal to the first mass moment of the platform with respect to the point o, $\vec{c}_{p_0}$.

$$\vec{c}_{p_0} = \int_{\mathcal{P}} \vec{r}_p\ dm \tag{3.3}$$

Applying these results to Eq. 3.2 gives

$$\vec{p}_p = m_p \vec{v}_o + \vec{\omega} \times \vec{c}_{p_o} \tag{3.4}$$

Equation 3.4 is used in Section 3.1.3 to derive the equation for the linear momentum of a gyrostat.

3.1.2 Rotor ($\mathcal{R}$)

The linear momentum of one of the gyrostat rotors, $\vec{p}_r$, is

$$\vec{p}_r = \int_{\mathcal{R}} \vec{v}_o + \vec{\omega} \times \vec{b} + \vec{\omega}_r \times \vec{r}_r\ dm \tag{3.5}$$

where $\vec{b}$ is the vector directed from the point o to the center of mass of the rotor, $\vec{\omega}_r$ is the angular velocity of the rotor with respect to inertial space, and $\vec{r}_r$ is a vector directed from the rotor center of mass to the infinitesimal mass element dm. The values of $\vec{v}_o$, $\vec{\omega}$, $\vec{b}$, and $\vec{\omega}_r$ do not vary over the rotor, and may therefore be moved outside of the integral over the rotor $\mathcal{R}$.

$$\vec{p}_r = \int_{\mathcal{R}} dm\ \left(\vec{v}_o + \vec{\omega} \times \vec{b}\right) + \vec{\omega}_r \times \int_{\mathcal{R}} \vec{r}_r\ dm \tag{3.6}$$

The integral in the first term is equal to the total mass of the rotor, m_r. The integral in the second term in Eq. 3.2 is equal to the first mass moment of the rotor with respect to the rotor center of mass, witch is equal to $\vec{0}$.

$$\int_{\mathcal{R}} \vec{r}_r\ dm = \vec{0} \tag{3.7}$$

Applying these terms to Eq. 3.6 results in

$$\vec{p}_r = m_r \left(\vec{v}_o + \vec{\omega} \times \vec{b}\right) \tag{3.8}$$

Equation 3.8 is used in Section 3.1.3 to derive the equation for the linear momentum of a gyrostat.

3.1.3 Gyrostat ($\mathcal{G}$)

The total linear momentum of a gyrostat, $\vec{p}$, is the sum of the linear momenta of the platform $\mathcal{P}$ and the rotors $\mathcal{R}$.

$$\vec{p} = \vec{p}_p + \sum_i^n \vec{p}_{r_i} \tag{3.9}$$

Plugging Eqs. 3.4 and 3.8 into Eq. 3.9 results in

$$\vec{p} = m_p\vec{v}_o + \vec{\omega} \times \vec{c}_{p_o} + \sum_i^n m_{r_i}\left(\vec{v}_o + \vec{\omega} \times \vec{b}_i\right) \tag{3.10}$$

Equation 3.10 can be rewritten as

$$\vec{p} = \left(m_p + \sum_i^n m_{r_i}\right)\vec{v}_o + \vec{\omega} \times \left(\vec{c}_{p_o} + \sum_i^n m_{r_i}\vec{b}_i\right) \tag{3.11}$$

The quantity in parentheses in the first term is equal to the total mass of the gyrostat, m.

$$m = m_p + \sum_i^n m_{r_i} \tag{3.12}$$

The quantity in parentheses in the second term is equal to the first mass moment of the gyrostat with respect to the point o, $\vec{c}_o$.

$$\vec{c}_o = \vec{c}_{p_o} + \sum_i^n m_{r_i}\vec{b}_i \tag{3.13}$$

Applying these terms to Eq. 3.11 results in

$$\vec{p} = m\vec{v}_o + \vec{\omega} \times \vec{c}_o \tag{3.14}$$

If the point o is chosen to be the center of mass of the gyrostat, the value of $\vec{c}_o$ is $\vec{0}$, and Eq. 3.14 simplifies to

$$\vec{p} = m\vec{v} \tag{3.15}$$

Equation 3.15 is used in Section 3.4.1 to derive the translational equations of motion for a gyrostat-satellite.

3.2 Moment of Momentum

The equations defining the moment of momentum of a gyrostat are derived in this section. First, equations are derived for the moments of momentum of the platform, Section 3.2.1, and a single rotor, Section 3.2.2. The moments of momentum are summed to arrive at the equation of moment of momentum for a gyrostat in Section 3.2.3.

3.2.1 Platform ($\mathcal{P}$)

The moment of momentum of the platform $\mathcal{P}$ is

$$\vec{H}_{p_o} = \int_{\mathcal{P}} \vec{r}_p \times (\vec{v}_o + \vec{\omega} \times \vec{r}_p)\ dm \tag{3.16}$$

Recognizing that $\vec{v}_o$ is constant over the platform $\mathcal{P}$ and using Eq. 3.3, Eq. 3.16 may be rewritten as

$$\begin{aligned} \vec{H}_{p_o} &= \left(\int_{\mathcal{P}} \vec{r}_p\ dm\right) \times \times \vec{v}_o + \int_{\mathcal{P}} \vec{r}_p \times (\vec{\omega} \times \vec{r}_p)\ dm \\ &= \vec{c}_{p_o} \times \vec{v}_o + \int_{\mathcal{P}} \vec{r}_p \times (\vec{\omega} \times \vec{r}_p)\ dm \end{aligned} \tag{3.17}$$

The vector triple product in the integrand of the second term of Eq. 3.17 may be rewritten so that the platform angular velocity vector, $\vec{\omega}$, can be pulled outside of the integrand.

$$\vec{H}_{p_o} = \vec{c}_{p_o} \times \vec{v}_o + \left(\int_{\mathcal{P}} \vec{r}_p \cdot \vec{r}_p \vec{1} - \vec{r}_p \vec{r}_p\ dm\right) \cdot \vec{\omega} \tag{3.18}$$

The integral term inside the parentheses is equal to the interia tensor of the platform.

$$\vec{I}_{p_o} = \int_{\mathcal{P}} \vec{r}_p \cdot \vec{r}_p \vec{1} - \vec{r}_p \vec{r}_p\ dm \tag{3.19}$$

Equation 3.18 becomes

$$\vec{H}_{p_o} = \vec{c}_{p_o} \times \vec{v}_o + \vec{I}_{p_o} \cdot \vec{\omega} \tag{3.20}$$

after applying the definition in Eq. 3.19. Equation 3.20 is used in Section 3.2.3 to derive the equation for the moment of momentum of a gyrostat.

3.2.2 Rotor ($\mathcal{R}$)

The moment of momentum of a rotor $\mathcal{R}$ is

$$\vec{H}_{r_o} = \int_{\mathcal{R}} \left(\vec{b} + \vec{r}_r\right) \times \left(\vec{v}_o + \vec{\omega} \times \vec{b} + \vec{\omega}_r \times \vec{r}_r\right)\ dm \tag{3.21}$$

Equation 3.21 can be rewritten as

$$\begin{aligned} \vec{H}_{r_o} &= \vec{b} \times \int_{\mathcal{R}} \left(\vec{v}_o + \vec{\omega} \times \vec{b} + \vec{\omega}_r \times \vec{r}_r\right)\ dm \\ &+ \left(\int_{\mathcal{R}} \vec{r}_r\ dm\right) \times \left(\vec{v}_o + \vec{\omega} \times \vec{b}\right) + \int_{\mathcal{R}} \vec{r}_r \times (\vec{\omega}_r \times \vec{r}_r)\ dm \end{aligned} \tag{3.22}$$

The integral in the first term of Eq. 3.22 is equal to the linear momentum of the rotor with respect to inertial space (Eq. 3.8). The integral in the second term of Eq. 3.22 is equal to

the first mass moment of the rotor about its center of mass, which is equal to $\vec{0}$ (Eq. 3.7). Applying these two findings allows Eq. 3.22 to be simplified to

$$\vec{H}_{r_o} = \vec{b} \times \vec{p}_r + \int_{\mathcal{R}} \vec{r}_r \times (\vec{\omega}_r \times \vec{r}_r)\ dm \tag{3.23}$$

The vector triple product in the integrand of the second term of Eq. 3.23 may be rewritten so that the rotor angular velocity vector, $\vec{\omega}_r$, can be pulled outside of the integrand.

$$\vec{H}_{r_o} = \vec{b} \times \vec{p}_r + \left(\int_{\mathcal{R}} \vec{r}_r \cdot \vec{r}_r \vec{1} - \vec{r}_r \vec{r}_r\ dm \right) \cdot \vec{\omega}_r \tag{3.24}$$

The integral term inside the parentheses is equal to the interia tensor of the rotor.

$$\vec{I}_r = \int_{\mathcal{R}} \vec{r}_r \cdot \vec{r}_r \vec{1} - \vec{r}_r \vec{r}_r\ dm \tag{3.25}$$

Equation 3.24 becomes

$$\vec{H}_{r_o} = \vec{b} \times \vec{p}_r + \vec{I}_r \cdot \vec{\omega}_r \tag{3.26}$$

after applying the definition in Eq. 3.25. Equation 3.26 is used in Section 3.2.3 to derive the equation for the moment of momentum of a gyrostat.

3.2.3 Gyrostat ($\mathcal{G}$)

The moment of momentum of the gyrostat $\mathcal{G}$ is the sum of the moments of momentum of the platform and all rotors.

$$\vec{H}_o = \vec{H}_{p_o} + \sum_i^n \vec{H}_{r_{i_o}} \tag{3.27}$$

Plugging in the equations for the moments of momentum for the platform (Eq. 3.20) and the rotors (Eq. 3.26) results in

$$\vec{H}_o = \vec{c}_{p_o} \times \vec{v}_o + \vec{I}_{p_o} \cdot \vec{\omega} + \sum_i^n \left(\vec{b}_i \times \vec{p}_{r_i} + \vec{I}_{r_i} \cdot \vec{\omega}_{r_i} \right) \tag{3.28}$$

and becomes

$$\vec{H}_o = \vec{c}_{p_o} \times \vec{v}_o + \vec{I}_{p_o} \cdot \vec{\omega} + \sum_i^n \left(\vec{b}_i \times m_{r_i} \left(\vec{v}_o + \vec{\omega} \times \vec{b}_i \right) + \vec{I}_{r_i} \cdot \vec{\omega}_{r_i} \right) \tag{3.29}$$

when replacing $\vec{p}_r$ with its definition (Eq. 3.8). The angular velocity of the rotor with respect to inertial space, $\vec{\omega}_r$, is equal to

$$\vec{\omega}_r = \vec{\omega} + \vec{\omega}_s \tag{3.30}$$

where $\vec{\omega}_s$ is the angular velocity of the rotor with respect to the platform. Applying Eq. 3.30 to Eq. 3.29 and gathering terms crossed with $\vec{v}_o$ and multiplied by $\vec{\omega}$ results in

$$\begin{aligned} \vec{H}_o &= \left(\vec{c}_{p_o} + \sum_i^n \left(m_{r_i}\vec{b}_i\right)\right) \times \vec{v}_o \\ &+ \left(\vec{I}_{p_o} + \sum_i^n \left(\vec{I}_{r_i} + m_{r_i}\left(\vec{b}_i \cdot \vec{b}_i\vec{1} - \vec{b}_i\vec{b}_i\right)\right)\right) \cdot \vec{\omega} + \sum_i^n \left(\vec{I}_{r_i} \cdot \vec{\omega}_{s_i}\right) \end{aligned} \tag{3.31}$$

The quantity in parentheses in the first term is equal to the first mass moment of the gyrostat with respect to the point o. If the point o is chosen to conincide with the center of mass of the gyrostat, the first mass moment is equal to $\vec{0}$.

$$\vec{c}_{p_o} + \sum_i^n \left(m_{r_i}\vec{b}_i\right) = \vec{0} \tag{3.32}$$

The quantity in parentheses in the second term is equal to the inertia tensor of the gyrostat.

$$\vec{I} = \vec{I}_{p_o} + \sum_i^n \left(\vec{I}_{r_i} + m_{r_i}\left(\vec{b}_i \cdot \vec{b}_i\vec{1} - \vec{b}_i\vec{b}_i\right)\right) \tag{3.33}$$

The final term in Eq. 3.31 is the relative angular momentum vector of the gyrostat, $\vec{h}_s$.

$$\vec{h}_s = \sum_i^n \left(\vec{I}_{r_i} \cdot \vec{\omega}_{s_i}\right) \tag{3.34}$$

Using these definitions simplifies Eq. 3.31 to

$$\vec{h} = \vec{I} \cdot \vec{\omega} + \vec{h}_s \tag{3.35}$$

Equation 3.35 is used in Section 3.4.2 to derive the rotational equations of motion for a gyrostat-satellite.

3.3 Gravitational Effects on a Gyrostat-Satellite

The gravitational force and torque acting on a gyrostat-satellite are derived in this section. The following assumptions are used in the derivations:

1. The gyrostat-satellite is only affected by the gravitation of a single celestial primary.
2. The celestial primary has a spherically symmetrical mass distribution.
3. The gyrostat is small compared to its distance from the center of mass of the celestial primary.

These represent the standard set assumptions pertaining to gravitational effects used throughout the literature on the dynamics and control of a gyrostat-satellite. The reader is referred to Hughes[11] for a detailed discussion on the implications of each of these assumptions and a qualitative assessment of the error incurred.

The gravitational force acting on a gyrostat-satellite is derived in Section 3.3.1. The gravitational torque acting on a gyrostat-satellite is derived in Section 3.3.2.

3.3.1 Gravitational Force

The gravitational force on the differential mass element dm, $d\vec{f}$, is

$$d\vec{f} = -\mu \frac{\vec{r}}{r^3}\, dm \tag{3.36}$$

where μ is the gravitational constant of the celestial primary, $\vec{r}$ is the vector starting at the center of the celestial primary and extending to the differential mass element dm, and r is the magnitude of $\vec{r}$. The total gravitational force acting on the gyrostat $\vec{f}$ is

$$\vec{f} = \int_{\mathcal{G}} d\vec{f} = -\mu \int_{\mathcal{G}} \frac{\vec{r}}{r^3}\, dm \tag{3.37}$$

The vector $\vec{r}$ can be written as the sum of the vector from the center of the celestial primary to the center of mass of the gyrostat, $\vec{r}_c$, and the vector from the center of mass of the gyrostat to the differential mass element dm, $\vec{r}_g$.

$$\vec{r} = \vec{r}_c + \vec{r}_g \tag{3.38}$$

The denominator of Eq. 3.37 can be written as a funtion of $\vec{r}_c$ and $\vec{r}_g$.

$$\begin{aligned} r^{-3} &= [(\vec{r}_c + \vec{r}_g) \cdot (\vec{r}_c + \vec{r}_g)]^{-\frac{3}{2}} \\ &= (\vec{r}_c \cdot \vec{r}_c + 2\vec{r}_c \cdot \vec{r}_g + \vec{r}_g \cdot \vec{r}_g)^{-\frac{3}{2}} \\ &= \left(r_c^2 + 2\vec{r}_c \cdot \vec{r}_g + r_g^2\right)^{-\frac{3}{2}} \\ &= r_c^3 \left(1 + 2\frac{\vec{r}_c \cdot \vec{r}_g}{r_c^2} + \left(\frac{r_g}{r_c}\right)^2\right)^{-\frac{3}{2}} \end{aligned} \tag{3.39}$$

The class of gyrostat-satellites that are of practical engineering interest generally satisfy the following relation.

$$\frac{r_g}{r_c} \ll 1 \tag{3.40}$$

Equation 3.40 requires that the "characteristic length" of the gyrostat is significantly smaller than the distance from the celestial primary. Applying Eq. 3.40 allows Eq. 3.39 to be

approximated to first order using binomial expansion as[11,31]

$$r^{-3} \approx r_c^{-3}\left(1 - 3\frac{\vec{r}_c \cdot \vec{r}_g}{r_c^2}\right) \tag{3.41}$$

Plugging Eq. 3.41 into Eq. 3.37 results in

$$\begin{aligned} \vec{f} &= -\mu \int_{\mathcal{G}} \frac{\vec{r}_c + \vec{r}_g}{r_c^3}\left(1 - 3\frac{\vec{r}_c \cdot \vec{r}_g}{r_c^2}\right)\, dm \\ &= -\frac{\mu}{r_c^3}\int_{\mathcal{G}}\left(\vec{r}_c + \vec{r}_g - 3\frac{\vec{r}_c \cdot \vec{r}_g}{r_c^2}\vec{r}_c - 3\frac{\vec{r}_c \cdot \vec{r}_g}{r_c^2}\vec{r}_g\right)\, dm \\ &= -\frac{\mu}{r_c^3}\left(m\vec{r}_c + \int_{\mathcal{G}} \vec{r}_g\, dm\right) + \frac{3\mu}{r_c^5}\left(\vec{r}_c\vec{r}_c \cdot \int_{\mathcal{G}} \vec{r}_g\, dm + \int_{\mathcal{G}} \vec{r}_g\vec{r}_g\, dm \cdot \vec{r}_c\right) \end{aligned} \tag{3.42}$$

Because $\vec{r}_g$ eminates from center of mass of the gyrostat, the first mass moment is

$$\int_{\mathcal{G}} \vec{r}_g\, dm = \vec{0} \tag{3.43}$$

Equation 3.42 simplifies to

$$\begin{aligned} \vec{f} &= -\frac{\mu}{r_c^3}\left(m\vec{1} + \frac{3\mu}{r_c^2}\int_{\mathcal{G}} \vec{r}_g\vec{r}_g\, dm\right) \cdot \vec{r}_c \\ &= -\frac{\mu}{r_c^3}\left(m\vec{1} + \frac{3\mu}{r_c^2}\vec{M}\right) \cdot \vec{r}_c \end{aligned} \tag{3.44}$$

where

$$\vec{M} = \int_{\mathcal{G}} \vec{r}_g\vec{r}_g\, dm \tag{3.45}$$

The inertia-like matrix $\vec{M}$ can be expressed in terms of the moments and products of inertia.

$$\mathbf{M} = \begin{bmatrix} \frac{1}{2}\left(I_{22} + I_{33} - I_{11}\right) & I_{12} & I_{13} \\ I_{12} & \frac{1}{2}\left(I_{11} + I_{33} - I_{22}\right) & I_{23} \\ I_{13} & I_{23} & \frac{1}{2}\left(I_{11} + I_{22} - I_{33}\right) \end{bmatrix} \tag{3.46}$$

The second term in the parentheses is significantly smaller than the first term for systems satisfying Eq. 3.40 and can therefore be ignored. The resulting equation for the gravitational force, $\vec{f}$, applied to the gyrostat-satellite is

$$\vec{f} = -\frac{\mu m}{r_c^3}\vec{r}_c \tag{3.47}$$

Equation 3.47 depends on the position of the gyrostat-satellite with respect to the celestial primary, and is independent of the orientation of the gyrostat-satellite. Equation 3.47 is used in Section 3.4.1 to derive the translational equations of motion for a gyrostat-satellite.

3.3.2 Gravitational Torque

The total gravitational torque acting on the gyrostat $\vec{g}$ is

$$\vec{g} = \int_{\mathcal{G}} \vec{r}_g \times d\vec{f} = -\mu \int_{\mathcal{G}} \vec{r}_g \times \frac{\vec{r}}{r^3}\, dm \tag{3.48}$$

Substituting Eq. 3.38 into Eq. 3.48 results in

$$\begin{aligned} \vec{g} &= -\mu \int_{\mathcal{G}} \vec{r}_g \times \frac{(\vec{r}_c + \vec{r}_g)}{r^3}\, dm \\ &= \vec{r}_c \times \mu \int_{\mathcal{G}} \frac{\vec{r}_g}{r^3}\, dm \end{aligned} \tag{3.49}$$

From Eq. 3.48, it is clear that the gravitational torque does not have a component along the vector directed from the center of mass of the celestial primary to the center of mass of the gyrostat. Applying the same approximation for r^{-3} used in the derivation of the gravitational force acting on the gyrostat, Eq. 3.41, gives

$$\begin{aligned} \vec{g} &= \vec{r}_c \times \mu \int_{\mathcal{G}} \frac{\vec{r}_g}{r_c^3} \left(1 - 3\frac{\vec{r}_c \cdot \vec{r}_g}{r_c^2}\right) dm \\ &= \vec{r}_c \times \left(\frac{\mu}{r_c^3} \int_{\mathcal{G}} \vec{r}_g\, dm - 3\frac{\mu}{r_c^5} \int_{\mathcal{G}} (\vec{r}_c \cdot \vec{r}_g)\, \vec{r}_g\, dm\right) \end{aligned} \tag{3.50}$$

Utilizing the vector triple product identity and Eq. 3.43 allows Eq. 3.51 to be rewritten as

$$\begin{aligned} \vec{g} &= -3\frac{\mu}{r_c^5}\vec{r}_c \times \left(\int_{\mathcal{G}} \vec{r}_g \times (\vec{r}_c \times \vec{r}_g) - (\vec{r}_g \cdot \vec{r}_g)\, \vec{r}_c\, dm\right) \\ &= -3\frac{\mu}{r_c^5} \left(\vec{r}_c \times \int_{\mathcal{G}} \vec{r}_g \times (\vec{r}_c \times \vec{r}_g)\; dm - \left(\int_{\mathcal{G}} \vec{r}_g \cdot \vec{r}_g\, dm\right) \vec{r}_c \times \vec{r}_c\right) \\ &= -3\frac{\mu}{r_c^5}\vec{r}_c \times \int_{\mathcal{G}} \vec{r}_g \times (\vec{r}_c \times \vec{r}_g)\; dm \end{aligned} \tag{3.51}$$

The vector triple product identity is used again to arrive at

$$\vec{g} = -3\frac{\mu}{r_c^5}\vec{r}_c \times \left(\int_{\mathcal{G}} (\vec{r}_g \cdot \vec{r}_g)\, \vec{1} - \vec{r}_g\vec{r}_g\, dm\right) \cdot \vec{r}_c \tag{3.52}$$

The term in parentheses is the interia matrix of the gyrostat, $\vec{I}$. Equation 3.52 becomes

$$\vec{g} = 3\frac{\mu}{r_c^3}\vec{o}_3 \times \vec{I} \cdot \vec{o}_3 \tag{3.53}$$

Equation 3.53 depends on the distance of the gyrostat-satellite from the center of they celestial primary, and the orientation of the gyrostat-satellite. Equation 3.53 is used in Section 3.4.2 to derive the rotational equations of motion for a gyrostat-satellite.

3.4 Equations of Motion

The equations of motion of a gyrostat-satellite are presented in this section. The translational equations of motion are derived in Section 3.4.1, and the rotational equations of motion are derived in Section 3.4.2.

3.4.1 Translational

Newton's second law of motion can be written as

$$\frac{d}{dt}\left(\vec{p}\right)_i = \vec{f} \tag{3.54}$$

where the subscript i indicates that the time derivative is taken with respect to inertial space, and $\vec{f}$ is the total external force applied to the gyrostat. Based on the linear momentum of a gyrostat derived in Section 3.1, the first time derivative of the linear momentum of a gyrostat with respect to inertial space is

$$\frac{d}{dt}\left(\vec{p}\right)_i = m\frac{d}{dt}\left(\vec{v}\right)_i = m\vec{a} \tag{3.55}$$

where $\vec{a}$ is the second time derivative of the gyrostat position vector taken with respect to inertial space, and it has been assumed that the total mass of the gyrostat, m, is a constant. Plugging in the equation for the gravitational force acting on a gyrostat (Eq. 3.47) results in

$$m\vec{a} = -\frac{\mu m}{r_c^3}\vec{r}_c \tag{3.56}$$

The total mass m appears on both the left- and right-hand sides of Eq. 3.56, and can therefore be canceled out. Thus, simplifying Eq. 3.56 to

$$\vec{a} = -\frac{\mu}{r_c^3}\vec{r}_c \tag{3.57}$$

Equation 3.57 is the standard translational equations of motion for a small object orbiting a single celestial primary. The solutions to Equation 3.57 are Keplerian orbits. Throughout the rest of this dissertation, it is assumed that gyrostat-satellite is in a circular orbit about the celestial primary. The fractional quantity in Eq. 3.57 is equal to the square of the instantaneous orbital rate, which for circular orbits is a constant.[2]

$$\omega_o = \sqrt{\frac{\mu}{r_c^3}} \tag{3.58}$$

Plugging Eq. 3.58 into Eq. 3.57 results in

$$\vec{a} = -\omega_o^2\vec{r}_c \tag{3.59}$$

The translational equations of motion are decoupled from the rotational motion of the gyrostat-satellite.

3.4.2 Rotational

Euler's second law of motion can be written as

$$\frac{d}{dt}\left(\vec{h}\right)_i = \vec{g} \tag{3.60}$$

where $\vec{g}$ is the total external torque applied to the gyrostat. Based on the moment of momentum of a gyrostat (about its center of mass) derived in Section 3.2, the first time derivative of the moment of momentum of a gyrostat (about its center of mass) with respect to inertial space is

$$\frac{d}{dt}\left(\vec{h}\right)_i = \vec{I}\cdot\dot{\vec{\omega}} + \dot{\vec{h}}_s + \vec{\omega}\times\left(\vec{I}\cdot\vec{\omega} + \vec{h}_s\right) \tag{3.61}$$

where $\dot{\vec{\omega}}$ is the angular acceleration of the gyrostat platform with respect to a platform fixed reference frame, $\dot{\vec{h}}_s$ is the first time derivative of the relative angular momentum vector with respect to a platform fixed reference frame, and it has been assumed that the inertia tensor of the gyrostat, $\vec{I}$, is constant. Plugging in the equation for the gravitational torque acting on a gyrostat (Eq. 3.52) results in

$$\vec{I}\cdot\dot{\vec{\omega}} + \dot{\vec{h}}_s + \vec{\omega}\times\left(\vec{I}\cdot\vec{\omega} + \vec{h}_s\right) = 3\frac{\mu}{r_c^3}\vec{o}_3\times\vec{I}\cdot\vec{o}_3 \tag{3.62}$$

The term $\vec{\omega}\times\left(\vec{I}\cdot\vec{\omega} + \vec{h}_s\right)$ is often referred to as "gyroscopic" torque. Equation 3.62 is the standard formulation of the rotational equations of motion for a gyrostat-satellite found in the literature. The rotational equations of motion are coupled to the distance from the gyrostat to the center of the celestial primary. Assuming the gyrostat-satellite is restricted to a circular orbit, Eq. 3.62 simplifies to

$$\vec{I}\cdot\dot{\vec{\omega}} + \dot{\vec{h}}_s + \vec{\omega}\times\left(\vec{I}\cdot\vec{\omega} + \vec{h}_s\right) = 3\omega_o^2\vec{o}_3\times\vec{I}\cdot\vec{o}_3 \tag{3.63}$$

Equation 3.63 is the standard rotational equations of motion for a gyrostat-satellite in a circular orbit, and is the form of the rotational equations of motion used throughout most of the literature. Equation 3.63 is decoupled from the translational equations of motion.

3.5 Summary

The equations of motion for a gyrostat-satellite were derived in this chapter. It was shown that, if the gyrostat-satellite is restricted to a circular orbit, the rotational dynamics decouple from the translational dynamics. Therefore, only the rotational equations of motion are considered throughout the rest of the dissertation. Equation 3.63 is the form of the rotational equations of motion that is used.

Chapter 4

Relative Equilibria of a Gyrostat-Satellite

Equilibrium solutions to the rotational equations of motion developed in Chapter 3 are presented and analyzed. A significant portion of the presentation already exists in the literature (Hughes,[11] Longman,[15] etc.). New contributions to the literature are explicitly noted.

Section 4.1 introduces the concept of relative equilibrium. The necessary and sufficient condition that allows an attitude to be made into a relative equilibrium by the proper selection of the relative momentum vector is derived and presented in Section 4.2. Section 4.3 presents a three-variable parameterization of all possible relative equilibrium attitudes. Section 4.4 presents a detailed development of the directions of the basis vectors of the orbital and principal reference frames that admit relative equilibrium attitudes, which represents a new contribution to the literature. The local stability characteristics of relative equilibria are briefly investigated in Section 4.5.

4.1 Definition of Concept

A dynamical equilibrium occurs when the attitude and relative angular momentum vector of a gyrostat-satellite are constant with respect to the orbital reference frame, and the net external torque applied to the gyrostat-satellite is zero.[11] Therefore, a dynamical equilibrium occurs when the following conditions are met,

$$\vec{\omega} = -\omega_o \vec{o}_2 \tag{4.1}$$

$$\dot{\vec{h}}_s = \vec{0} \tag{4.2}$$

$$\vec{g} = \vec{0} \tag{4.3}$$

The vector $\vec{o}_2$ is a basis vector of the orbital reference frame, and is anti-parallel to the orbit normal of the gyrostat-satellite. The vectors $\vec{o}_1$ and $\vec{o}_3$ complete the orthonormal triad of basis vectors for the orbital reference frame. The vector $\vec{o}_3$ is directed from the gyrostat-satellite center of mass toward the center of the celestial primary. The vector $\vec{o}_1$ is parallel to the velocity vector of the gyrostat-satellite.* If the conditions expressed in Eqs. 4.1 through 4.3 are satisfied, the system momentum is constant with respect to the principal or orbital reference frames and is perpendicular to the orbital plane. The principal reference frame is a body-fixed reference frame in which each basis vector is aligned with a principal axis of the gyrostat-satellite. The inertia matrix expressed in the principal reference frame is a diagonal matrix.

The literature classifies the dynamical equilibria of a gyrostat satellite as being either of the cylindrical or hyperbolic case (See Section 2.1). A dynamical equilibrium is said to be of the cylindrical case if the relative angular momentum vector is perpendicular to the orbital plane. These equilibrium attitudes are the same as the equilibrium attitudes for a rigid-body satellite. A dynamical equilibrium is said to be of the hyperbolic case if the relative angular momentum vector is in the plane perpendicular to $\vec{o}_3$, but not perpendicular to the orbital plane. In this case, the projection of the relative angular momentum vector onto $\vec{o}_1$ is canceled by the projection of the platform angular momentum vector onto $\vec{o}_1$.

A relative equilibrium occurs when the attitude and relative angular momentum vector of a gyrostat-satellite are constant with respect to the orbital reference frame.[11] Therefore, a relative equilibrium occurs when the following conditions are met,

$$\vec{\omega} = -\omega_o \vec{o}_2 \tag{4.4}$$

$$\dot{\vec{h}}_s = \vec{0} \tag{4.5}$$

If the conditions expressed in Eqs. 4.4 and 4.5 are satisfied, the system momentum is constant with respect to the principal or orbital reference frames. Relative equilibria may be thought of as generalization of dynamical equilibria wherein the third condition (Eq. 4.3) is removed. The literature classifies the relative equilibria of a gyrostat satellite as being either of the conical or offset hyperbolic case. A relative equilibrium is said to be of the conical case if the relative angular momentum vector is perpendicular to $\vec{o}_1$, but not perpendicular to the orbital plane. A relative equilibrium is said to be of the offset hyperbolic case if the relative angular momentum vector is not contained in a plane perpendicular to one of the orbital reference frame basis axes. In this case, the projection of the relative angular momentum vector onto $\vec{o}_1$ is canceled by the projection of the platform angular momentum vector onto $\vec{o}_1$.

The gravitational torque applied to a gyrostat-satellite in a relative equilibrium is counteracted by the "gyroscopic" torque exerted by the relative angular momentum vector rotating at orbital rate about the orbit normal. In Section 3.3.2, it was determined, based on Eq. 3.48, that the projection of the gravitational torque along $\vec{o}_3$ is zero. This requires that

* It is assumed that the gyrostat-satellite is in a circular orbit.

the gravitational torque lies in the plane perpendicular to $\vec{o}_3$. The gyroscopic torque term in Eq. 3.62 that must cancel out the gravitational torque applied to the gyrostat-satellite is $\vec{\omega} \times \left(\vec{I} \cdot \vec{\omega} + \vec{h}_s\right)$, which is the cross product of the angular velocity of the platform with the system angular momentum. The first relative equilibrium condition (Eq. 4.4) requires that $\vec{\omega}$ is anti-parallel to $\vec{o}_2$. Therefore, in order for the gyroscopic torque term to satisfy Eq. 4.4 and lie in the same plane as the gravitational torque (perpendicular to $\vec{o}_3$), the system angular momentum must lie in the plane perpendicular to $\vec{o}_1$.

4.2 Necessary and Sufficient Condition

The derivation of the necessary and sufficient conditions for a relative equilibrium attitude presented in this section generally follows the presentations in Longman and Roberson[20] and Hughes.[11] As derived in Chapter 3, the equation of motion for a gyrostat-satellite is

$$\vec{I} \cdot \dot{\vec{\omega}} + \vec{\omega} \times \left(\vec{I} \cdot \vec{\omega} + \vec{h}_s\right) = 3\omega_o^2 \vec{o}_3 \times \vec{I} \cdot \vec{o}_3$$

Satisfying the first relative equilibrium condition, Eq. 4.4, requires that the angular acceleration of the principal reference frame, $\dot{\vec{\omega}}$, is $\vec{0}$, so that

$$\vec{\omega} \times \left(\vec{I} \cdot \vec{\omega} + \vec{h}_s\right) = 3\omega_o^2 \vec{o}_3 \times \vec{I} \cdot \vec{o}_3 \tag{4.6}$$

The gyroscopic torque, $\vec{\omega} \times \left(\vec{I} \cdot \vec{\omega} + \vec{h}_s\right)$, must cancel the gravitational torque, $3\omega_o^2 \vec{o}_3 \times \vec{I} \cdot \vec{o}_3$. Plugging in the first relative equilibrium condition, Eq. 4.4, into Eq. 4.6 and simplifying results in

$$-\omega_o \vec{o}_2 \times \left(-\omega_o \vec{I} \cdot \vec{o}_2 + \vec{h}_s\right) = 3\omega_o^2 \vec{o}_3 \times \vec{I} \cdot \vec{o}_3 \tag{4.7}$$

$$\omega_o^2 \vec{o}_2 \times \vec{I} \cdot \vec{o}_2 - \omega_o \vec{o}_2 \times \vec{h}_s = 3\omega_o^2 \vec{o}_3 \times \vec{I} \cdot \vec{o}_3 \tag{4.8}$$

$$\vec{o}_2 \times \vec{I} \cdot \vec{o}_2 - \vec{o}_2 \times \vec{j}_s = 3\vec{o}_3 \times \vec{I} \cdot \vec{o}_3 \tag{4.9}$$

where the scaled relative angular momentum vector, $\vec{j}_s$, is defined

$$\vec{j}_s = \frac{\vec{h}_s}{\omega_o} \tag{4.10}$$

Both Longman and Roberson[20] and Hughes[11] determine the requirements for a relative equilibrium atttiude by taking the inner products of Eq. 4.9 with the orbital frame basis vectors. The inner product of Eq. 4.9 with $\vec{o}_1$ is

$$\vec{o}_1 \cdot \left(\vec{o}_2 \times \vec{I} \cdot \vec{o}_2 - \vec{o}_2 \times \vec{j}_s\right) = \vec{o}_1 \cdot \left(3\vec{o}_3 \times \vec{I} \cdot \vec{o}_3\right) \tag{4.11}$$

$$\vec{o}_3 \cdot \vec{I} \cdot \vec{o}_2 - \vec{o}_3 \cdot \vec{j}_s = -3\vec{o}_2 \cdot \vec{I} \cdot \vec{o}_3 \tag{4.12}$$

$$\vec{o}_3 \cdot \vec{j}_s = 4\vec{o}_2 \cdot \vec{I} \cdot \vec{o}_3 \tag{4.13}$$

The inner product of Eq. 4.9 with $\vec{o}_2$ is

$$\vec{o}_2 \cdot \left(\vec{o}_2 \times \vec{I} \cdot \vec{o}_2 - \vec{o}_2 \times \vec{j}_s\right) = \vec{o}_2 \cdot \left(3\vec{o}_3 \times \vec{I} \cdot \vec{o}_3\right) \quad (4.14)$$

$$0 = \vec{o}_1 \cdot \vec{I} \cdot \vec{o}_3 \quad (4.15)$$

The inner product of Eq. 4.9 with $\vec{o}_3$ is

$$\vec{o}_3 \cdot \left(\vec{o}_2 \times \vec{I} \cdot \vec{o}_2 - \vec{o}_2 \times \vec{j}_s\right) = \vec{o}_3 \cdot \left(3\vec{o}_3 \times \vec{I} \cdot \vec{o}_3\right) \quad (4.16)$$

$$-\vec{o}_1 \cdot \vec{I} \cdot \vec{o}_2 + \vec{o}_1 \cdot \vec{j}_s = 0 \quad (4.17)$$

$$\vec{o}_1 \cdot \vec{j}_s = \vec{o}_1 \cdot \vec{I} \cdot \vec{o}_2 \quad (4.18)$$

Recognizing that the elements of the inertia tensor of the gyrostat-satellite expressed in the orbital frame are

$$J_{ij} = \vec{o}_i \cdot \vec{I} \cdot \vec{o}_j \quad (4.19)$$

and the elements of the scaled relative angular momentum vector ($\vec{j}_s$) expressed in the orbital frame are

$$j_i = \vec{o}_i \cdot \vec{j}_s \quad (4.20)$$

the necessary and sufficient conditions for a relative equilibrium are

$$j_3 = 4J_{23} \quad (4.21)$$

$$J_{13} = 0 \quad (4.22)$$

$$j_1 = J_{12} \quad (4.23)$$

Equations 4.21 through 4.23 allow for two conclusions to be drawn about the relative equilibrium attitudes of a gyrostat-satellite:[20]

1. A necessary and sufficient condition that an attitude can be made into a relative equilibrium by the proper choice of j_1 and j_3 is that $J_{13} = 0$.
2. The projection of the relative angular momentum vector, $\vec{h}_s$, on to the orbit normal does not affect the attitude of a relative equilibrium.*

An alternative, though exactly equivalent, method for obtaining the necessary and sufficient conditions (Eqs. 4.21 through 4.23) would be to simply express all of the quantities in Eq. 4.9 in the orbital reference frame.

$$\left(\mathbf{o}_2^o\right)^\times \mathbf{J}\mathbf{o}_2^o - \left(\mathbf{o}_2^o\right)^\times \mathbf{j}_s^o = 3\left(\mathbf{o}_3^o\right)^\times \mathbf{J}\mathbf{o}_3^o \quad (4.24)$$

* However, in Section 4.5 it is shown that the stability of the relative equilibrium is dependent on the projection of the relative angular momentum vector, $\vec{h}_s$, on to the orbit normal.

where $\mathbf{o}_2^o$ and $\mathbf{o}_3^o$ are defined,

$$\mathbf{o}_2^o = \begin{bmatrix} 0 & 1 & 0 \end{bmatrix}^\mathsf{T} \tag{4.25}$$

$$\mathbf{o}_3^o = \begin{bmatrix} 0 & 0 & 1 \end{bmatrix}^\mathsf{T} \tag{4.26}$$

Carrying out the matrix multiplication in Eq. 4.24 results in the following vector equation.

$$\begin{bmatrix} J_{23} \\ 0 \\ -J_{12} \end{bmatrix} - \begin{bmatrix} j_3 \\ 0 \\ -j_1 \end{bmatrix} = 3 \begin{bmatrix} -J_{23} \\ J_{13} \\ 0 \end{bmatrix} \tag{4.27}$$

This result matches Eqs. 4.21 through 4.23.

4.3 Parametrization of Relative Equilibrium Attitudes

The set of all possible attitudes that can be made into a relative equilibrium attitude is a three parameter family of orientations. The first two parameters, θ_1 and θ_2, define the direction of the nadir vector, $\vec{o}_3$, with respect to the principal reference frame. The angle θ_1 is defined as the angle between $\vec{p}_3$ and the projection of $\vec{o}_3$ onto the $\vec{p}_2$-$\vec{p}_3$ plane with positive values representing a counterclockwise rotation about $\vec{p}_1$. The angle θ_2 is defined as the angle between $\vec{o}_3$ and the projection of $\vec{o}_3$ onto the $\vec{p}_2$-$\vec{p}_3$ plane with positive angular values resulting in a negative value of the projection of $\vec{o}_3$ onto $\vec{p}_1$. The nadir vector ($\vec{o}_3$) expressed in the principal reference frame, $\mathbf{o}_3$, is calculated from θ_1 and θ_2 using

$$\mathbf{o}_3 = \begin{bmatrix} -\sin(\theta_2) \\ \sin(\theta_1)\cos(\theta_2) \\ \cos(\theta_1)\cos(\theta_2) \end{bmatrix} \tag{4.28}$$

The necessary and sufficient condition for an attitude to be a relative equilibrium attitude is

$$J_{13} = \vec{o}_1 \cdot \vec{I} \cdot \vec{o}_3 = 0 \tag{4.29}$$

The vectors $\vec{o}_1$ and $\vec{o}_3$ are members of an orthonormal triad (the set of basis vectors of the orbital reference frame), and therefore must satisfy the following equality constraint.

$$\vec{o}_1 \cdot \vec{o}_3 = 0 \tag{4.30}$$

Therefore, $\vec{o}_1$ must be perpendicular to both $\vec{o}_3$ and $\vec{I} \cdot \vec{o}_3$. If $\|\vec{o}_3 \times \vec{I} \cdot \vec{o}_3\| \neq 0$, there are two solutions for $\vec{o}_1$, which can be determined using

$$\vec{o}_1 = \pm \frac{\vec{o}_3 \times \vec{I} \cdot \vec{o}_3}{\|\vec{o}_3 \times \vec{I} \cdot \vec{o}_3\|} \tag{4.31}$$

Equation (4.31) shows that for each $\vec{o}_3$ there are precisely two possible relative equilibrium attitudes, which are separated by a 180° rotation about $\vec{o}_3$.

When $\|\vec{o}_3 \times \vec{I} \cdot \vec{o}_3\| = 0$, the gravitational torque is zero, and the gyrostat-satellite is at a dynamical equilibrium. If $\|\vec{o}_3 \times \vec{I} \cdot \vec{o}_3\| = 0$, there are an infinite number of solutions for $\vec{o}_1$. This occurs when $\vec{o}_3$ satisfies,

$$\lambda \vec{o}_3 \quad = \quad \vec{I} \cdot \vec{o}_3 \tag{4.32}$$

where λ is an arbitrary positive scalar. Equation 4.32 is true when $\vec{o}_3$ is aligned with an eigenvector of the inertia matrix $\vec{I}$, or equivalently when $\vec{o}_3$ is aligned with a principal axis of the gyrostat-satellite. In this configuration, any vector lying in the plane perpendicular to $\vec{o}_3$ represents a $\vec{o}_1$ vector of a dynamical equilibrium attitude. Therefore, a third parameter θ_3 is introduced to uniquely define a single attitude. The angle θ_3 is defined as the first angle in a 3-2-1 Euler angle sequence defining the rotation from the orbital to principal reference frame. So, if $\|\vec{o}_3 \times \vec{I} \cdot \vec{o}_3\| = 0$, the vector $\vec{o}_1$ expressed in the principal frame, $\mathbf{o}_1$, is calculated from θ_1, θ_2, and θ_3 using

$$\mathbf{o}_1 \quad = \quad \begin{bmatrix} \cos(\theta_2)\cos(\theta_3) \\ -\cos(\theta_1)\sin(\theta_3) + \sin(\theta_1)\sin(\theta_2)\cos(\theta_3) \\ \sin(\theta_1)\sin(\theta_3) + \cos(\theta_1)\sin(\theta_2)\cos(\theta_3) \end{bmatrix} \tag{4.33}$$

Because $\vec{o}_1$, $\vec{o}_2$, and $\vec{o}_3$ form an orthonormal triad, $\vec{o}_2$ is

$$\vec{o}_2 \quad = \quad \vec{o}_3 \times \vec{o}_1 \tag{4.34}$$

Once $\vec{o}_1$, $\vec{o}_2$, and $\vec{o}_3$ have been determined, the projections of the relative angular momentum vector on $\vec{o}_1$ and $\vec{o}_3$ required to make the attitude a relative equilibrium are determined by applying Eqs. 4.21 and 4.23. The scaled relative angular momentum vector expressed in the orbital frame is calculated using

$$\mathbf{j}^o \quad = \quad \begin{bmatrix} \mathbf{o}_1^\mathsf{T}\mathbf{I}\mathbf{o}_2 & j_2 & 4\mathbf{o}_2^\mathsf{T}\mathbf{I}\mathbf{o}_3 \end{bmatrix}^\mathsf{T} \tag{4.35}$$

where the value of j_2 may be arbitrarily chosen. The relative angular momentum vector expressed in the principal reference frame ($\mathbf{h}_s$) may then be calculated using

$$\mathbf{h}_s \quad = \quad \omega_o \begin{bmatrix} \mathbf{o}_1 & \mathbf{o}_2 & \mathbf{o}_3 \end{bmatrix} \mathbf{j}^o \tag{4.36}$$

An algorithm for calculating the parameters of a relative equilibrium is presented in Algorithm 4.1. The algorithm takes the gyrostat-satellite inertia matrix expressed in a body-fixed reference frame ($\mathbf{I}$), the three relative equilibrium attitude parameters (θ_1, θ_2, and θ_3), and the component of the relative angular momentum vector along the orbit normal (j_2) as input. The algorithm is valid for an inertia matrix expressed in any body-fixed reference frame, therefore it is not limited to the principal reference frame. The algorithm outputs the direction cosine matrix for the rotation from the orbital to the body-fixed reference frame ($\mathbf{R}^{bo}$) and the relative angular momentum vector expressed in the body-fixed reference frame ($\mathbf{h}_s$).

Input : θ_1, θ_2, θ_3, j_2, $\mathbf{I}$
Output: $\mathbf{R}^{bo}$, $\mathbf{h}_s$

$\mathbf{o}_3 \leftarrow \begin{bmatrix} -\sin(\theta_2) \\ \sin(\theta_1)\cos(\theta_2) \\ \cos(\theta_1)\cos(\theta_2) \end{bmatrix}$;
if $\|\mathbf{o}_3^{\times}\mathbf{I}\mathbf{o}_3\| = 0$ **then**
  $\mathbf{o}_1 \leftarrow \begin{bmatrix} \cos(\theta_2)\cos(\theta_3) \\ -\cos(\theta_1)\sin(\theta_3) + \sin(\theta_1)\sin(\theta_2)\cos(\theta_3) \\ \sin(\theta_1)\sin(\theta_3) + \cos(\theta_1)\sin(\theta_2)\cos(\theta_3) \end{bmatrix}$;
else
  $\mathbf{o}_1 \leftarrow \operatorname{sgn}(\theta_3)\frac{\mathbf{o}_3^{\times}\mathbf{I}\mathbf{o}_3}{\|\mathbf{o}_3^{\times}\mathbf{I}\mathbf{o}_3\|}$;
end
$\mathbf{o}_2 \leftarrow \mathbf{o}_3^{\times}\mathbf{o}_1$;
$\mathbf{R}^{bo} \leftarrow \begin{bmatrix} \mathbf{o}_1 & \mathbf{o}_2 & \mathbf{o}_3 \end{bmatrix}$;
$\mathbf{h}_s \leftarrow \omega_o \mathbf{R}^{bo} \begin{bmatrix} \mathbf{o}_1^{\mathsf{T}}\mathbf{I}\mathbf{o}_2 & j_2 & 4\mathbf{o}_2^{\mathsf{T}}\mathbf{I}\mathbf{o}_3 \end{bmatrix}^{\mathsf{T}}$;

Algorithm 4.1: Algorithm to calculate the relative equilibrium attitude and relative angular momentum vector

4.4 Admissible Basis Vector Directions

This section presents a detailed analysis into the directions of the basis vectors of the orbital and principal reference frames that admit a relative equilibrium attitude. The work presented in this section represents a new contribution to the literature, however some of the results overlap results presented in Pascal and Stepanov.[23]

Section 4.4.1 defines the directions of the orbital reference frame basis vectors that admit relative equilibrium attitudes. Section 4.4.2 defines the directions of the principal reference frame basis vectors that admit relative equilibrium attitudes.

4.4.1 Orbital Reference Frame

The parameterization of the relative equilibrium attitudes presented in Section 4.3 demonstrates that a relative equilibrium attitude may be found that aligns $\vec{o}_3$ with any direction with respect to the principal reference frame. An examination of the equations in Section 4.3 shows that a similar parameterization could be generated to define the direction of $\vec{o}_1$ with respect to the principal reference frame. Therefore, a relative equilibrium attitude may be found that aligns $\vec{o}_1$ with any direction with respect to the principal reference frame.

It is only left to determine the directions of $\vec{o}_2$ that admit a relative equilibrium attitude.

The direction of $\vec{o}_2$ with respect to the principal reference frame is chosen arbitrarily, and the orientation of $\vec{o}_1$ and $\vec{o}_3$ are parameterized as functions of $\vec{o}_2$ and a "clocking" angle about $\vec{o}_2$, θ.

$$\vec{o}_1 = \cos\theta\vec{t}_1 + \sin\theta\vec{t}_3 \tag{4.37}$$
$$\vec{o}_3 = -\sin\theta\vec{t}_1 + \cos\theta\vec{t}_3 \tag{4.38}$$

The vectors $\vec{t}_i$ are a set of basis vectors of a temporary reference frame where $\vec{t}_2$ is aligned with $\vec{o}_2$, and the orientation of the temporary reference frame about $\vec{o}_2$ is chosen arbitrarily.

If there exists an angle θ that satisfies the necessary and sufficient condition for the existence of a relative equilibrium attitude, then the current direction of $\vec{o}_2$ with respect to the principal reference frame admits a relative equilibrium attitude. Using Eqs. 4.37 and 4.38 to calculate J_{13} gives

$$J_{13} = \left(\cos^2\theta - \sin^2\theta\right)\vec{t}_1\cdot\vec{I}\cdot\vec{t}_3 - \cos\theta\sin\theta\vec{t}_1\cdot\vec{I}\cdot\vec{t}_1 + \cos\theta\sin\theta\vec{t}_3\cdot\vec{I}\cdot\vec{t}_3 \tag{4.39}$$

The quantities $\vec{t}_i\cdot\vec{I}\cdot\vec{t}_j$ in Eq. 4.39 are entries of the inertia matrix expressed in the temporary reference frame, J^t_{ij}. Applying this result and using some trigonometric identities, Eq. 4.39 simplifies to

$$\begin{aligned} J_{13} &= \left(\cos^2\theta - \sin^2\theta\right)J^t_{13} - \cos\theta\sin\theta J^t_{11} + \cos\theta\sin\theta J^t_{33} \\ &= \cos(2\theta)J^t_{13} + \frac{1}{2}\sin(2\theta)\left(J^t_{33} - J^t_{11}\right) \end{aligned} \tag{4.40}$$

The values of θ that result in $J_{13} = 0$ are summarized below:

1. If $J^t_{13} = 0$ and $J^t_{11} = J^t_{33}$, then θ is unconstrained.
2. If $J^t_{13} = 0$ and $J^t_{11} \neq J^t_{33}$, then
$$\theta = k\frac{\pi}{2} \quad k \in 0, 1, 2, ... \tag{4.41}$$
3. If $J^t_{13} \neq 0$ and $J^t_{11} = J^t_{33}$, then
$$\theta = \frac{\pi}{4} + k\frac{\pi}{2} \quad k \in 0, 1, 2, ... \tag{4.42}$$
4. If $J^t_{13} \neq 0$ and $J^t_{11} \neq J^t_{33}$, then
$$\theta = \frac{1}{2}\arctan\left(\frac{2J^t_{13}}{J^t_{11} - J^t_{33}}\right) + k\frac{\pi}{2} \quad k \in 0, 1, 2, ... \tag{4.43}$$

In summary, it was determined that (in general) for each direction of

- $\vec{o}_1$ on the unit sphere fixed in the principal reference frame there are two possible relative equilibrium attitudes separated by rotations of 180^o about $\vec{o}_1$,
- $\vec{o}_2$ on the unit sphere fixed in the principal reference frame there are four possible relative equilibrium attitudes separated by rotations of 90^o about $\vec{o}_2$, and
- $\vec{o}_3$ on the unit sphere fixed in the principal reference frame there are two possible relative equilibrium attitudes separated by rotations of 180^o about $\vec{o}_3$.

4.4.2 Principal Reference Frame

The directions of the basis vectors of the principal reference frame that admit relative equilibrium attitudes are determined in this section. The distinction between basis vectors of the principal reference frame is arbitrary. Therefore, without loss of generality, only the directions of $\vec{p}_1$ with respect to the orbital reference frame are analyzed.

The direction of $\vec{p}_1$ with respect to the orbital reference frame is chosen arbitrarily, and the orientation of $\vec{p}_2$ and $\vec{p}_3$ are parameterized as functions of $\vec{p}_1$ and a "clocking" angle about $\vec{p}_1$, θ.

$$\vec{p}_2 = \cos\theta\vec{t}_2 + \sin\theta\vec{t}_3 \tag{4.44}$$
$$\vec{p}_3 = -\sin\theta\vec{t}_2 + \cos\theta\vec{t}_3 \tag{4.45}$$

The vectors $\vec{t}_i$ are a set of basis vectors of a temporary reference frame where $\vec{t}_1$ is aligned with $\vec{p}_1$, and the orientation of the temporary reference frame about $\vec{p}_1$ is chosen arbitrarily.

The basis vectors of the orbital reference frame expressed in the principal reference frame are related to the basis vectors of the principal reference frame through the following equation.

$$\mathbf{R}^{po} = \left[\begin{array}{ccc} \mathbf{o}_1 & \mathbf{o}_2 & \mathbf{o}_3 \end{array}\right] = \left[\begin{array}{ccc} \mathbf{p}_1 & \mathbf{p}_2 & \mathbf{p}_3 \end{array}\right]^{\mathsf{T}} \tag{4.46}$$

The 1 and 3 basis vectors of the orbital reference frame expressed in the principal reference frame may be calculated using,

$$\mathbf{o}_1 = \left[\begin{array}{ccc} p_{11} & p_{21} & p_{31} \end{array}\right]^{\mathsf{T}} \tag{4.47}$$
$$\mathbf{o}_3 = \left[\begin{array}{ccc} p_{13} & p_{23} & p_{33} \end{array}\right]^{\mathsf{T}} \tag{4.48}$$

Applying Eqs. 4.44, 4.45, 4.47, and 4.48, the 1-3 component of the gyrostat-satellite inertia matrix expressed in the orbital reference frame may be written as,

$$J_{13} = \mathbf{o}_1^{\mathsf{T}}\mathbf{I}\mathbf{o}_3 = A + B\cos\theta^2 + C\sin\theta^2 + D\cos\theta\sin\theta \tag{4.49}$$

where the coefficients A, B, C, and D are defined

$$\begin{aligned} A &= I_1 p_{11} p_{13} && (4.50)\\ B &= I_2 t_{21} t_{23} + I_3 t_{31} t_{33} && (4.51)\\ C &= I_3 t_{21} t_{23} + I_2 t_{31} t_{33} && (4.52)\\ D &= I_2 t_{21} t_{33} + I_2 t_{23} t_{31} - I_3 t_{21} t_{33} - I_3 t_{23} t_{31} && (4.53) \end{aligned}$$

Using a few trigonometric identities, Eq. 4.49 becomes,

$$J_{13} = A + \frac{1}{2}(B+C) + \frac{1}{2}\sqrt{(B-C)^2 + D^2}\sin\left(2\theta + \arctan\frac{D}{B-C}\right) \quad (4.54)$$

Equation 4.54 must be equal to zero in order to satisfy the necessary and sufficient condition for a relative equilibrium attitude.

$$A + \frac{1}{2}(B+C) + \frac{1}{2}\sqrt{(B-C)^2 + D^2}\sin\left(2\theta + \arctan\frac{D}{B-C}\right) = 0 \quad (4.55)$$

The direction of $\vec{p}_1$ admits a relative equilibrium attitude if a real value of θ exists such that Eq. 4.55 is satisfied. Solving for the value of the $\sin(\cdot)$ quantity in the third term in the left-hand side of Eq. 4.55 gives

$$\begin{aligned} \sin\left(2\theta + \arctan\frac{D}{B-C}\right) &= -\frac{A + \frac{1}{2}(B+C)}{\frac{1}{2}\sqrt{(B-C)^2 + D^2}}\\ &= \beta\gamma && (4.56) \end{aligned}$$

where the variables β and γ in Eq. 4.56 are defined

$$\begin{aligned} \beta &= \frac{p_{11}}{\sqrt{1-p_{11}^2}}\frac{p_{13}}{\sqrt{1-p_{13}^2}} && (4.57)\\ \gamma &= -2\frac{I_1 - \frac{1}{2}(I_2+I_3)}{\|I_2 - I_3\|} && (4.58) \end{aligned}$$

The absolute value of the product of β and γ must be less than or equal to one for a real solution to exist. The value of β is solely a function of the direction of $\vec{p}_1$ with respect to the orbital reference frame. The absolute value of β is always less than or equal to 1. The value of γ only depends on the mass distribution of the gyrostat-satellite and the selection of the principal axis.

If $\vec{p}_1$ is selected to be aligned with the intermediate axis of inertia, the absolute value of γ will be less than or equal to 1. Therefore, the product of β and γ will be less than or equal to 1, and a relative equilibrium attitude will exist for any selected direction of $\vec{p}_1$. If $\vec{p}_1$ is not the intermediate axis of inertia then there are some directions of $\vec{p}_1$ for which the absolute value of the product of β and γ will be greater than 1. And, therefore, do not admit relative equilibrium attitudes.

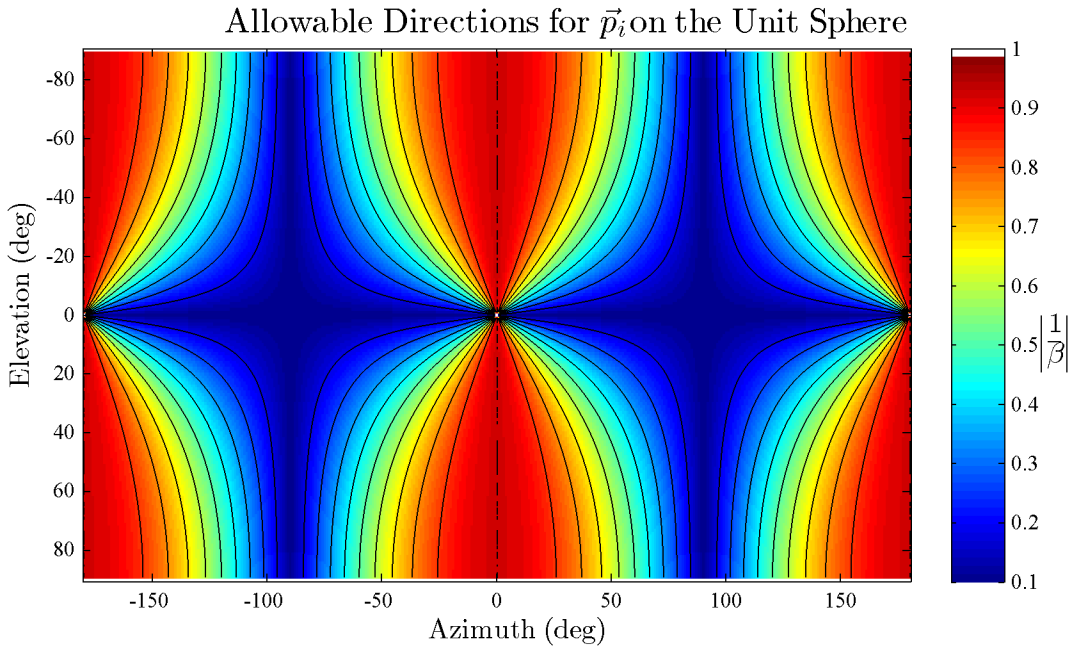

Figure 4.1: A pseudo-color plot showing the values of $\left|\frac{1}{\beta}\right|$ over the unit sphere, which defines the directions of $\vec{p}_i$ that admit a relative equilibrium attitude for a particular values of $\left|\frac{1}{\beta}\right|$.

Figure 4.1 is a pseudo-color plot showing the absolute value of the quantity $\left|\frac{1}{\beta}\right|$ for each direction of $\vec{p}_1$. The colorbar on the right-hand side of the figure defines the mapping from color to the value of $\left|\frac{1}{\beta}\right|$. The black lines overlaid on the plot represent level curves of constant $\left|\frac{1}{\beta}\right|$. The principal moments of inertia and the principal axis with which $\vec{p}_1$ is aligned define the characteristic value of $\left|\frac{1}{\beta}\right|$ for a specific gyrostat-satellite. The directions of $\vec{p}_1$ that admit a relative equilibrium attitude are those regions in Figure 4.1 that have a value less than the characteristic value for the specific gyrostat-satellite.

4.5 Stability of Relative Equilibria

Many authors have investigated the local stability characteristics of a gyrostat-satellite about a relative equilibrium (Hughes,[11] Longman,[15] etc.). This section presents a brief investigation that (in part) loosely follows Hughes,[11] and is included mostly for completeness. The current presentation includes an algorithm that calculates intervals of values for the projection of the relative momentum vector on $\vec{o}_2$, j_2, that result in statically stable relative equilibrium, which represents a new contribution to the literature.

The nonlinear equations of rotational motion, presented in Chapter 3, are linearized about a relative equilibrium in Section 4.5.1. The linearized equations of motion are used to derive

sufficient conditions for the local stability of a relative equilibrium in Section 4.5. Section 4.5 also presents a deterministic algorithm for determining the intervals of j_2 for which a relative equilibrium attitude is stable. Linear numeric simulation results are presented in Section 4.5.3 that validate the stability results.

4.5.1 Linearized Equations of Rotational Motion

The nonlinear equations of rotational motion derived and presented in Section 3.4.2 are linearized about a relative equilibrium. The full nonlinear equations of rotational motion are repeated below.

$$\vec{I}\cdot\dot{\vec{\omega}} + \dot{\vec{h}}_s + \vec{\omega}\times\left(\vec{I}\cdot\vec{\omega}+\vec{h}_s\right) \;=\; 3\omega_o^2\vec{o}_3\times\vec{I}\cdot\vec{o}_3$$

The states of the linearized system are the angular displacement vector and its first time derivative. The angular displacement vector is defined

$$\vec{\alpha} \;=\; \int_0^t \vec{\omega}dt + \vec{\alpha}(0) \tag{4.59}$$

It is assumed that the system experiences only small angular displacements from the relative equilibrium attitude. The initial value of the angular displacement vector can be approximated as

$$\vec{\alpha}(0) \;\approx\; 2\bar{q}^{p\hat{p}}(0) \tag{4.60}$$

where $\bar{q}^{p\hat{p}}$ is the vector part of the principal attitude quaternion* representing the rotation from a reference frame aligned with the relative equilibrium attitude ($\mathcal{F}_{\hat{p}}$) to the principal reference frame ($\mathcal{F}_p$). The first time derivative of the angular displacement vector is

$$\dot{\vec{\alpha}} \;=\; \vec{\omega}^{po} \tag{4.61}$$

Linear approximations of the variables appearing in Eq 4.59 are derived assuming small angular displacements from the relative equilibrium attitude. The angular velocity of $\mathcal{F}_p$ with respect to $\mathcal{F}_i$ can be formulated as

$$\vec{\omega} \;=\; \vec{\omega}^{po} + \vec{\omega}^{oi} \tag{4.62}$$

where $\vec{\omega}^{oi}$ is the angular velocity of $\mathcal{F}^o$ with respect to $\mathcal{F}_i$ and can be written as

$$\vec{\omega}^{oi} \;=\; -\omega_o\vec{o}_2 \tag{4.63}$$

Equation 4.63 is plugged into Eq. 4.62 to arrive at

$$\vec{\omega} \;=\; \vec{\omega}^{po} - \omega_o\vec{o}_2 \tag{4.64}$$

* The set of principal attitude quaternions is the subset of attitude quaternions with a scalar component greater than or equal to zero.

The first time derivative of $\vec{\omega}$ is calculated using

$$\dot{\vec{\omega}} = \dot{\vec{\omega}}^{po} + \omega_o \vec{\omega}^{po} \times \vec{o}_2 \tag{4.65}$$

where the time derivative of $\vec{o}_2$ (defined below) has already been applied.

$$\dot{\vec{o}}_2 = -\vec{\omega}^{po} \times \vec{o}_2 \tag{4.66}$$

The vector $\mathbf{o}_2$ may be written as a function of the equilibrium value of the $\mathbf{o}_2$, $\hat{\mathbf{o}}_2$,

$$\mathbf{o}_2 = \mathbf{R}^{p\hat{p}} \hat{\mathbf{o}}_2 \tag{4.67}$$

where $\mathbf{R}^{p\hat{p}}$ is the direction cosine matrix to rotate vectors from $\mathcal{F}_{\hat{p}}$ to $\mathcal{F}_p$. Assuming small angular displacements from the relative equilibrium attitude, $\mathbf{R}^{p\hat{p}}$ may be approximated as

$$\mathbf{R}^{p\hat{p}} \approx \mathbf{1} - \boldsymbol{\alpha}^{\times} \tag{4.68}$$

The $\mathcal{F}_o$ basis vectors expressed in $\mathcal{F}_p$ may then be approximated as

$$\mathbf{o}_i \approx \left(\mathbf{1} - \boldsymbol{\alpha}^{\times}\right) \hat{\mathbf{o}}_i = \hat{\mathbf{o}}_i + \hat{\mathbf{o}}_i^{\times} \boldsymbol{\alpha} \qquad \text{for} \quad i \in 1, 2, 3 \tag{4.69}$$

Plugging Eqs. 4.61 and 4.69 into Eq. 4.65 results in

$$\dot{\boldsymbol{\omega}} \approx \ddot{\boldsymbol{\alpha}} + \omega_o \dot{\boldsymbol{\alpha}}^{\times} \left(\hat{\mathbf{o}}_2 + \hat{\mathbf{o}}_2^{\times} \boldsymbol{\alpha}\right) \approx \ddot{\boldsymbol{\alpha}} - \omega_o \hat{\mathbf{o}}_2^{\times} \dot{\boldsymbol{\alpha}} \tag{4.70}$$

where terms of the linear states of second-order or higher have been approximated as zero. Plugging Eqs. 4.61 and 4.69 into Eq. 4.62 results in

$$\boldsymbol{\omega} \approx \dot{\boldsymbol{\alpha}} - \omega_o \hat{\mathbf{o}}_2 + \omega_o \hat{\mathbf{o}}_2^{\times} \boldsymbol{\alpha} \tag{4.71}$$

The linear approximations for $\dot{\boldsymbol{\omega}}$ and $\boldsymbol{\omega}$ from Eqs. 4.70 and 4.71 are plugged into Eq. 4.59 to arrive at

$$\mathbf{I}\ddot{\boldsymbol{\alpha}} + \omega_o \mathbf{G}\dot{\boldsymbol{\alpha}} + \omega_o^2 \mathbf{K}\boldsymbol{\alpha} = \mathbf{0} \tag{4.72}$$

where

$$\mathbf{G} = -\mathbf{I}\hat{\mathbf{o}}_2^{\times} + (\mathbf{I}\hat{\mathbf{o}}_2)^{\times} - \hat{\mathbf{o}}_2^{\times}\mathbf{I} - \mathbf{j}_s^{\times} \tag{4.73}$$

$$\mathbf{K} = \hat{\mathbf{o}}_2^{\times}\mathbf{I}\hat{\mathbf{o}}_2^{\times} - (\mathbf{I}\hat{\mathbf{o}}_2)^{\times}\hat{\mathbf{o}}_2^{\times} + \mathbf{j}_s^{\times}\hat{\mathbf{o}}_2^{\times} - 3\hat{\mathbf{o}}_3^{\times}\mathbf{I}\hat{\mathbf{o}}_3^{\times} + 3(\mathbf{I}\hat{\mathbf{o}}_3)^{\times}\hat{\mathbf{o}}_3^{\times} \tag{4.74}$$

As noted by Hughes,[11] "some stamina is required to carry out the matrix algebra," including frequent use of the following equalities.

$$\hat{\mathbf{o}}_1^{\times}\hat{\mathbf{o}}_2 = \hat{\mathbf{o}}_3 \tag{4.75}$$

$$\hat{\mathbf{o}}_2^{\times}\hat{\mathbf{o}}_3 = \hat{\mathbf{o}}_1 \tag{4.76}$$

$$\hat{\mathbf{o}}_3^{\times}\hat{\mathbf{o}}_1 = \hat{\mathbf{o}}_2 \tag{4.77}$$

$$-\omega_o \hat{\mathbf{o}}_2^{\times}(-\omega_o \mathbf{I}\hat{\mathbf{o}}_2 + \mathbf{h}_s) = 3\omega_o^2 \hat{\mathbf{o}}_3^{\times}\mathbf{I}\hat{\mathbf{o}}_3 \tag{4.78}$$

Equations 4.75 through 4.77 come from the fact that $\mathbf{o}_1$, $\mathbf{o}_2$, and $\mathbf{o}_3$ form an orthonormal triad of vectors. Equation 4.78 is the result of the linearization state being a relative equilibrium, so that the gyroscopic and gravitational torque terms cancel one another.

4.5.2 Sufficient Conditions for Stability

The linearized equations of motion of a gyrostat-satellite were derived in Section 4.5.1. Equation 4.72 represents a conservative gyric system.[11] A sufficient condition for a conservative gyric system to be stable is that it is statically stable.[11] A conservative gyric system is statically stable if $\mathbf{K}$ is a positive-definite matrix.[11] Longman[16] notes that even if $\mathbf{K}$ is sign-indefinite the gyrostat-satellite may be infinitesimally stable due to gyroscopic effects.

One method to determine if a matrix is positive-definite is to check sign of the eigenvalues of the matrix. The matrix $\mathbf{K}$ expressed in the orbital frame is

$$\mathbf{K} = \begin{bmatrix} 4\Delta_{23} - j_{s_2} & -3J_{12} & 0 \\ -3J_{12} & 3\Delta_{13} & 3J_{23} \\ 0 & 3J_{23} & -\Delta_{12} - J_{s_2} \end{bmatrix} \tag{4.79}$$

where

$$\Delta_{12} = J_{11} - J_{22} \tag{4.80}$$
$$\Delta_{13} = J_{11} - J_{33} \tag{4.81}$$
$$\Delta_{23} = J_{22} - J_{33} \tag{4.82}$$

The $\mathbf{K}$ matrix is a real symmetric matrix and thus has only real eigenvalues. The Routh-Hurwitz criteria are used to determine the requirements for all of the eigenvalues of the $\mathbf{K}$ matrix to be positive. The characteristic equation of $\mathbf{K}$ is

$$\lambda^3 + a_1\lambda^2 + a_2\lambda + a_3 = \mathbf{0} \tag{4.83}$$

where

$$a_1 = c_{11}j_2 + c_{10} \tag{4.84}$$
$$a_2 = c_{22}j_2^2 + c_{21}j_2 + c_{20} \tag{4.85}$$
$$a_3 = c_{32}j_2^2 + c_{31}j_2 + c_{30} \tag{4.86}$$

The coefficients of the j_2 terms, c_{ij}, are provided below.

$$c_{11} = 2 \tag{4.87}$$
$$c_{10} = \Delta_{12} - 3\Delta_{13} - 4\Delta_{23} \tag{4.88}$$
$$c_{22} = 1 \tag{4.89}$$
$$c_{21} = \Delta_{12} - 6\Delta_{13} - 4\Delta_{23} \tag{4.90}$$
$$c_{20} = -3\Delta_{12}\Delta_{13} - 4\Delta_{12}\Delta_{23} + 12\Delta_{13}\Delta_{23} \tag{4.91}$$
$$c_{32} = -3\Delta_{13} \tag{4.92}$$
$$c_{31} = -3\Delta_{12}\Delta_{13} + 12\Delta_{13}\Delta_{23} - 9J_{12}^2 - 9J_{23}^2 \tag{4.93}$$
$$c_{30} = 12\Delta_{12}\Delta_{13}\Delta_{23} - 9J_{12}^2\Delta_{12} + 36J_{23}^2\Delta_{23} \tag{4.94}$$

The eigenvalues of $\mathbf{K}$ are positive if[11]

$$a_1, a_3, \Delta_2 \;>\; 0 \tag{4.95}$$

where Δ_2 is defined[11]

$$\Delta_2 \;=\; \det\left(\begin{bmatrix} a_1 & a_3 \\ 1 & a_2 \end{bmatrix}\right) \tag{4.96}$$

Plugging Eqs. 4.84 through 4.98 into Eq. (4.96) results in

$$\Delta_2 \;=\; c_{43}j_2^3 + c_{42}j_2^2 + c_{41}j_2 + c_{40} \tag{4.97}$$

where

$$c_{43} \;=\; 2 \tag{4.98}$$

$$c_{42} \;=\; 3\Delta_{12} - 12\Delta_{13} - 12\Delta_{23} \tag{4.99}$$

$$c_{41} \;=\; \Delta_{12}^2 - 12\Delta_{12}\Delta_{13} - 16\Delta_{12}\Delta_{23} + 18\Delta_{13}^2 + 48\Delta_{13}\Delta_{23} + 16\Delta_{23}^2 - 9J_{12}^2 - 9J_{23}^2 \tag{4.100}$$

$$c_{40} \;=\; -3\Delta_{12}^2\Delta_{13} - 4\Delta_{12}^2\Delta_{23} + 9\Delta_{12}\Delta_{13}^2 + 24\Delta_{12}\Delta_{13}\Delta_{23} + 16\Delta_{12}\Delta_{23}^2 - 9J_{23}^2\Delta_{12} - 36\Delta_{13}^2\Delta_{23} - 48\Delta_{13}\Delta_{23}^2 + 27J_{12}^2\Delta_{13} + 27J_{23}^2\Delta_{13} + 36J_{12}^2\Delta_{23} \tag{4.101}$$

Equations 4.84, 4.98, and 4.97 are polynomials in j_2. An algorithm was developed and implemented in MATLAB® that determines the values of j_2 that result in a positive-definite $\mathbf{K}$ matrix. The algorithm determines all of the intervals of j_2 for which $a_1 > 0$, $a_3 > 0$, and $\Delta_2 > 0$ are positive. The output of the algorithm is the intervals denoting the values of j_2 that result in a positive-definite $\mathbf{K}$ and therefore a stable relative equilibrium. The steps executed by the algorithm are shown below:

1. Calculate the values of j_2 that are the roots of a_1, a_3, and Δ_2
2. Sort the list of roots in ascending order
3. Evaluate each polynomial at each root
4. Remove any roots from the list that evaluate to negative values for any of the polynomials. The remaining roots are the ends of open intervals that define where all the polynomials are positive.
5. Evaluate each polynomial at a value less than the minimum root, if all values are positive, the first interval is from negative infinity to the minimum root, and it is added to the interval list

6. Evaluate each polynomial at the mean of each sequential pair of roots in the list, if all values are positive, the interval between the pair of roots is a positive interval, and it is added to the interval list

7. Evaluate each polynomial at a value greater than the maximum root, if all values are positive, the last interval is from the maximum root to positive infinity, and it is added to the interval list

This algorithm was used to select a value for j_2 that would result in a stable relative equilibrium for the numeric simulation presented in the next section.

4.5.3 Linear Numeric Simulation Results

In the previous section, Section 4.5.2, sufficient conditions for the infinitesimal stability of a relative equilibrium were presented. Numeric simulation of the linear equations of rotational motion (Eq. 4.72) is performed to validate these stability results. The simulation is performed in MATLAB® using the built in `ode45()` ordinary differential equation solver.

The parameters chosen for the relative equilibrium are

$$\theta_1 = 72.7461^\circ \tag{4.102}$$
$$\theta_2 = 48.4836^\circ \tag{4.103}$$
$$\theta_3 = 1.0 \tag{4.104}$$

The resulting nadir vector expressed in the body frame is

$$\mathbf{o}_3 = \begin{bmatrix} -0.74877 & 0.63301 & 0.1966 \end{bmatrix}^\mathsf{T} \tag{4.105}$$

The interia matrix of the gyrostat-satellite expressed in the body frame is set to

$$\mathbf{I} = \begin{bmatrix} 65.0 & 0.0 & 0.0 \\ 0.0 & 53.0 & 0.0 \\ 0.0 & 0.0 & 86.0 \end{bmatrix} \tag{4.106}$$

The attitude quaternion from the orbital to the relative equilibrium attitude is

$$\mathbf{q}^{\hat{po}} = \begin{bmatrix} 0.4118 & 0.4818 & -0.0042 & 0.7735 \end{bmatrix}^\mathsf{T} \tag{4.107}$$

The algorithm presented in Section 4.5.2 is used to determine that the relative equilibrium is statically stable if j_2 satisfies the following inequality.

$$-\infty < j_2 < -36.873 \tag{4.108}$$

The value selected for j_2 is -150, which satisfies Eq. 4.108. The $\mathbf{K}$ matrix expressed in the orbital reference frame is

$$\mathbf{K} = \begin{bmatrix} 168.3413 & 7.0896 & 25.0467 \\ 7.0896 & 106.4694 & 69.8303 \\ 25.0467 & 69.8303 & 89.3266 \end{bmatrix} \tag{4.109}$$

The eigenvalues of the $\mathbf{K}$ matrix are 190.8184, 147.1992, and 26.1196, which are all positive. The $\mathbf{K}$ matrix is positive-definite and the relative equilibrium is confirmed to meet the sufficient conditions for stability. The initial conditions of the simulation are set to

$$\boldsymbol{\alpha} = \begin{bmatrix} 0.81403^\circ & -0.10645^\circ & -0.57098^\circ \end{bmatrix}^\mathsf{T} \tag{4.110}$$

$$\dot{\boldsymbol{\alpha}} = \begin{bmatrix} 0.0045312^\circ/s & -0.00075365^\circ/s & -0.001975^\circ/s \end{bmatrix}^\mathsf{T} \tag{4.111}$$

The results of the numeric simulation are presented as Figures 4.2 through 4.4. Figure 4.2 is a plot of the time history of the components of the angular displacement vector on the abscissa and the elapsed simulation time on the ordinate. The 1, 2, and 3 components of the angular displacement vector (α_i) are shown as blue, green, and red curves, respectively. Figure 4.3 is a plot of the time history of the rates of the components of the angular displacement vector on the abscissa and the elapsed simulation time on the ordinate. The rates of the 1, 2, and 3 component of the angular displacement vector ($\dot{\alpha}_i$) are shown as blue, green, and red curves, respectively. The upper-left, upper-right, and lower-left plots in Figure 4.4 depict the trajectory of the gyrostat-satellite in the phase plane of each axis. The lower-right plot in Figure 4.4 shows the path of the angular displacement vector in three-space. The simulation results depicted in Figures 4.2 through 4.4 are consistent with the expected motions of a system at a stable equilibrium. All of the states remain bounded and in the neighborhood of the origin. The simulation results also show that the equilibrium, while stable, is not asymptotically stable. The lack of asymptotic stability is due to there being no mechanism for damping, resulting in continual oscillations.

4.6 Summary

Equilibrium solutions to the nonlinear equations of rotational motion derived in Chapter 3 were analyzed. In particular, the concept of relative equilibria was introduced and defined. The necessary and sufficient condition that allows an attitude to be made into a relative equilibrium by the proper selection of the relative momentum vector was derived. A three-variable parameterization of all possible relative equilibrium attitudes was presented. A detailed analysis into the directions of the basis vectors of the orbital and principal reference frames that admit relative equilibrium attitudes was presented. This analysis represents a new contribution to the literature. The local stability characteristics of relative equilibria were briefly investigated. An algorithm was presented that calculates intervals of values

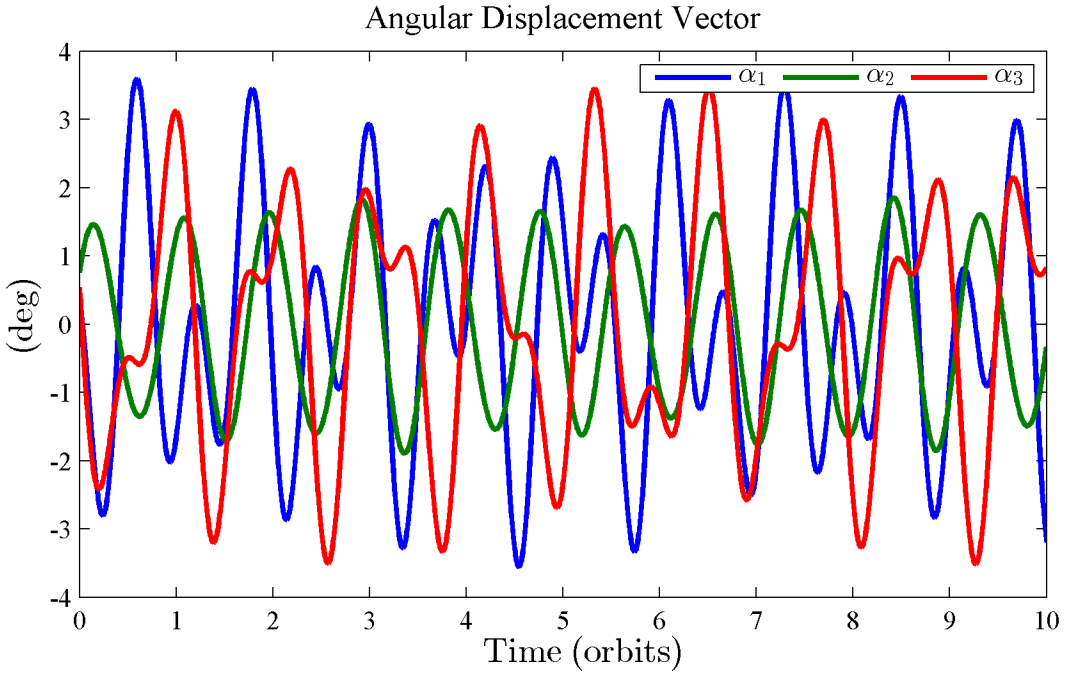

Figure 4.2: Angular displacements from the equilibrium attitude to the principal reference frame

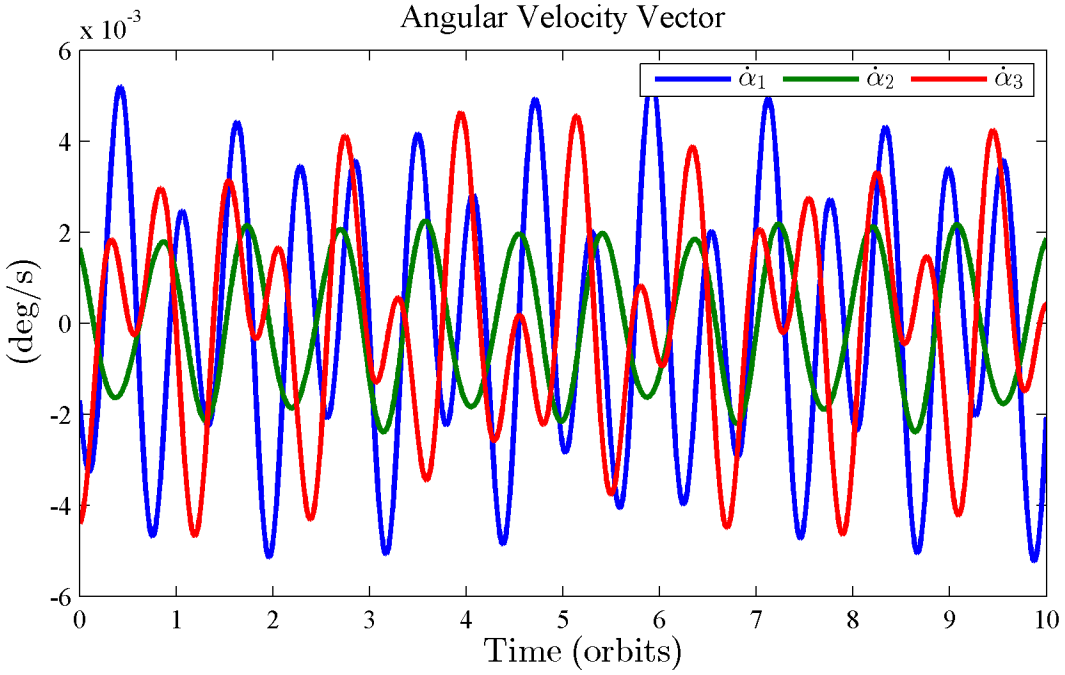

Figure 4.3: Angular rates with respect to the orbital reference frame expressed in the principal reference frame

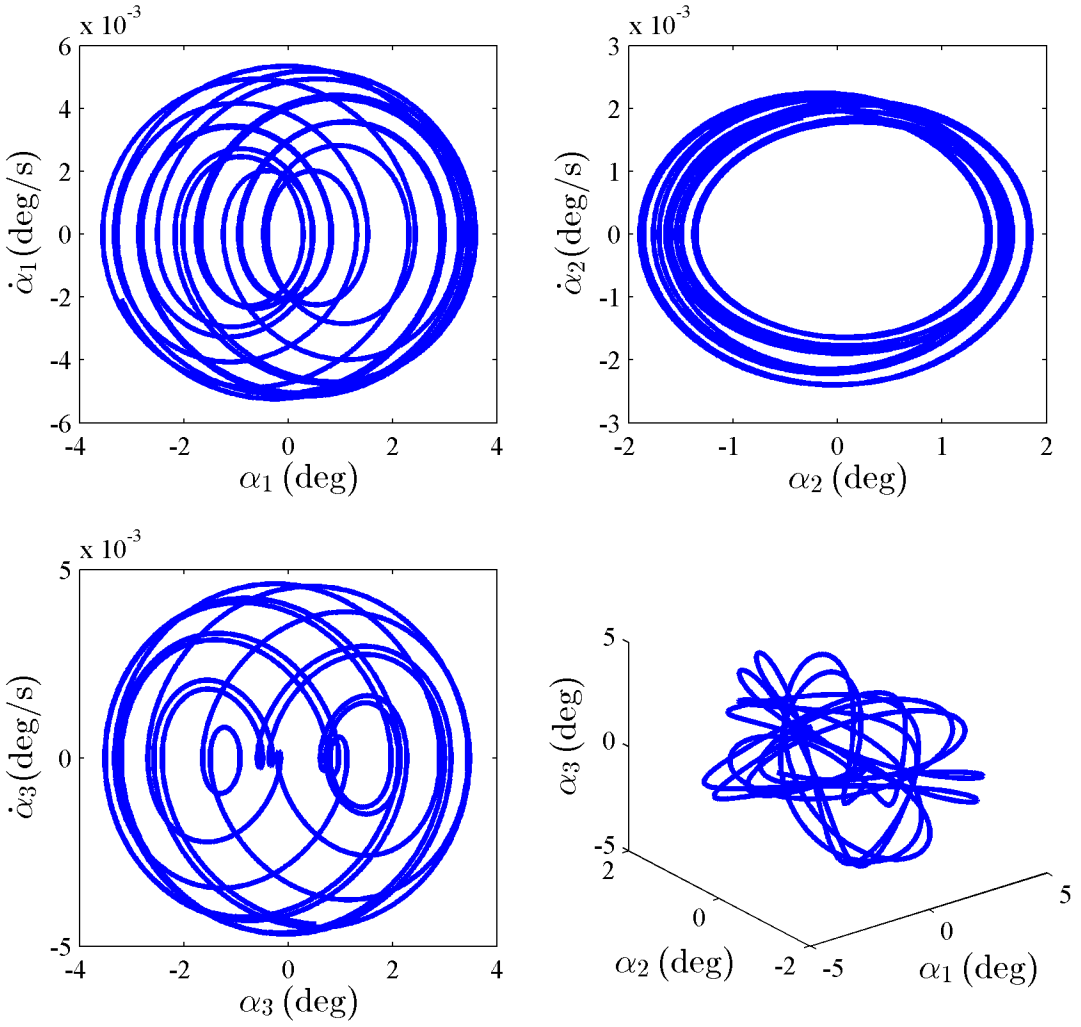

Figure 4.4: Time history of the attitude trajectory throughout the simulation in the $\alpha_1 - \dot{\alpha}_1$ phase plane (upper-left), $\alpha_2 - \dot{\alpha}_2$ phase plane (upper-right), $\alpha_3 - \dot{\alpha}_3$ phase plane (lower-left), and $\boldsymbol{\alpha}$ configuration space

for the projection of the relative momentum vector on $\vec{o}_2$, j_2, that result in stable relative equilibrium, which represents a new contribution to the literature. The concept of relative equilibrium presented in this chapter is extended in the next chapter with the introduction of constant orbital momentum equilibrium trajectories or COMETs.

Chapter 5

Constant Orbital Momentum Equilibrium Trajectories of a Gyrostat-Satellite

Chapter 4 introduced the concepts of dynamic and relative equilibrium of a gyrostat-satellite. It was shown that relative equilibrium may be thought of as a generalization of dynamic equilibrium obtained by relaxing the condition that the net external torque applied to the gyrostat-satellite is equal to zero. In this chapter, a new concept, the Constant Orbital Momentum Equilibrium Trajectory (COMET), is introduced that results from a further generalization that relaxes the condition that the gyrostat-satellite is at rest when viewed by an observer embedded in the orbital reference frame. Table 5.1 provides a comparison of some of the key characteristics of the three concepts. The purpose of this chapter is to introduce, define, and investigate the new concept of Constant Orbital Momentum Equilibrium Trajectories (COMETs).

Section 5.1 presents the derivation of the equilibrium solutions to the system angular momentum expressed in the orbital reference frame. Section 5.2 gives a mathematical definition for a

Table 5.1: High-level comparison of dynamic equilibria, relative equilibria, and COMETs

Class of Equilibrium	Dynamic	Relative	COMET
System Angular Momentum (Orbit Referenced)	Constant	Constant	Constant
Platform Angular Velocity (Orbit Referenced)	Constant	Constant	Time-Varying
Rotor Speeds (Platform Referenced)	Constant	Constant	Time-Varying
Gravitational Torque (Orbit Referenced)	Zero	Constant	Constant
Gravitational Torque (Platform Referenced)	Zero	Constant	Time-Varying

family of attitude trajectories that satisfy the equilibrium conditions presented in Section 5.1. Section 5.3 introduces a coordinate chart for COMETs and presents a method to generate a mapping from that coordinate chart to an attitude quaternion. Section 5.4 presents a method to generate visualizations of families of COMETs, and applies the method to generate multiple examples. Section 5.5 discusses the existence of critical points on COMETs, which are observable in the visualizations. Section 5.6 presents the results of two numeric simulations of a gyrostat-satellite traversing a COMET. Section 5.7 summarizes the results of the chapter and highlights the new contributions to the literature.

5.1 Orbital Momentum Equilibria

The conditions necessary for the system angular momentum of a gyrostat-satellite to remain constant when expressed in the orbital reference frame are derived in this section. Euler's second law of motion for a gyrostat-satellite is

$$\left.\frac{d}{dt}\right|_i \left(\vec{h}\right) = 3\omega_o^2 \vec{o}_3 \times \vec{I} \cdot \vec{o}_3 \tag{5.1}$$

where the right-hand side is the gravitational torque (Eq. 3.53). The first time derivative of the system angular momentum vector with respect to the inertial reference frame may be written as the sum of the first time derivative with respect to the orbital reference frame and the rate induced due to the rotation of the orbital reference frame.

$$\left.\frac{d}{dt}\right|_i \left(\vec{h}\right) = \left.\frac{d}{dt}\right|_o \left(\vec{h}\right) + \vec{\omega}_o \times \vec{h} \tag{5.2}$$

Plugging in Eqs. 5.2 into Eq. 5.1 results in

$$\left.\frac{d}{dt}\right|_o \left(\vec{h}\right) + \vec{\omega}_o \times \vec{h} = 3\omega_o^2 \vec{o}_3 \times \vec{I} \cdot \vec{o}_3 \tag{5.3}$$

The scalar equations expressed in the orbital reference frame are

$$\dot{h}_1^o - \omega_o h_3^o = -3\omega_o^2 J_{23} \tag{5.4}$$
$$\dot{h}_2^o = 3\omega_o^2 J_{13} \tag{5.5}$$
$$\dot{h}_3^o + \omega_o h_1^o = 0 \tag{5.6}$$

The "pitch" angular momentum dynamics (Eq. 5.5) are decoupled from the roll-yaw angular momentum dynamics (Eqs. 5.4 and 5.6). The pitch angular momentum is at an equilibrium if the following condition is met.

$$J_{13} = 0 \tag{5.7}$$

Equation 4.22 is the sufficient condition for an attitude to be a relative equilibrium attitude (Eq. 4.22). Equilibrium solutions to the roll-yaw angular momentum dynamics (Eqs. 5.4 and 5.6) occur when the following conditions are met.

$$h_3^o = 3\omega_o J_{23} \tag{5.8}$$
$$h_1^o = 0 \tag{5.9}$$

Equations 5.8 and 5.9 are now shown to be equivalent to conditions on the "roll" and yaw components of the relative angular momentum vector (Eqs. 4.21 and 4.23) for a gyrostat-satellite to be at a relative equilibrium. The system angular momentum is related to relative angular momentum vector through Eq. 3.35. The 1 and 3 components in the orbital reference frame of these two vectors are related by the following equations,

$$h_1^o = -\omega_o J_{12} + h_{s_1}^o \tag{5.10}$$
$$h_3^o = -\omega_o J_{23} + h_{s_3}^o \tag{5.11}$$

where it has been assumed the gyrostat-satellite is in a relative equilibrium so that Eq.4.4 is true. Applying Eqs. 5.8 and 5.9 and solving for the 1 and 3 components of the relative angular momentum vector expressed in the orbital reference frame results in

$$h_{s_3}^o = 4\omega_o J_{23} \tag{5.12}$$
$$h_{s_1}^o = \omega_o J_{12} \tag{5.13}$$

Equations 5.12 and 5.13 are equivalent to Eqs. 4.21 and 4.23. Thus, it has been verified that the conditions for a relative equilibrium are the same as those for an orbital momentum equilibrium with the addition of requiring that the gyrostat-satellite is stationary with respect to the orbital reference frame.

5.2 COMET Definition

Constant Orbital Momentum Equilibrium Trajectories (COMETs) are attitude trajectories where the system angular momentum and the gravity-gradient torque are constant (when expressed in the orbital reference frame) and balance forming a stationary solution to Euler's equation. In the previous section, it was determined that if Eq. 5.7 through Eq. 5.9 are satisfied the system angular momentum expressed in the orbital reference frame will be at equilibrium. In this section, a class of non-trivial* attitude trajectories that satisfy Eqs. 5.7 through 5.9 are determined.

The attitude of the gyrostat-satellite affects the dynamics of the system angular momentum vector expressed in the orbital frame through the 1-3 and 2-3 products of inertia expressed

* Relative equilibria are the class of "trivial" attitude trajectories that satisfy Eqs. 5.7 through 5.9.

in the orbital reference frame (J_{13} and J_{23}). From Eq. 5.8 and Eq. 5.9, it can be seen that the system angular momentum will remain at equilibrium if

$$\dot{J}_{23} = \dot{J}_{13} = 0 \tag{5.14}$$

and the initial state is an orbital momentum equilibrium. The first time derivatives of J_{23} and J_{13} are

$$\dot{J}_{23} = \frac{d}{dt}\left(\vec{o}_2 \cdot \vec{I} \cdot \vec{o}_3\right) = \dot{\vec{o}}_2 \cdot \vec{I} \cdot \vec{o}_3 + \vec{o}_2 \cdot \vec{I} \cdot \dot{\vec{o}}_3 \tag{5.15}$$

$$\dot{J}_{13} = \frac{d}{dt}\left(\vec{o}_1 \cdot \vec{I} \cdot \vec{o}_3\right) = \dot{\vec{o}}_1 \cdot \vec{I} \cdot \vec{o}_3 + \vec{o}_1 \cdot \vec{I} \cdot \dot{\vec{o}}_3 \tag{5.16}$$

The first time derivative of a basis axis of the orbital reference frame is

$$\dot{\vec{o}}_i = -\vec{\omega}_{po} \times \vec{o}_i \tag{5.17}$$

The angular velocity of the principal reference frame with respect to the orbital reference frame can be formulated as

$$\vec{\omega}_{po} = \omega_1 \vec{o}_1 + \omega_2 \vec{o}_2 + \omega_3 \vec{o}_3 \tag{5.18}$$

where ω_1, ω_2, and ω_3 are the projections $\vec{\omega}_{po}$ on the orbital reference frame basis vectors, so that

$$\boldsymbol{\omega}^o_{po} = \begin{bmatrix} \omega_1 & \omega_2 & \omega_3 \end{bmatrix}^\mathsf{T} \tag{5.19}$$

Plugging Eq. 5.18 into Eq. 5.17 results in

$$\dot{\vec{o}}_1 = \omega_2 \vec{o}_3 - \omega_3 \vec{o}_2 \tag{5.20}$$

$$\dot{\vec{o}}_2 = -\omega_1 \vec{o}_3 + \omega_3 \vec{o}_1 \tag{5.21}$$

$$\dot{\vec{o}}_3 = \omega_1 \vec{o}_2 - \omega_2 \vec{o}_1 \tag{5.22}$$

Using this result with Eqs. 5.15 and 5.16 gives

$$\begin{bmatrix} \dot{J}_{23} \\ \dot{J}_{13} \end{bmatrix} = \begin{bmatrix} J_{22} - J_{33} & -J_{12} & J_{13} \\ J_{12} & J_{33} - J_{11} & -J_{23} \end{bmatrix} \boldsymbol{\omega}^o_{po} \tag{5.23}$$

Equation 5.14 is satisfied if $\boldsymbol{\omega}^o_{po}$ is $\mathbf{0}^*$ or is contained in the null space of the coefficient matrix. The null space of the 2×3 matrix in Eq. 5.23 can be determined by calculating the cross product of the first and second rows.

$$\mathbf{v} = \begin{bmatrix} J_{12}J_{23} - J_{13}\left(J_{33} - J_{11}\right) \\ J_{23}\left(J_{22} - J_{33}\right) + J_{13}J_{12} \\ \left(J_{22} - J_{33}\right)\left(J_{33} - J_{11}\right) + J_{12}^2 \end{bmatrix} \tag{5.24}$$

* This is the trivial solution and corresponds to a relative equilibrium.

The necessary condition for the existence of a stationary solution of the pitch system angular momentum is given by Eq. 5.7. Applying this to Eq. 5.24 results in

$$\mathbf{v} = \begin{bmatrix} J_{12}J_{23} \\ J_{23}\left(J_{22}-J_{33}\right) \\ \left(J_{22}-J_{33}\right)\left(J_{33}-J_{11}\right)+J_{12}^2 \end{bmatrix} \tag{5.25}$$

The angular velocity of the principal reference frame with respect to the orbital reference frame is restricted to satisfy

$$\boldsymbol{\omega}_{po} = \sigma \mathbf{R}^{po}\mathbf{v} \tag{5.26}$$

where σ is an arbitrary, real, and scalar-valued continuous function. Therefore, any attitude trajectory that is contains a relative equilibrium attitude and whose angular velocity satisfies Eq. 5.26 is a COMET.

The set of relative equilibrium attitudes is the subset of all attitudes that result in $J_{13} = 0$. Each COMET is a subset of the set of all relative equilibrium attitudes that result in the same value of J_{23}. However, two relative equilibrium attitudes that result in the same value J_{23} do not necessarily share the same COMET. This situation occurs when all members of the set of continuous paths connecting the two relative equilibrium attitudes result in a varying value for J_{23}. The next section presents a method to determine the subset of relative equilibrium attitudes that make up an individual COMET.

5.3 Mapping of COMETs

A necessary first step to analyze COMETs is the determination of their full shape and extent within SO(3). A method to fully map a COMET is presented in this section. First, a coordinate chart for COMETs is developed. The coordinate s of the coordinate chart is defined as

$$s = \int \sigma\sqrt{\mathbf{v}^{\mathsf{T}}\mathbf{v}}dt \tag{5.27}$$

The coordinate s can be thought of as a "signed pseudo-arclength" measured along the path defined by the COMET. This is apparent when it is recognized that the absolute value of the integrand in Eq. 5.27 is equal to the magnitude of the angular velocity vector.

$$|\boldsymbol{\omega}^{po}| = \left|\sigma\sqrt{\mathbf{v}^{\mathsf{T}}\mathbf{v}}\right| \tag{5.28}$$

The first time derivative of the coordinate s is

$$\dot{s} = \sigma\sqrt{\mathbf{v}^{\mathsf{T}}\mathbf{v}} \tag{5.29}$$

The scalar function σ connects the kinematics of the principal reference frame with respect to the orbital reference frame to the time history of the coordinate s. Solving Eq. 5.29 for σ results in

$$\sigma = \frac{\dot{s}}{\sqrt{\mathbf{v}^{\mathsf{T}}\mathbf{v}}} \tag{5.30}$$

It was shown in Section 5.2 that the angular velocity of a gyrostat-satellite traversing a COMET is restricted to satisfy Eq. 5.26. Plugging Eq. 5.30 into Eq. 5.26 results in

$$\boldsymbol{\omega}^{po} = \dot{s}\frac{\mathbf{R}^{po}\mathbf{v}}{\sqrt{\mathbf{v}^{\mathsf{T}}\mathbf{v}}} \tag{5.31}$$

Equation 5.31 is a nonholonomic constraint. Numeric integration must be used to map a COMET because of the nonholonomic constraint. The attitude quaternions that make up the COMET may now be calculated by integrating the following kinematic relation.

$$\dot{\bar{\mathbf{q}}}^{po} = \frac{1}{2}\bar{\boldsymbol{\omega}}^{po} \otimes \bar{\mathbf{q}}^{po} \tag{5.32}$$

A discrete approximation of the integration of the attitude quaternion is

$$\bar{\mathbf{q}}^{po}_{k+1} = \begin{bmatrix} \frac{\mathbf{R}^{po}\mathbf{v}}{\sqrt{\mathbf{v}^{\mathsf{T}}\mathbf{v}}} \sin\left(\frac{1}{2}\Delta s\right) \\ \cos\left(\frac{1}{2}\Delta s\right) \end{bmatrix} \otimes \bar{\mathbf{q}}^{po}_{k} \tag{5.33}$$

where it is assumed that $\bar{\boldsymbol{\omega}}^{po}$ is constant over each integration step, Δs. The corresponding value of the coordinate s for each $\bar{\mathbf{q}}^{po}_{k}$ is calculated using

$$s_{k+1} = s_k + \Delta s \tag{5.34}$$

The accumulation of numerical errors is an issue that arises due to the use of numeric integration to relate the coordinate s to the attitude quaternion $\bar{\mathbf{q}}^{po}$. The result of the accumulated error is that (eventually) the attitude quaternion will drift off of the COMET being mapped. It is therefore necessary to devise a method to "correct" the propagated attitude quaternion so that errors do not accumulate. The "drift" in the propagated attitude quaternion is observable via changes in values of the 1-3 and 2-3 products of inertia expressed in the orbital reference frame (J_{13} and J_{23}). The value of J_{13} should remain zero throughout the propagation. The value of J_{23} should remain constant throughout the propagation.

An algorithm is developed that maps observed errors in the values of J_{13} and J_{23} to an attitude correction defined by the angular displacement vector ($\boldsymbol{\alpha}$). The products of inertia are calculated using

$$J_{ij} = \mathbf{o}_i^{\mathsf{T}}\mathbf{I}\mathbf{o}_j \quad \forall\, i,j \in 1,2,3 \tag{5.35}$$

Assuming the angular distance between the true value of $\bar{\mathbf{q}}^{po}$ and the propagated value of $\bar{\mathbf{q}}^{po}$ is small, the linear approximation to $\mathbf{o}_i$ determined in Chapter 4 (Eq. 4.69) may be plugged into Eq. 5.35 to give

$$\begin{aligned} J_{ij} &\approx \hat{\mathbf{o}}_i^{\mathsf{T}} \left(\mathbf{1} + \boldsymbol{\alpha}^{\times}\right) \mathbf{I} \left(\mathbf{1} - \boldsymbol{\alpha}^{\times}\right) \hat{\mathbf{o}}_j \\ &\approx \hat{\mathbf{o}}_i^{\mathsf{T}} \mathbf{I} \hat{\mathbf{o}}_j - \hat{\mathbf{o}}_i^{\mathsf{T}} \mathbf{I} \boldsymbol{\alpha}^{\times} \hat{\mathbf{o}}_j + \hat{\mathbf{o}}_i^{\mathsf{T}} \boldsymbol{\alpha}^{\times} \mathbf{I} \hat{\mathbf{o}}_j - \hat{\mathbf{o}}_i^{\mathsf{T}} \boldsymbol{\alpha}^{\times} \mathbf{I} \boldsymbol{\alpha}^{\times} \hat{\mathbf{o}}_j \\ &\approx \hat{J}_{ij} + \left(\hat{\mathbf{o}}_i^{\mathsf{T}} \mathbf{I} \hat{\mathbf{o}}_j^{\times} + \hat{\mathbf{o}}_j^{\mathsf{T}} \mathbf{I} \hat{\mathbf{o}}_i^{\times}\right) \boldsymbol{\alpha} + O(2) \end{aligned} \tag{5.36}$$

The functional relationship between the angular displacement vector and J_{13} and J_{23} is

$$J_{23} \approx \hat{J}_{23} + \left(\hat{\mathbf{o}}_2^{\mathsf{T}} \mathbf{I} \hat{\mathbf{o}}_3^{\times} + \hat{\mathbf{o}}_3^{\mathsf{T}} \mathbf{I} \hat{\mathbf{o}}_2^{\times}\right) \boldsymbol{\alpha} \tag{5.37}$$

$$J_{13} \approx \hat{J}_{13} + \left(\hat{\mathbf{o}}_1^{\mathsf{T}} \mathbf{I} \hat{\mathbf{o}}_3^{\times} + \hat{\mathbf{o}}_3^{\mathsf{T}} \mathbf{I} \hat{\mathbf{o}}_1^{\times}\right) \boldsymbol{\alpha} \tag{5.38}$$

where terms of 2nd order and higher have been approximated as zero. Rewritten in matrix form, Eqs. 5.37 and 5.38 become

$$\begin{bmatrix} J_{23} - \hat{J}_{23} \\ J_{13} - \hat{J}_{13} \end{bmatrix} \approx \begin{bmatrix} \hat{\mathbf{o}}_2^{\mathsf{T}} \mathbf{I} \hat{\mathbf{o}}_3^{\times} + \hat{\mathbf{o}}_3^{\mathsf{T}} \mathbf{I} \hat{\mathbf{o}}_2^{\times} \\ \hat{\mathbf{o}}_1^{\mathsf{T}} \mathbf{I} \hat{\mathbf{o}}_3^{\times} + \hat{\mathbf{o}}_3^{\mathsf{T}} \mathbf{I} \hat{\mathbf{o}}_1^{\times} \end{bmatrix} \boldsymbol{\alpha} \tag{5.39}$$

Solving Eq. 5.39 for the angular displacement vector $\boldsymbol{\alpha}$ results in

$$\boldsymbol{\alpha} \approx \begin{bmatrix} \hat{\mathbf{o}}_2^{\mathsf{T}} \mathbf{I} \hat{\mathbf{o}}_3^{\times} + \hat{\mathbf{o}}_3^{\mathsf{T}} \mathbf{I} \hat{\mathbf{o}}_2^{\times} \\ \hat{\mathbf{o}}_1^{\mathsf{T}} \mathbf{I} \hat{\mathbf{o}}_3^{\times} + \hat{\mathbf{o}}_3^{\mathsf{T}} \mathbf{I} \hat{\mathbf{o}}_1^{\times} \end{bmatrix}^{+} \begin{bmatrix} J_{23} - \hat{J}_{23} \\ J_{13} - \hat{J}_{13} \end{bmatrix} \tag{5.40}$$

where the $(\cdot)^{+}$ operator indicates the Moore-Penrose pseudoinverse. Equation 5.40 represents an underdetermined linear system of equations (2 equations and 3 unknowns). The use of the Moore-Penrose pseudoinverse results in the solution for $\boldsymbol{\alpha}$ being the minimum magnitude vector solution. The attitude quaternion representing the rotation from the propagated principal reference frame ($\hat{p}$) to the true principal reference frame residing on the COMET (p) may be approximated, assuming small angles, as

$$\bar{\mathbf{q}}^{p\hat{p}} \approx \frac{\begin{bmatrix} \frac{1}{2}\boldsymbol{\alpha} & 1.0 \end{bmatrix}}{\sqrt{\frac{1}{4}\boldsymbol{\alpha}^{\mathsf{T}}\boldsymbol{\alpha} + 1}} \tag{5.41}$$

An algorithm using these equations to correct the propagated attitude quaternion is presented as Algorithm 5.1. The algorithm takes an "estimated" attitude quaternion $\bar{\mathbf{q}}^{\hat{po}}$ (assumed to be close to the COMET), the J_{23} value of the COMET, and the inertia matrix of the gyrostat-satellite ($\mathbf{I}$). The algorithm returns the attitude quaternion on the COMET that is closest to the "estimated" attitude quaternion.

An algorithm that maps a COMET is presented as Algorithm 5.2. The algorithm generates a set of coordinates (s_k, $\bar{\mathbf{q}}_k^{po}$) that are (generally) evenly spaced around the full extent of the COMET. The inputs to the algorithm are an initial $\bar{\mathbf{q}}^{po}$ ($\bar{\mathbf{q}}_1^{po}$), the true value of J_{23} for

Input : $\bar{\mathbf{q}}^{\hat{p}o}$, J_{23}, $\mathbf{I}$
Output: $\bar{\mathbf{q}}^{po}$

1 $\mathbf{R}^{po} \leftarrow R\left(\bar{\mathbf{q}}^{po}\right)$;
2 $\mathbf{o}_1 \leftarrow \mathbf{R}^{po} \begin{bmatrix} 1.0 & 0.0 & 0.0 \end{bmatrix}^{\mathsf{T}}$;
3 $\mathbf{o}_2 \leftarrow \mathbf{R}^{po} \begin{bmatrix} 0.0 & 1.0 & 0.0 \end{bmatrix}^{\mathsf{T}}$;
4 $\mathbf{o}_3 \leftarrow \mathbf{R}^{po} \begin{bmatrix} 0.0 & 0.0 & 1.0 \end{bmatrix}^{\mathsf{T}}$;
5 $\hat{J}_{23} \leftarrow \mathbf{o}_2^{\mathsf{T}} \mathbf{I} \mathbf{o}_3$;
6 $\hat{J}_{13} \leftarrow \mathbf{o}_1^{\mathsf{T}} \mathbf{I} \mathbf{o}_3$;
7 $\boldsymbol{\alpha} \leftarrow \begin{bmatrix} \hat{\mathbf{o}}_2^{\mathsf{T}} \mathbf{I} \hat{\mathbf{o}}_3^{\times} + \hat{\mathbf{o}}_3^{\mathsf{T}} \mathbf{I} \hat{\mathbf{o}}_2^{\times} \\ \hat{\mathbf{o}}_1^{\mathsf{T}} \mathbf{I} \hat{\mathbf{o}}_3^{\times} + \hat{\mathbf{o}}_3^{\mathsf{T}} \mathbf{I} \hat{\mathbf{o}}_1^{\times} \end{bmatrix}^{+} \begin{bmatrix} J_{23} - \hat{J}_{23} \\ -\hat{J}_{13} \end{bmatrix}$;
8 $\bar{\mathbf{q}}^{p\hat{p}} \leftarrow \frac{\begin{bmatrix} \frac{1}{2}\boldsymbol{\alpha} & 1.0 \end{bmatrix}}{\sqrt{\frac{1}{4}\boldsymbol{\alpha}^{\mathsf{T}}\boldsymbol{\alpha}+1}}$;
9 $\bar{\mathbf{q}}^{po} \leftarrow \bar{\mathbf{q}}^{p\hat{p}} \otimes \bar{\mathbf{q}}^{\hat{p}o}$;

Algorithm 5.1: Algorithm to calculate the attitude quaternion on a COMET that is closest to a specified attitude quaternion

the COMET, the inertia matrix ($\mathbf{I}$), the step size in the coordinate s (Δs), and an iteration limit (i_{max}). The algorithm executes discrete propagation steps using Eqs. 5.33 and 5.34 and the input Δs until the propagated attitude quaternion $\bar{\mathbf{q}}_k^{po}$ is close to the initial attitude quaternion $\bar{\mathbf{q}}_1^{po}$. Algorithm 5.2 calls Algorithm 5.1 on Line 14 in order to correct for numerical errors due to the propagation performed on Line 13. The values of Δs and i_{max} must be set such that the algorithm is able to take enough discrete propagation steps to fully traverse the COMET.

Algorithm 5.2 was implemented in MATLAB®, and used to map five example COMETs. The parameters used to map the example COMETs are summarized in Table 5.2. The first three columns are the values of the parameters defining the initial attitude quaternions ($\bar{\mathbf{q}}_1^{po}$), which were calculated using Algorithm 4.1. The fourth column contains the magnitude of the propagation step Δs used, which was held constant over all COMETs mapped. The fifth column contains the "true" value of J_{23}, which is used by Algorithm 5.1 to correct for accumulated propagation errors. The inertia matrix of the gyrostat-satellite is the same for all five COMETs and is provided in Table 5.3 as the inertias for Gyrostat-Satellite I. The results of the mapping are presented in Figure 5.1. The figure shows the paths of the vector part of the attitude quaternion throughout each COMET. Each curve is color-coded based on the J_{23} value of the COMET. The colorbar on the right-hand side of the figure provides the mapping from the color to the numeric value for J_{23}. The COMETs have very different shapes and perimeters, but are all closed curves.

Input : $\bar{\mathbf{q}}_1^{po}$, J_{23}, $\mathbf{I}$, Δs, i_{max}
Output: $\bar{\mathbf{q}}_i^{po} \quad \forall \quad i \in 2, 3, ..., n$

$i \leftarrow 1$;
$s_1 \leftarrow 0.0$;
$\phi \leftarrow 0.0$;
$\Delta\phi \leftarrow 1.0$;
while $(\Delta\phi > 0.0)$ AND $(\phi_i > \Delta s)$ AND $(i \leq i_{max})$ **do**
  $i \leftarrow i + 1$;
  $s_i \leftarrow s_{i-1} + \Delta s$;
  $\mathbf{R}^{po} \leftarrow R\left(\bar{\mathbf{q}}_{i-1}^{po}\right)$;
  $\mathbf{J} \leftarrow \left(\mathbf{R}^{po}\right)^{\mathsf{T}} \mathbf{I}\mathbf{R}^{po}$;
  $\mathbf{v}^o \leftarrow \begin{bmatrix} J_{12}J_{23} \\ J_{23}\left(J_{22} - J_{33}\right) \\ \left(J_{22} - J_{33}\right)\left(J_{33} - J_{11}\right) + J_{12}^2 \end{bmatrix}$;
  $\hat{\mathbf{v}} \leftarrow \frac{1}{\sqrt{\left(\mathbf{v}^o\right)^{\mathsf{T}}\mathbf{v}^o}}\mathbf{R}^{po}\mathbf{v}^o$;
  $\Delta\bar{\mathbf{q}}_i \leftarrow \begin{bmatrix} \hat{\mathbf{v}}\sin\left(\frac{1}{2}\Delta s\right) \\ \cos\left(\frac{1}{2}\Delta s\right) \end{bmatrix}$;
  $\bar{\mathbf{q}}_i^{po} \leftarrow \Delta\bar{\mathbf{q}}_i \otimes \bar{\mathbf{q}}_{i-1}^{po}$;
  $\bar{\mathbf{q}}_i^{po} \leftarrow$ Algorithm 5.1 $\left(\bar{\mathbf{q}}_i^{po}, \mathbf{I}, J_{23}\right)$;
  $\bar{\mathbf{q}}^{p_i|p_1} \leftarrow \bar{\mathbf{q}}_i^{po} \otimes \left(\bar{\mathbf{q}}_1^{po}\right)$;
  $\phi_i \leftarrow 2\arcsin\left(\left(\mathbf{q}^{p_i|p_1}\right)^{\mathsf{T}}\mathbf{q}^{p_i|p_1}\right)$;
  $\Delta\phi \leftarrow \phi_i - \phi_{i-1}$;
end

Algorithm 5.2: Algorithm to generate a map of the COMET on which $\bar{\mathbf{q}}_1^{po}$ resides

Table 5.2: Parameters used to map five example COMETs

θ_1	θ_2	θ_3	Δs	J_{23}
-10.0°	-10.0°	1.0	0.1°	-5.3637 kg-m^2
-12.7°	-12.7°	1.0	0.1°	-6.6499 kg-m^2
-15.0°	-15.0°	1.0	0.1°	-7.7037 kg-m^2
-15.5°	-15.5°	1.0	0.1°	-7.9183 kg-m^2
-20.0°	-20.0°	1.0	0.1°	-9.6627 kg-m^2
-30.0°	-30.0°	1.0	0.1°	-12.1456 kg-m^2

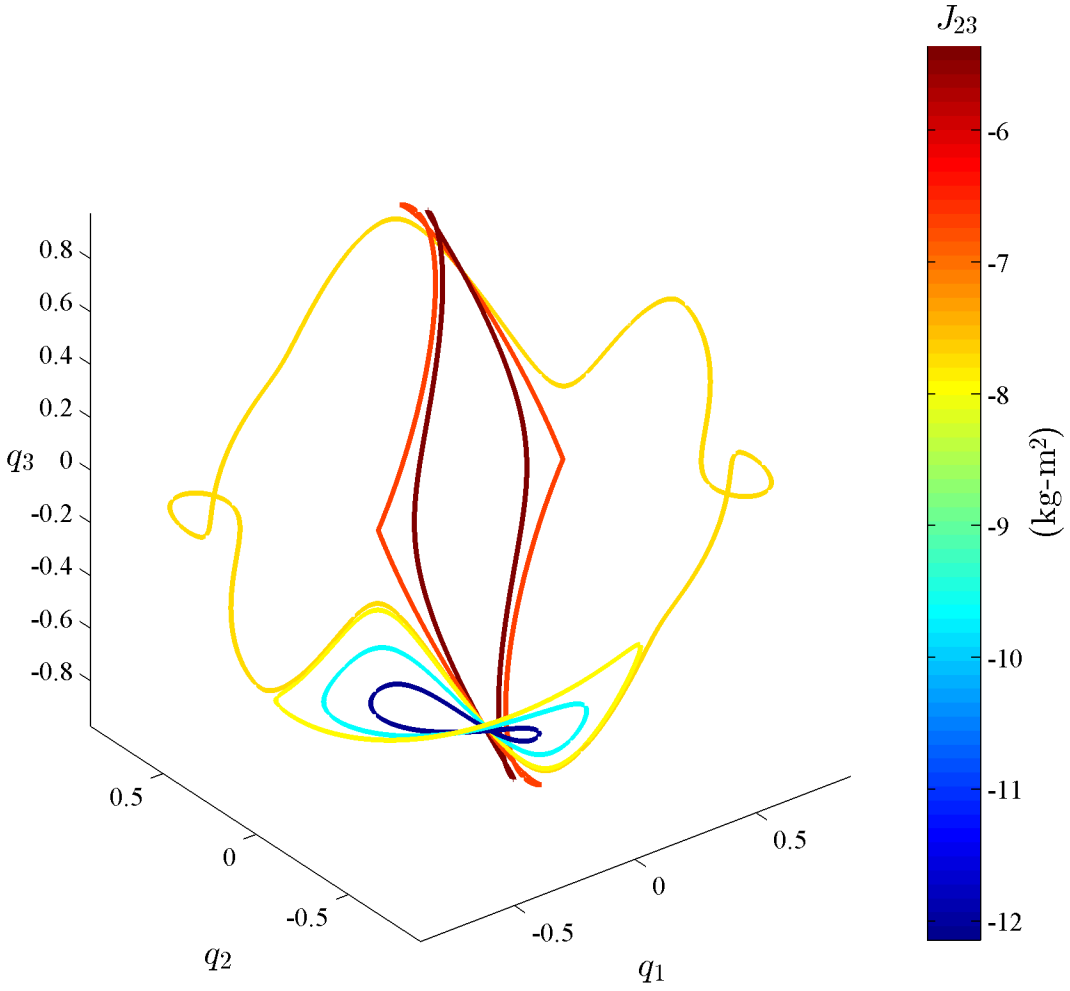

Figure 5.1: Paths in the configuration space of the vector part of the attitude quaternion ($\mathbf{q}^{po}$) of several different COMETs

Table 5.3: Principal moments of inertia of example gyrostat-satellites

Moment of Inertia	Gyrostat-Satellite I	Gyrostat-Satellite II
I_1	96.2	80.0
I_2	80.6	70.0
I_3	67.3	20.0

5.4 Visualizations of Families of COMETs

The purpose of this section is to develop visualizations of families of COMETs to facilitate qualitative investigation of the characteristics of COMETs. The paths of the orbital basis vectors on the unit sphere fixed in the principal reference frame and the paths of the principal basis vectors on the unit sphere fixed in the orbital reference frame are used to visualize families of COMETs.

Relative equilibrium attitudes residing on the same COMET will all have $J_{13} = 0$ and the same value for J_{23}. In general, for a given direction of a basis vector there are a small number ($\leq$4) of attitudes that meet the condition $J_{13} = 0$. Therefore, level curves of the values of J_{23} over all possible directions of each basis vector (principal and orbital) represent the paths of the basis vectors of a gyrostat-satellite traversing a COMET.

In Section 4.4, equations for calculating the relative equilibrium attitudes for specified directions of each orbital or principal basis vector were developed. For each possible direction of a basis vector, the equations from Section 4.4 are used to determine all of the admissible relative equilibrium attitudes. The value of J_{23} for each admissible relative equilibrium attitude is calculated. Pseudo-color plots of J_{23} over the azimuth and elevation of each direction of a basis vector are then generated. A contour plot showing level curves of J_{23} in the azimuth-elevation plane are overlaid onto the pseudo-color plots. Continuous portions of the level curves represent the paths of the basis vectors while the gyrostat-satellite is traversing a COMET. Visualizations are developed for two example gyrostat-satellites. Table 5.3 summarizes the two sets of principal moments of inertia investigated.

Section 5.4.1 presents and discusses figures showing the paths of the orbital basis vectors on a unit sphere fixed in the principal reference frame. Section 5.4.2 presents and discusses figures showing the paths of the principal basis vectors on a unit sphere fixed in the orbital reference frame.

5.4.1 Orbital Reference Frame Basis Vectors

Visualizations of the paths of the orbital basis vectors for a gyrostat-satellite traversing a COMET are presented in the following sections. In Section 4.4.1, it was determined that at

least two relative equilibrium attitudes could be determined given any direction of $\vec{o}_1$, $\vec{o}_2$, or $\vec{o}_3$. The following three sections present the results for $\vec{o}_1$, $\vec{o}_2$, and $\vec{o}_3$. Each section presents the algorithms used to calculate the J_{23} values and example figures using the moments of inertia of the gyrostat-satellites provided in Table 5.3.

Example Paths of $\vec{o}_1$ on COMETs

Algorithm 5.3 calculates the value of J_{23} given the direction of $\vec{o}_1$ expressed in the principal reference frame. The direction of $\vec{o}_1$ is parameterized as an azimuth and elevation angle. As determined in Section 4.4.1, there are two relative equilibrium attitudes for each direction of $\vec{o}_1$. This is accounted for on Line 3 of Algorithm 5.3 with the $\pm$ in the calculation of $\mathbf{o}_3$. However, the selection of the sign in that equation does not affect the value of J_{23} that is calculated. Both relative equilibrium attitudes have the same value of J_{23}.

Figures 5.2 and 5.3 are pseudo-color plots of the values of J_{23} for each direction of $\vec{o}_1$ on the unit sphere embedded in the principal reference frame for Gyrostat-Satelite I and Gyrostat-Satellite II, respectively. The azimuth and elevation angles are the abscissa and ordinate of the plots, respectively. The value of J_{23} for a given azimuth and elevation angle is indicated by the color at those coordinates on the plot. A colorbar is included on the right-hand side of the figure to indicate the mapping from color to numeric value. Black curves are overlaid on the plots to indicate level-curves of constant J_{23}. The black curves represent a discrete sub-sample of the continuous set of COMETs.

Figures 5.2 and 5.3 have "convergent points" that occur when $\alpha, \epsilon = k\frac{\pi}{2}$ for $k \in \mathbf{Z}$. At these values, $\vec{o}_1$ is aligned with one of the principal axes of the inertia matrix. This results in a continuum of admissible relative equilibrium attitudes that differ by rotations about $\vec{o}_1$. Algorithm 5.3 returns a value of zero for J_{23} in these cases, which represents only one of the continuum of possible values. Because of this, the figure depicts multiple level curves representing different values of J_{23} converging at these points.

Example Paths of $\vec{o}_2$ on COMETs

Algorithm 5.4 calculates the value of J_{23} given the direction of $\vec{o}_2$ expressed in the principal reference frame. The direction of $\vec{o}_2$ is parameterized as an azimuth and elevation angle. As determined in Section 4.4.1, there are four relative equilibrium attitudes available for each direction of $\vec{o}_2$. This is accounted for using the input k to select between the four available relative equilibrium attitudes. The selection of the k affects the value of J_{23} that is calculated. Each possible relative equilibrium attitude has a distinct value of J_{23}. The relative equilibrium attitudes separated by 180^o ($k \in 0, 2$ and $k \in 1, 3$) have the same absolute value but opposite signs.

Figures 5.4 and 5.5 are pseudo-color plots of the absolute values of J_{23} for each direction

Input : α, ϵ, $\mathbf{I}$
Output: J_{23}

$\mathbf{o}_1 \leftarrow \begin{bmatrix} \cos(\epsilon)\cos(\alpha) \\ \cos(\epsilon)\sin(\alpha) \\ \sin(\epsilon) \end{bmatrix}$;
if $\|\mathbf{o}_1^{\times}\mathbf{I}\mathbf{o}_1\| \neq 0$ **then**
  $\mathbf{o}_3 \leftarrow \pm\frac{\mathbf{o}_1^{\times}\mathbf{I}\mathbf{o}_1}{|\mathbf{o}_1^{\times}\mathbf{I}\mathbf{o}_1|}$;
  $\mathbf{o}_2 \leftarrow \mathbf{o}_3^{\times}\mathbf{o}_1$;
  $J_{23} = \mathbf{o}_2^{\mathsf{T}}\mathbf{I}\mathbf{o}_3$;
else
  $J_{23} = 0$;
end

Algorithm 5.3: Algorithm to calculate the equilibrium value of J_{23} given the azimuth α and elevation ϵ of $\vec{o}_1$ in the principal reference frame

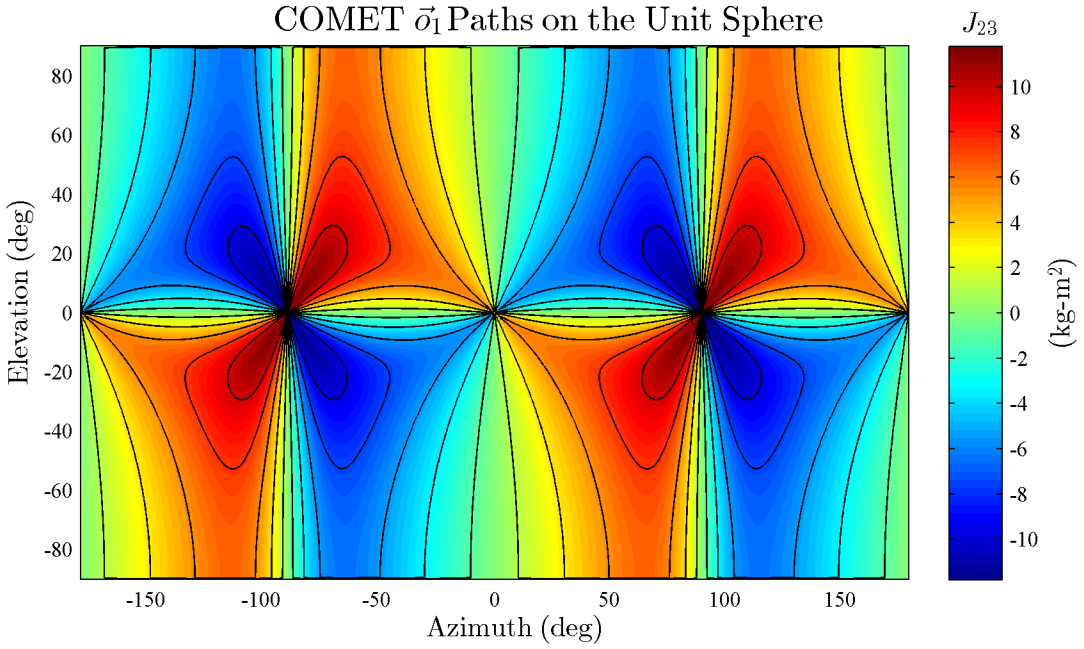

Figure 5.2: The pseudo-color plot for Gyrostat-Satellite I of the values of J_{23} for each direction of $\vec{o}_1$ expressed in the principal reference frame with level curves overlaid indicating constant values of J_{23} and COMETs

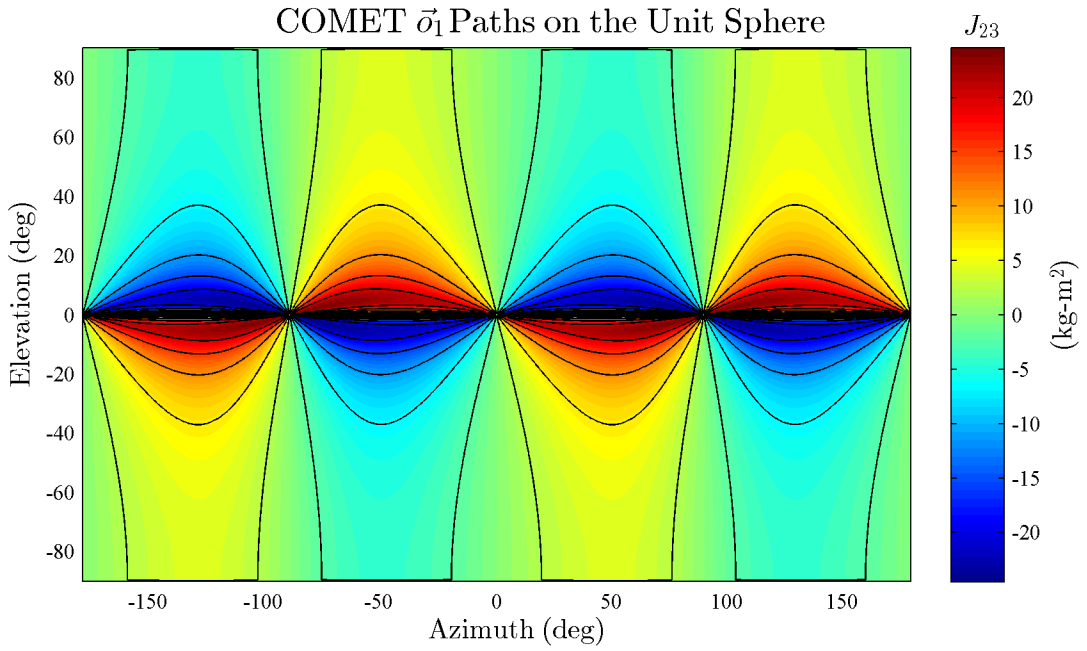

Figure 5.3: The pseudo-color plot for Gyrostat-Satellite II of the values of J_{23} for each direction of $\vec{o}_1$ expressed in the principal reference frame with level curves overlaid indicating constant values of J_{23} and COMETs

of $\vec{o}_2$ on the unit sphere embedded in the principal reference frame for Gyrostat-Satelite I. Figures 5.7 and 5.8 are pseudo-color plots of the absolute values of J_{23} for each direction of $\vec{o}_2$ on the unit sphere embedded in the principal reference frame for Gyrostat-Satelite II.

The existence of four relative equilibrium attitudes for each direction of $\vec{o}_2$ complicates the interpretation of the figures. The figures show evenly-spaced "convergence points" of the paths of $\vec{o}_2$. The "convergence points" occur at $\alpha = k\pi$ for $k \in \mathbf{Z}$ and $\epsilon \approx \pm 42.7°$ for Gyrostat-Satellite I and $\epsilon \approx \pm 65.7°$ for Gyrostat-Satellite II. These points represent "switch" points for the value of the parameter k of the relative equilibrium attitudes on a particular COMET. Several COMETs that pass near the $\alpha = 0°$, $\epsilon = 42.7°$ "convergence point" for Gyrostat-Satellite I are mapped using Algorithm 5.2 to verify this assertion. The parameters used to map the the COMETs are summarized in Table 5.4. The first three columns are the values of parameters defining the initial attitude quaternions ($\bar{\mathbf{q}}_1^{po}$), which were calculated using Algorithm 5.4. The fourth column contains the magnitude of the propagation step Δs used, which was held constant over all COMETs mapped. The fifth column contains the value of J_{23} for the COMET. Figure 5.6 is a plot of the paths of $\vec{o}_2$ in the α-ϵ plane of the mapped COMETs. The plot clearly shows that the paths are combinations of the level curves from the figures generated using $k \in 0, 2$ and $k \in 1, 3$, and that the "switch" point is indeed the "convergence" point.

The figures show that local extrema and saddle points of the absolute value of J_{23} occur when

Table 5.4: Parameters used to map four COMETs that pass near a "convergence" point

α	ϵ	k	Δs	J_{23}
0.0°	41.0°	0	0.1°	-14.3094 kg-m^2
1.0°	41.0°	0	0.1°	-13.9954 kg-m^2
5.0°	41.0°	0	0.1°	-11.8379 kg-m^2
10.0°	41.0°	0	0.1°	-10.6814 kg-m^2

$\vec{o}_2$ bisects the angle between two principal axes. These "critical points" represent either a COMET with an isolated $\vec{o}_2$ direction (where the path of $\vec{o}_2$ collapses to a single point) or a furcation in the available paths of $\vec{o}_2$ while traveling a COMET. These "critical points" are investigated in Section 5.5.

Example Paths of $\vec{o}_3$ on COMETs

Algorithm 5.5 calculates the value of J_{23} given the direction of $\vec{o}_3$ expressed in the principal reference frame. The direction of $\vec{o}_3$ is parameterized as an azimuth and elevation angle. As determined in Section 4.4.1, there are two relative equilibrium attitudes for each direction of $\vec{o}_3$. This is accounted for on Line 3 of Algorithm 5.5 with the $\pm$ in the calculation of $\mathbf{o}_1$. The selection of the sign in that equation determines the sign of J_{23} but does not affect the absolute value of J_{23} that is calculated.

Figures 5.9 and 5.10 are pseudo-color plots of the absolute values of J_{23} for each direction of $\vec{o}_3$ on the unit sphere embedded in the principal reference frame for Gyrostat-Satelite I and II. Figures 5.9 and 5.10 show concentric paths about a number of points in the α-ϵ plane. At points where $\alpha, \epsilon = k\frac{\pi}{2}$ for $k \in \mathbf{Z}$, the absolute value of J_{23} is zero. At these points, $\vec{o}_3$ is aligned with a principal axis of the inertia matrix, which results in a continuum of admitted relative equilibrium attitudes that differ by rotations about $\vec{o}_3$. All of the relative equilibrium attitudes in the continuum result in $J_{23} = 0$, and are therefore also dynamic equilibrium attitudes.

The figures show that local extrema and saddle points of the absolute value of J_{23} occur when $\vec{o}_3$ bisects the angle between two principal axes. Global maxima are reached when $\vec{o}_3$ bisects the angle between major and minor principal axes. These "critical points" represent either a COMET with an isolated $\vec{o}_3$ direction (where the path of $\vec{o}_3$ collapses to a single point) or a furcation in the available paths of $\vec{o}_3$ while traveling a COMET. These "critical points" are investigated in Section 5.5.

Input : α, ϵ, $\mathbf{I}$, k
Output: J_{23}

$\mathbf{o}_2 \leftarrow \begin{bmatrix} \cos(\epsilon)\cos(\alpha) \\ \cos(\epsilon)\sin(\alpha) \\ \sin(\epsilon) \end{bmatrix}$;
$\mathbf{v} \leftarrow \mathbf{0}$;
if $o_{21} < o_{22}, o_{23}$ **then**
  $v_1 \leftarrow 1$;
else
  if $o_{22} < o_{21}, o_{23}$ **then**
    $v_2 \leftarrow 1$;
  else
    if $o_{23} < o_{21}, o_{22}$ **then**
      $v_3 \leftarrow 1$;
    else
    end
  end
end
$\mathbf{t}_1 \leftarrow \frac{\mathbf{v}^\times \mathbf{o}_2}{|\mathbf{v}^\times \mathbf{o}_2|}$;
$\mathbf{t}_3 \leftarrow \mathbf{t}_1^\times \mathbf{o}_2$;
$J_{13}^t \leftarrow \mathbf{t}_1^\mathsf{T} \mathbf{I} \mathbf{t}_3$;
$J_{11}^t \leftarrow \mathbf{t}_1^\mathsf{T} \mathbf{I} \mathbf{t}_1$;
$J_{33}^t \leftarrow \mathbf{t}_3^\mathsf{T} \mathbf{I} \mathbf{t}_3$;
$\theta \leftarrow \frac{1}{2} \arctan\left(\frac{2J_{13}^t}{J_{11}^t - J_{33}^t}\right) + k\frac{\pi}{2}$;
$\mathbf{o}_1 \leftarrow \cos(\theta)\,\mathbf{t}_1 + \sin(\theta)\,\mathbf{t}_3$;
$\mathbf{o}_3 \leftarrow \mathbf{o}_1^\times \mathbf{o}_2$;
$J_{23} \leftarrow \mathbf{o}_2^\mathsf{T} \mathbf{I} \mathbf{o}_3$;

Algorithm 5.4: Algorithm to calculate the equilibrium value of J_{23} given the azimuth α and elevation ϵ of $\vec{o}_2$ in the principal reference frame and the value k selecting one of the (up to) four equilibrium attitudes

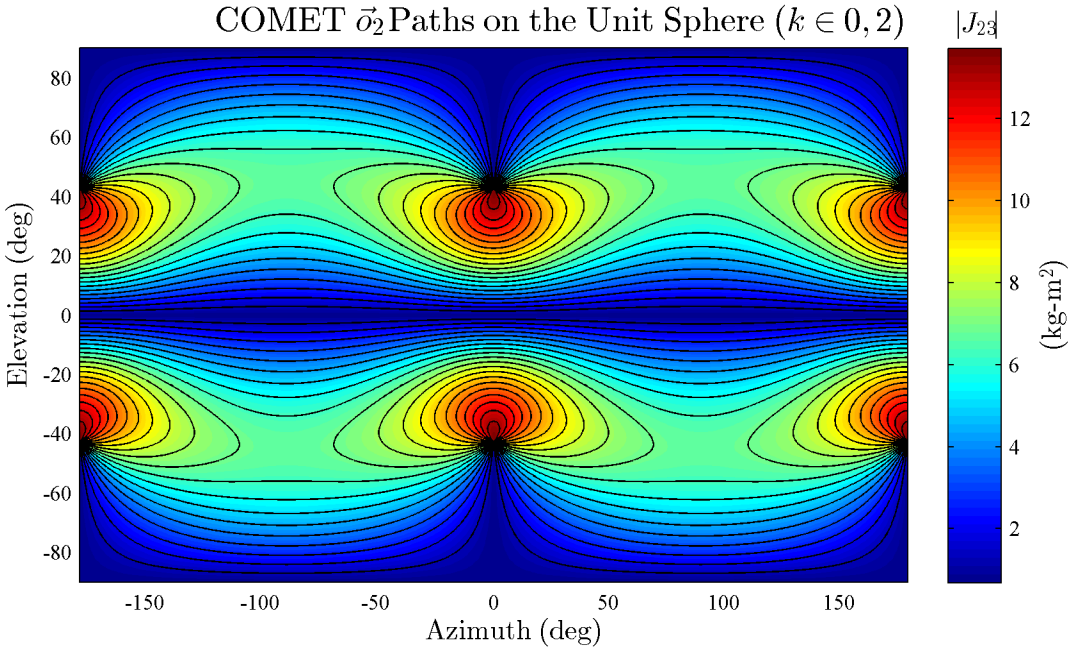

Figure 5.4: The pseudo-color plot for Gyrostat-Satellite I of the absolute values of J_{23} for each direction of $\vec{o}_2$ and $k \in 0, 2$ expressed in the principal reference frame with level curves overlaid indicating constant values of J_{23} and COMETs

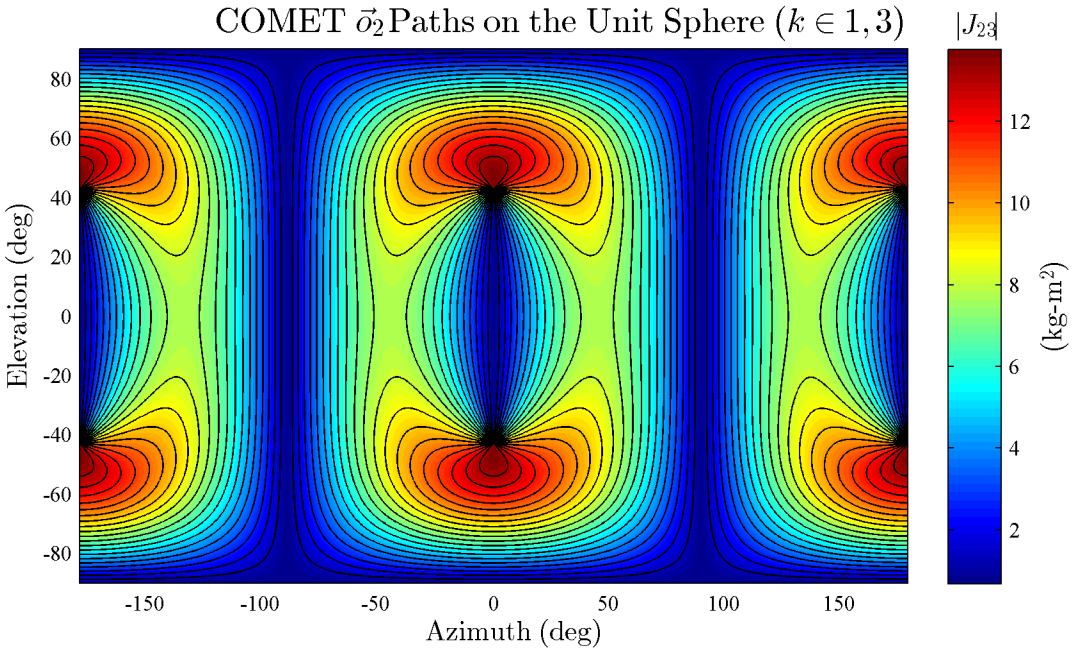

Figure 5.5: The pseudo-color plot for Gyrostat-Satellite I of the absolute values of J_{23} for each direction of $\vec{o}_2$ and $k \in 1, 3$ expressed in the principal reference frame with level curves overlaid indicating constant values of J_{23} and COMETs

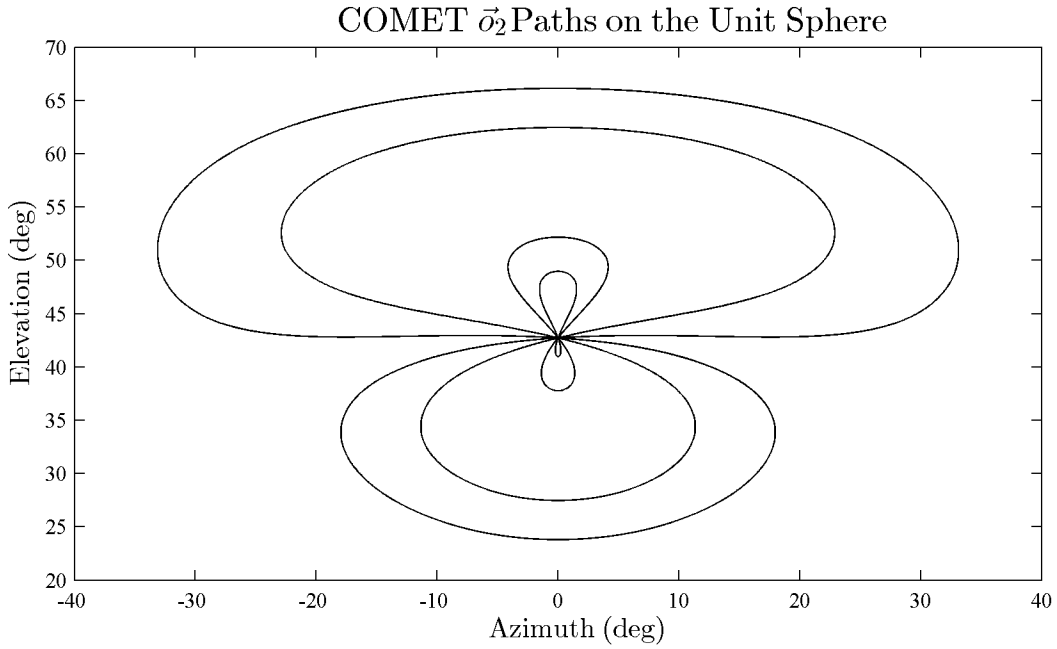

Figure 5.6: A plot for Gyrostat-Satellite I of the paths of $\vec{o}_2$ for multiple COMETs that pass near the "convergence point" in the α-ϵ plane

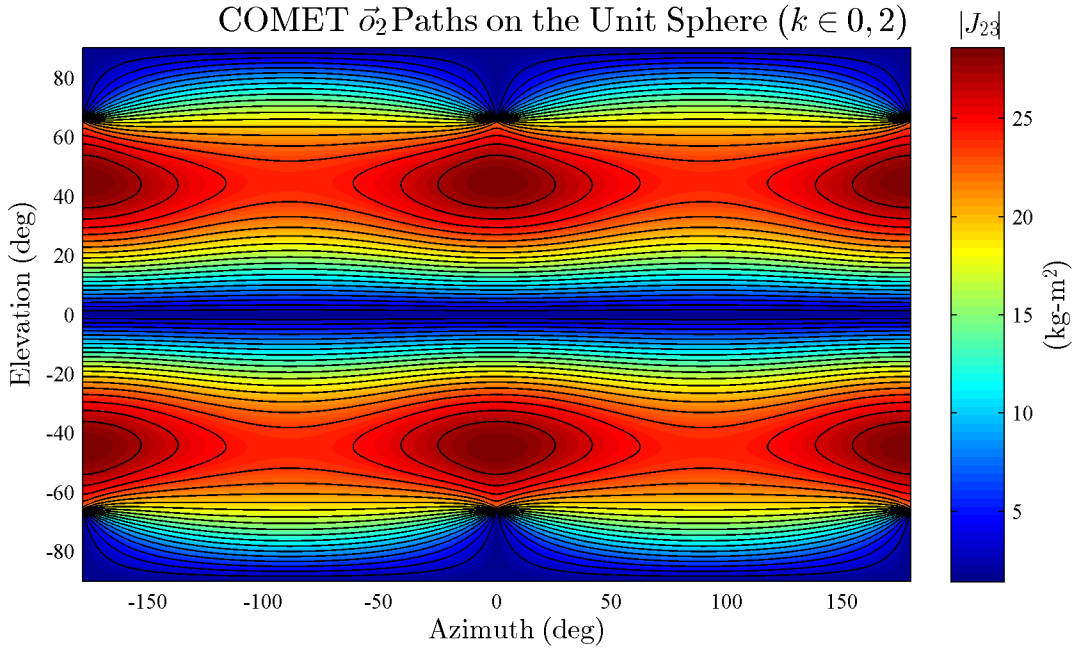

Figure 5.7: The pseudo-color plot for Gyrostat-Satellite II of the absolute values of J_{23} for each direction of $\vec{o}_2$ and $k \in 0, 2$ expressed in the principal reference frame with level curves overlaid indicating constant values of J_{23} and COMETs

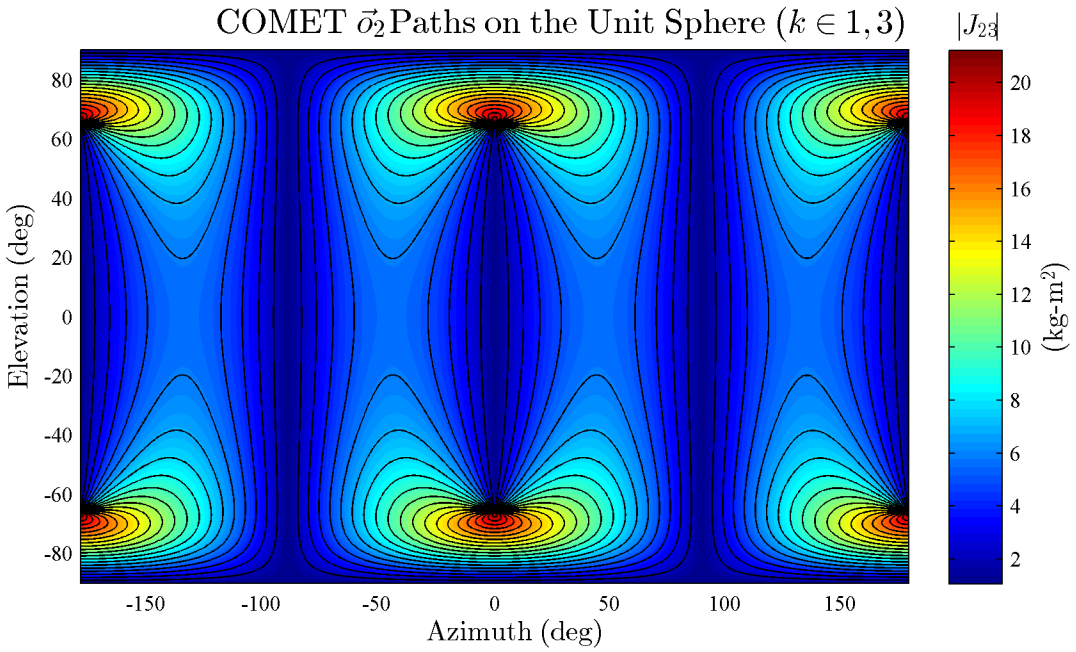

Figure 5.8: The pseudo-color plot for Gyrostat-Satellite II of the absolute values of J_{23} for each direction of $\vec{o}_2$ and $k \in 1,3$ expressed in the principal reference frame with level curves overlaid indicating constant values of J_{23} and COMETs

Input : α, ϵ, $\mathbf{I}$, $\pm$
Output: J_{23}

$\mathbf{o}_3 \leftarrow \begin{bmatrix} \cos(\epsilon)\cos(\alpha) \\ \cos(\epsilon)\sin(\alpha) \\ \sin(\epsilon) \end{bmatrix}$;
if $\|\mathbf{o}_3^{\times}\mathbf{I}\mathbf{o}_3\| \neq 0$ **then**
  $\mathbf{o}_1 \leftarrow \pm\frac{\mathbf{o}_3^{\times}\mathbf{I}\mathbf{o}_3}{|\mathbf{o}_3^{\times}\mathbf{I}\mathbf{o}_3|}$;
  $\mathbf{o}_2 \leftarrow \mathbf{o}_3^{\times}\mathbf{o}_1$;
  $J_{23} \leftarrow \mathbf{o}_2^{\mathsf{T}}\mathbf{I}\mathbf{o}_3$;
else
  $J_{23} \leftarrow 0$;
end

Algorithm 5.5: Algorithm to calculate the equilibrium value of J_{23} given the azimuth α and elevation ϵ of $\vec{o}_3$ in the principal reference frame and sign selecting the direction of $\vec{o}_1$

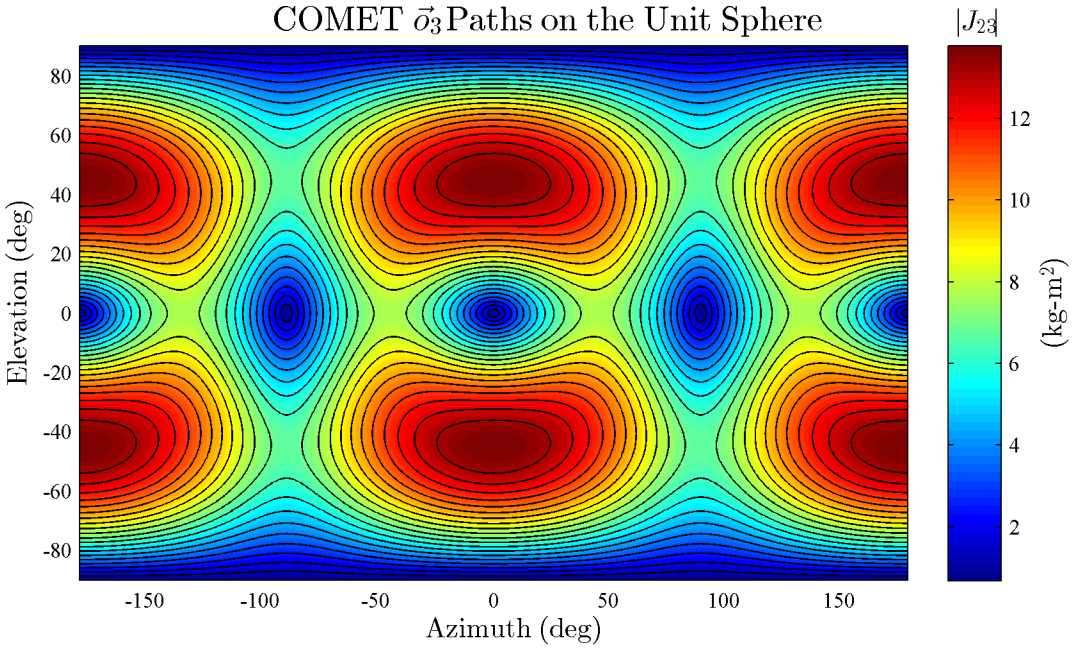

Figure 5.9: The pseudo-color plot for Gyrostat-Satellite I of the absolute values of J_{23} for each direction of $\vec{o}_3$ expressed in the principal reference frame with level curves overlaid indicating constant values of J_{23} and COMETs

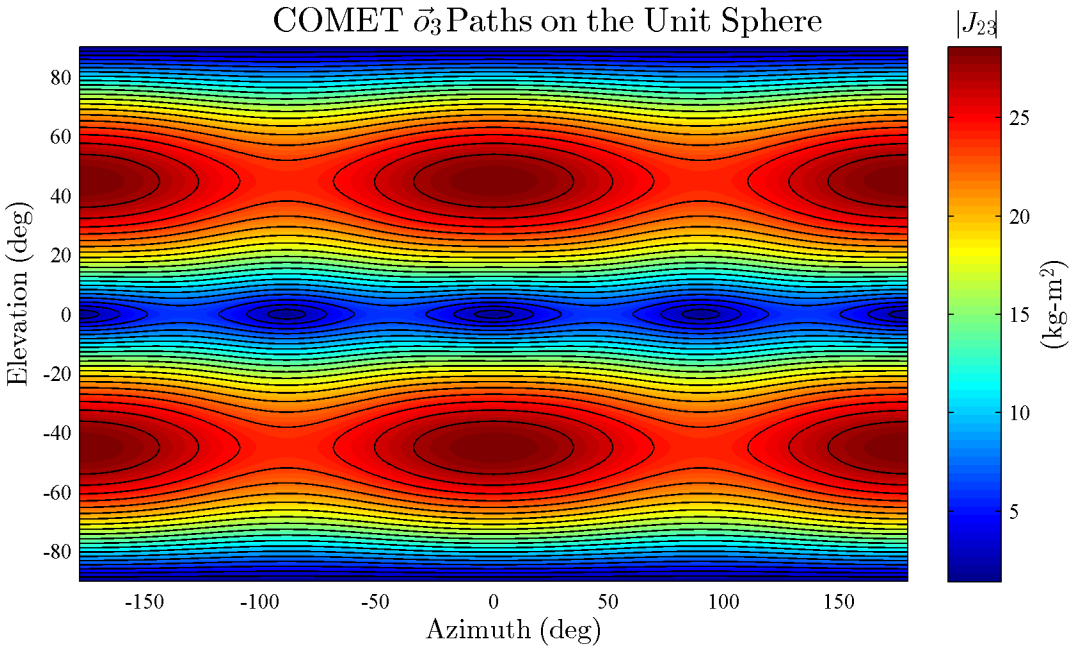

Figure 5.10: The pseudo-color plot for Gyrostat-Satellite II of the absolute values of J_{23} for each direction of $\vec{o}_3$ expressed in the principal reference frame with level curves overlaid indicating constant values of J_{23} and COMETs

5.4.2 Principal Reference Frame Basis Vectors

Visualizations of the paths of the principal basis vectors for a gyrostat-satellite traversing a COMET are presented in this section. Algorithm 5.6 calculates the value of J_{23} given the direction of $\vec{p}_i$ expressed in the orbital reference frame. The direction of $\vec{p}_i$ is parameterized as an azimuth and elevation angle. As determined in Section 4.4.2, there are two relative equilibrium attitudes for each direction of $\vec{p}_i$, if the following inequality is satisfied,

$$|\beta\gamma| \leq 1 \tag{5.42}$$

where β and γ are defined by Eqs. 4.57 and 4.58, respectively. This is accounted for on Line 3 of Algorithm 5.6 with the flag f, which is used to determine how to calculate θ. The selection of the flag f does (in general) affect the value of J_{23} that is calculated.

Figures 5.11 through 5.22 are pseudo-color plots of the values of J_{23} for each allowable direction of $\vec{p}_i$ on the unit sphere embedded in the orbital reference frame for Gyrostat-Satellite I and Gyrostat-Satellite II. The first set of figures (Figures 5.11 through 5.16) show the results for Gyrostat-Satellite I; and, the second set of figures (Figures 5.17 through 5.22) show the results for Gyrostat-Satellite II. Each set consists of two figures for each principal reference frame basis axis for a total of six figures. The first figure for each basis axis shows the results when the value of the flag f is 0, and the second figure shows the results when the value of the flag f is 1. The "white-space" in each figure represents directions of $\vec{p}_i$ that do not admit a relative equilibrium attitude.

In Section 4.4.2, an investigation into the principal basis vector directions that admit relative equilibrium attitudes was presented. The results of that investigation were summarized in Figure 4.1, which illustrated the admissible regions based on the value of the parameter β. The outlines of the "filled-in" regions shown in Figures 5.11 through 5.22 match those results. For both example gyrostat-satellites, $\vec{p}_2$ is aligned with an intermediate axis of inertia. The figures showing the results for $\vec{p}_2$ also match the finding determined in Section 4.4.2 that all directions of the intermediate axis of inertia admit relative equilibrium attitudes. As with the results for the orbital basis vectors (Section 5.4.1), the figures show local extrema and saddle points that occur when the principal basis vector bisects the angle between the $\vec{o}_2$ and $\vec{o}_3$ axes. These "critical points" represent either a COMET with an isolated $\vec{p}_i$ direction (where the path of $\vec{p}_i$ collapses to a single point) or a furcation in the available paths of $\vec{p}_i$ while traveling a COMET. These "critical points" are investigated in Section 5.5.

5.5 Critical Points on COMETs

The visualizations presented in Section 5.4 showed that critical points exist on a small subset of COMETs. The critical points either represent isolated relative equilibrium attitudes or points of furcation of the COMET. The critical points occurred at local extrema and saddle points of J_{23}. These critical points are investigated in this section.

Input : α, ϵ, $\mathbf{I}$, f
Output: J_{23}

$\mathbf{p}_i \leftarrow \begin{bmatrix} \cos(\epsilon)\cos(\alpha) \\ \cos(\epsilon)\sin(\alpha) \\ \sin(\epsilon) \end{bmatrix}$;
$\mathbf{v} \leftarrow \mathbf{0}$;
if $p_{i1} < p_{i2}, p_{i3}$ **then**
  $v_1 \leftarrow 1$;
end
if $p_{i2} < p_{i1}, p_{i3}$ **then**
  $v_2 \leftarrow 1$;
end
if $p_{i3} < p_{i1}, p_{i2}$ **then**
  $v_3 \leftarrow 1$;
end
$\mathbf{t}_j \leftarrow \frac{\mathbf{v}^\times \mathbf{p}_j}{|\mathbf{v}^\times \mathbf{p}_j|}$;
$\mathbf{t}_k \leftarrow \mathbf{p}_i^\times \mathbf{t}_j$;
$a \leftarrow t_{j1}t_{33} + t_{j3}t_{k1}$;
$b \leftarrow t_{j1}t_{23} - t_{k1}t_{k3}$;
$c \leftarrow -2\frac{I_1 - \frac{1}{2}(I_i + I_k)}{|I_j - I_k|}\frac{p_{i1}}{\sqrt{1-p_{i1}^2}}\frac{p_{i3}}{\sqrt{1-p_{i3}^2}}$;
if $\|c\| \leq 1$ **then**
  if $(I_j - I_k)\, a \geq 0$ **then**
    $\phi \leftarrow \arcsin\left(\frac{b}{\sqrt{a^2+b^2}}\right)$;
  else
    $\phi \leftarrow \pi - \arcsin\left(\frac{b}{\sqrt{a^2+b^2}}\right)$;
  end
  if $f == 0$ **then**
    $\theta \leftarrow \frac{1}{2}(\arcsin(c) - \phi)$;
  else
    $\theta \leftarrow \frac{1}{2}(\pi - \arcsin(c) - \phi)$;
  end
  $\mathbf{p}_j \leftarrow \cos(\theta)\mathbf{t}_j + \sin(\theta)\mathbf{t}_k$;
  $\mathbf{p}_k \leftarrow -\sin(\theta)\mathbf{t}_j + \cos(\theta)\mathbf{t}_k$;
  $\mathbf{o}_2 \leftarrow \begin{bmatrix} p_{i2} & t_{j2} & t_{k2} \end{bmatrix}^\mathsf{T}$;
  $\mathbf{o}_3 \leftarrow \begin{bmatrix} p_{i3} & t_{j3} & t_{k3} \end{bmatrix}^\mathsf{T}$;
  $J_{23} \leftarrow \mathbf{o}_2^\mathsf{T}\mathbf{I}\mathbf{o}_3$;
end

Algorithm 5.6: Algorithm to calculate the equilibrium value of J_{23} given the azimuth α and elevation ϵ of $\vec{p}_i$ in the orbital reference frame and flag f selecting the solution of θ.

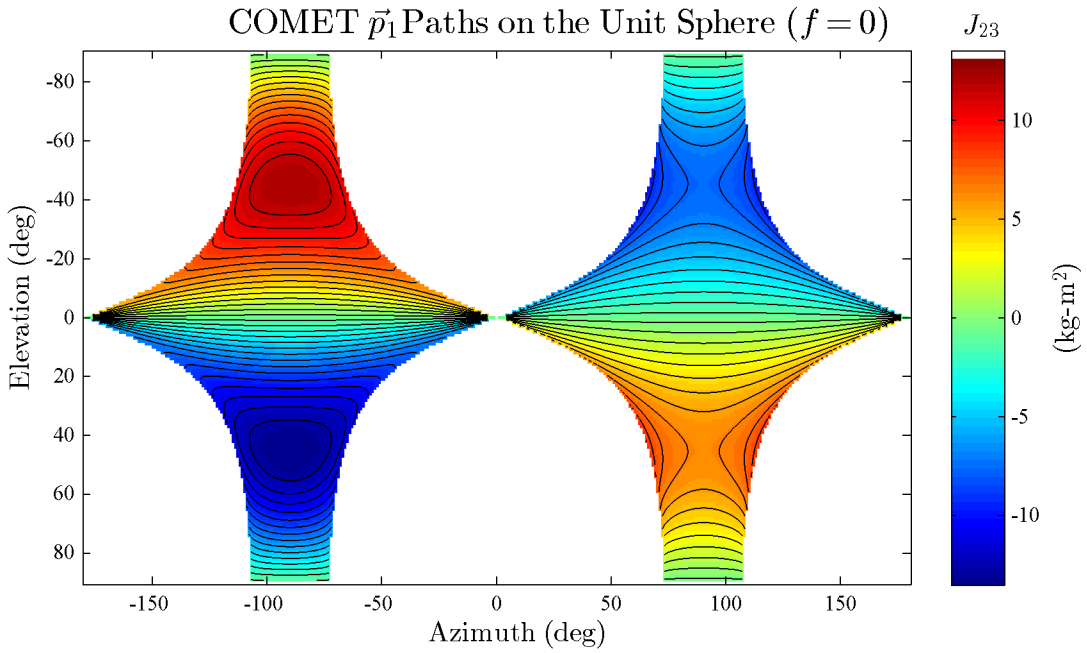

Figure 5.11: The pseudo-color plot for Gyrostat-Satellite I of the values of J_{23} for the allowable directions of $\vec{p}_1$ and $f = 0$ expressed in the orbital reference frame with level curves overlaid indicating constant values of J_{23} and COMETs

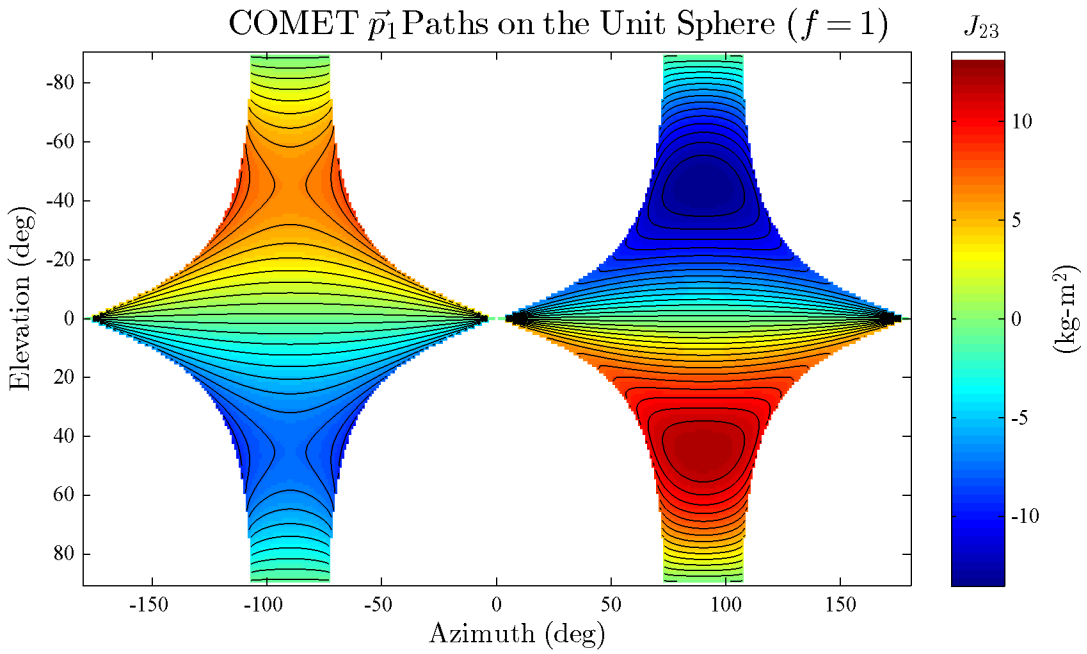

Figure 5.12: The pseudo-color plot for Gyrostat-Satellite I of the values of J_{23} for the allowable directions of $\vec{p}_1$ and $f = 1$ expressed in the orbital reference frame with level curves overlaid indicating constant values of J_{23} and COMETs

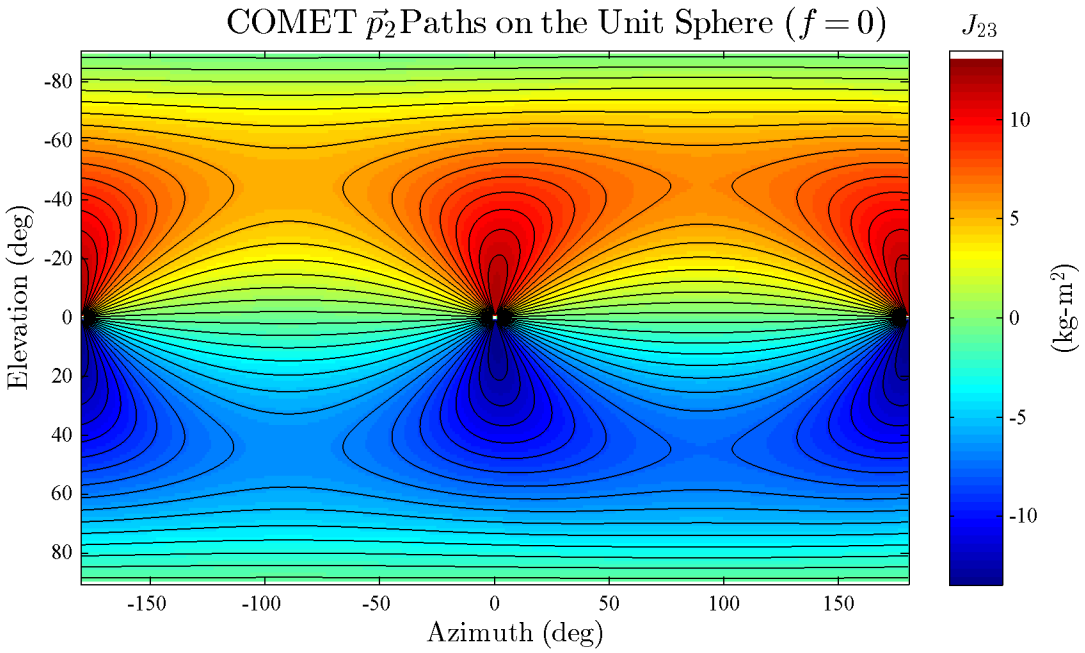

Figure 5.13: The pseudo-color plot for Gyrostat-Satellite I of the values of J_{23} for the allowable directions of $\vec{p}_2$ and $f = 0$ expressed in the orbital reference frame with level curves overlaid indicating constant values of J_{23} and COMETs

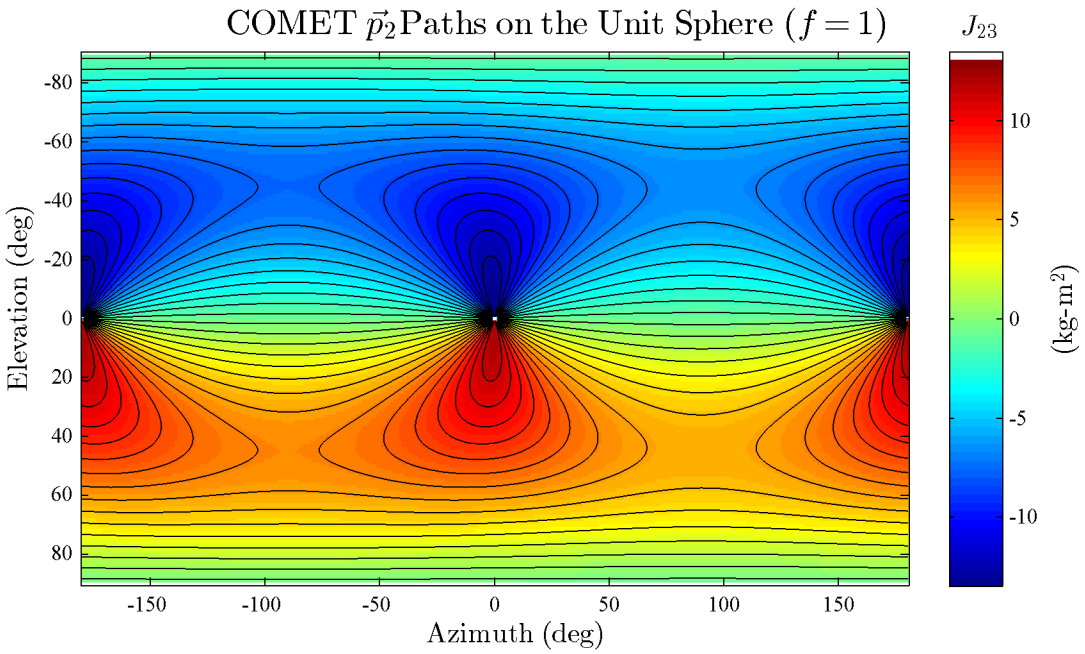

Figure 5.14: The pseudo-color plot for Gyrostat-Satellite I of the values of J_{23} for the allowable directions of $\vec{p}_2$ and $f = 1$ expressed in the orbital reference frame with level curves overlaid indicating constant values of J_{23} and COMETs

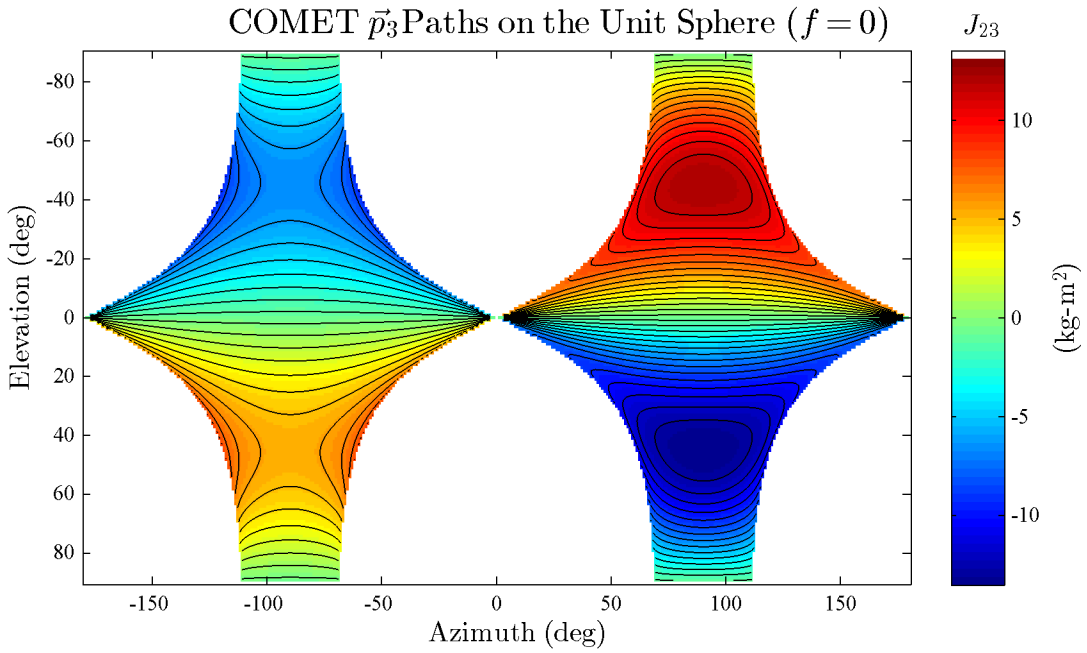

Figure 5.15: The pseudo-color plot for Gyrostat-Satellite I of the values of J_{23} for the allowable directions of $\vec{p}_3$ and $f = 0$ expressed in the orbital reference frame with level curves overlaid indicating constant values of J_{23} and COMETs

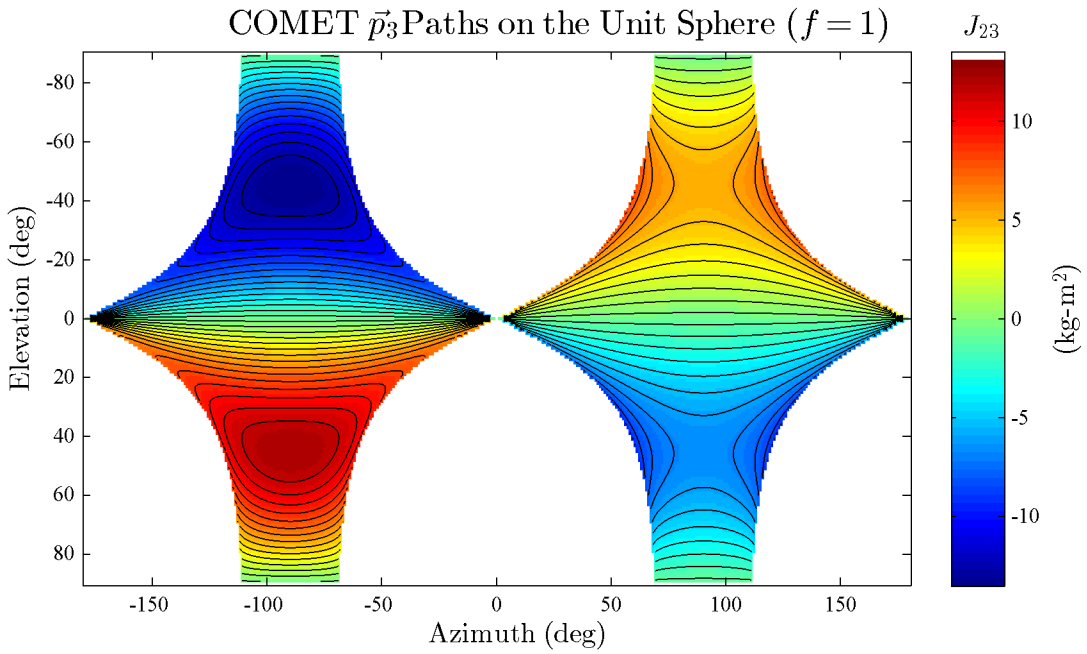

Figure 5.16: The pseudo-color plot for Gyrostat-Satellite I of the values of J_{23} for the allowable directions of $\vec{p}_3$ and $f = 1$ expressed in the orbital reference frame with level curves overlaid indicating constant values of J_{23} and COMETs

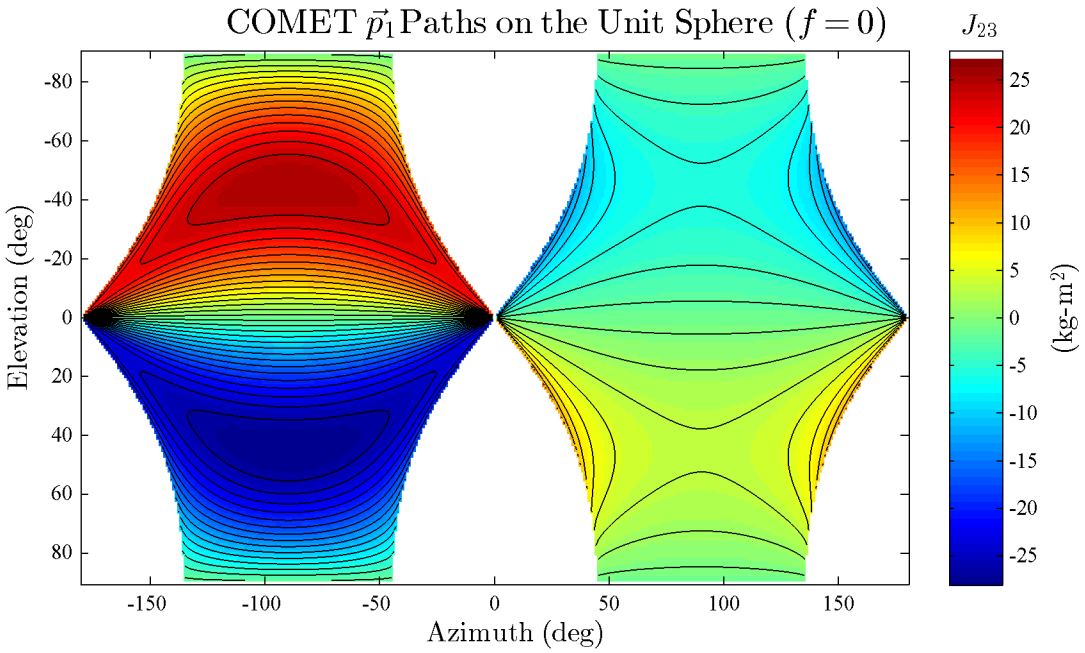

Figure 5.17: The pseudo-color plot for Gyrostat-Satellite II of the values of J_{23} for the allowable directions of $\vec{p}_1$ and $f = 0$ expressed in the orbital reference frame with level curves overlaid indicating constant values of J_{23} and COMETs

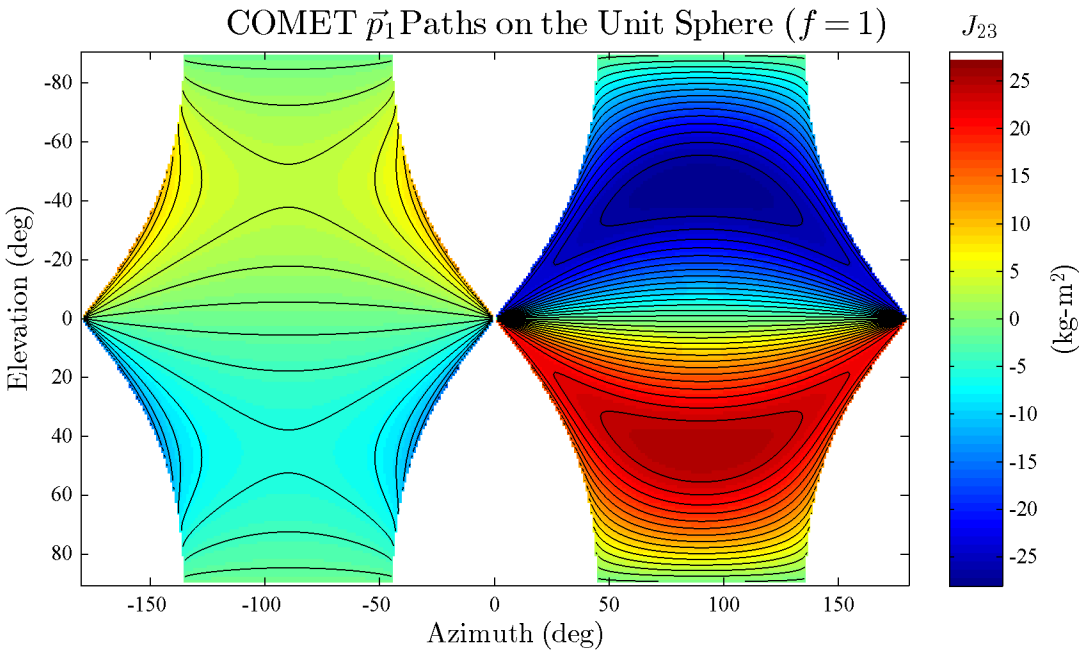

Figure 5.18: The pseudo-color plot for Gyrostat-Satellite II of the values of J_{23} for the allowable directions of $\vec{p}_1$ and $f = 1$ expressed in the orbital reference frame with level curves overlaid indicating constant values of J_{23} and COMETs

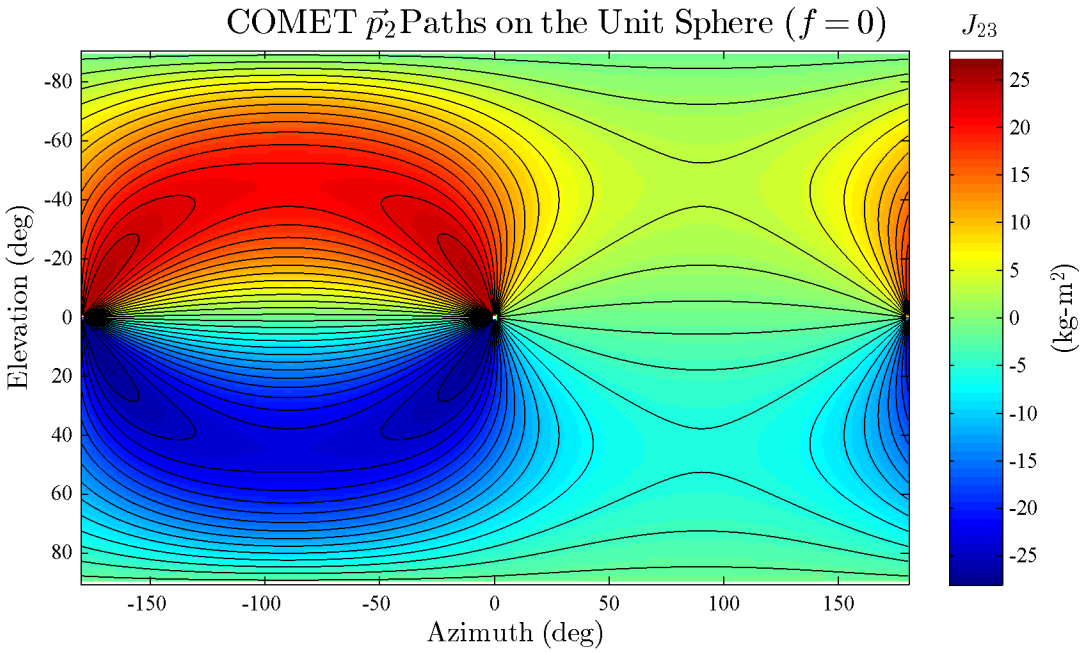

Figure 5.19: The pseudo-color plot for Gyrostat-Satellite II of the values of J_{23} for the allowable directions of $\vec{p}_2$ and $f = 0$ expressed in the orbital reference frame with level curves overlaid indicating constant values of J_{23} and COMETs

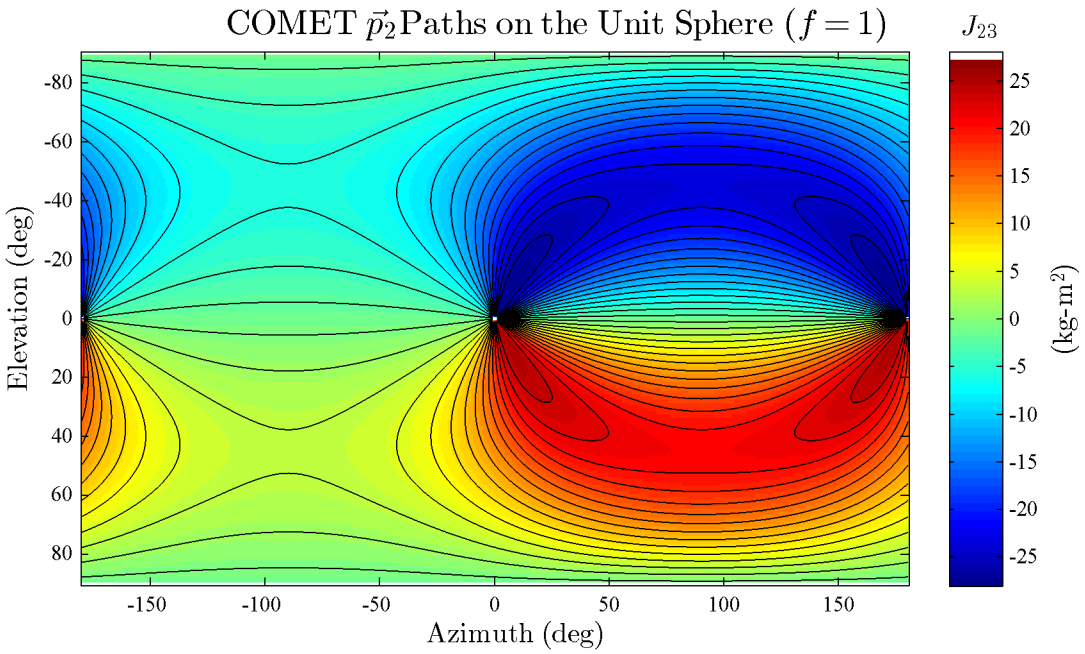

Figure 5.20: The pseudo-color plot for Gyrostat-Satellite II of the values of J_{23} for the allowable directions of $\vec{p}_2$ and $f = 1$ expressed in the orbital reference frame with level curves overlaid indicating constant values of J_{23} and COMETs

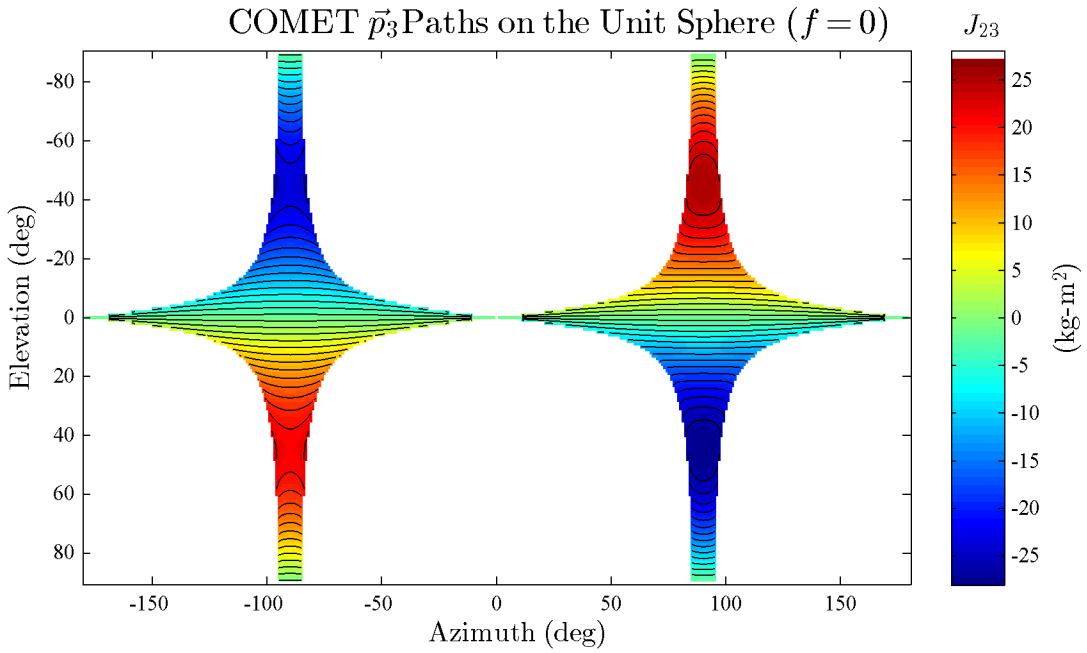

Figure 5.21: The pseudo-color plot for Gyrostat-Satellite II of the values of J_{23} for the allowable directions of $\vec{p}_3$ and $f = 0$ expressed in the orbital reference frame with level curves overlaid indicating constant values of J_{23} and COMETs

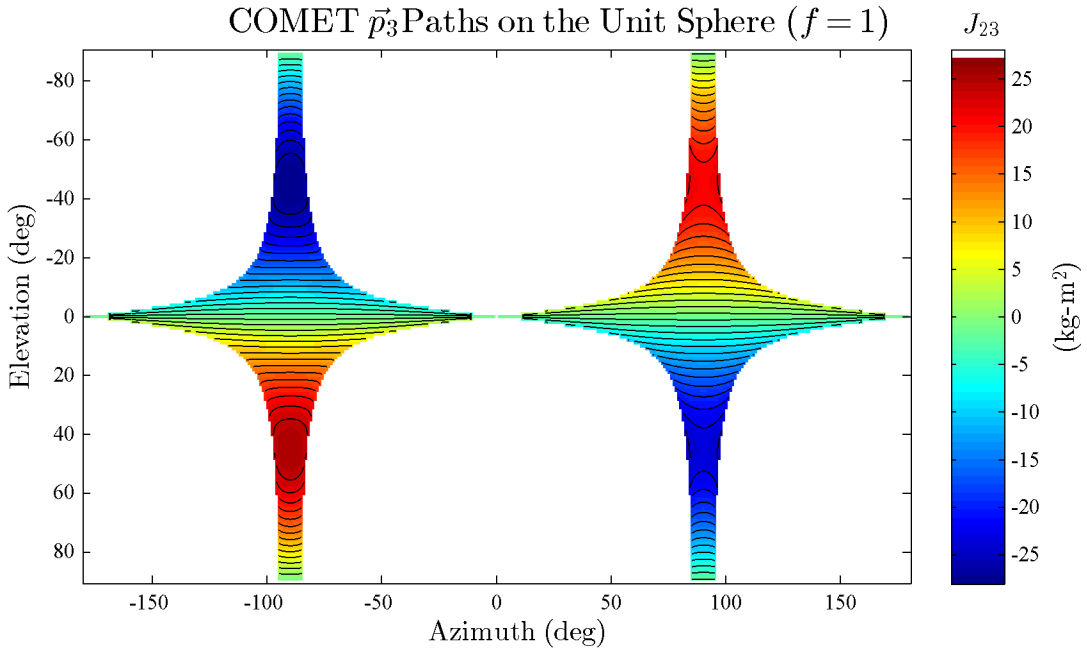

Figure 5.22: The pseudo-color plot for Gyrostat-Satellite II of the values of J_{23} for the allowable directions of $\vec{p}_3$ and $f = 1$ expressed in the orbital reference frame with level curves overlaid indicating constant values of J_{23} and COMETs

The definition of a COMET given in Section 5.2 is valid if the vector $\mathbf{v}$ fully spans the null space of the matrix $\mathbf{M}$, so that the path that maintains orbital momentum equilibrium is one-dimensional. Critical points occur on a COMET where the dimensionality of the null space of the matrix $\mathbf{M}$ (shown below) is greater than one. The magnitude of $\mathbf{v}$ at critical points is zero.

$$\mathbf{M} = \begin{bmatrix} J_{22} - J_{33} & -J_{12} & 0.0 \\ J_{12} & J_{33} - J_{11} & -J_{23} \end{bmatrix} \tag{5.43}$$

The dimensionality of the null space of the matrix $\mathbf{M}$ is greater than one when,

1. the magnitude of the first row of $\mathbf{M}$ is zero,
2. the magnitude of the second row of $\mathbf{M}$ is zero,
3. the magnitude of both rows of $\mathbf{M}$ is zero, or
4. the rows of $\mathbf{M}$ are linearly dependent.

Each of the cases enumerated above are examined in the following sections.

5.5.1 Magnitude of the First Row of M is Zero

In order for the magnitude of the first row of the $\mathbf{M}$ matrix to be zero, the following equalities must be satisfied.

$$J_{12} = 0 \tag{5.44}$$
$$\Delta_{23} = 0 \tag{5.45}$$

Equation 5.44 and the necessary condition for a relative equilibrium are

$$J_{12} = \vec{o}_2 \cdot \vec{I} \cdot \vec{o}_1 = 0 \tag{5.46}$$
$$J_{13} = \vec{o}_3 \cdot \vec{I} \cdot \vec{o}_1 = 0 \tag{5.47}$$

which require that

$$\rho\vec{o}_2 \times \vec{o}_3 = \vec{I} \cdot \vec{o}_1 \tag{5.48}$$
$$\rho\vec{o}_1 = \vec{I} \cdot \vec{o}_1 \tag{5.49}$$

Therefore, $\vec{o}_1$ must be an eigenvector of $\vec{I}$ so that

$$\vec{o}_1 = \pm\vec{p}_i \quad i \in 1, 2, 3 \tag{5.50}$$

To solve for the orientation about $\vec{o}_1$, $\vec{o}_2$ and $\vec{o}_3$ are parameterized as functions of the angle between $\vec{p}_j$ and $\vec{o}_2$, θ.

$$\vec{o}_2 = \pm\cos\theta\vec{p}_j \pm \sin\theta\vec{p}_k \quad (5.51)$$
$$\vec{o}_3 = \mp\sin\theta\vec{p}_j \mp \cos\theta\vec{p}_k \quad (5.52)$$

The angle θ is solved for by satisfying Eq. 5.45. The values of J_{22} and J_{33} as a function of θ are

$$J_{22} = \vec{o}_2 \cdot \vec{I} \cdot \vec{o}_2 = \cos^2\theta I_j + \sin^2\theta I_k \quad (5.53)$$
$$J_{33} = \vec{o}_3 \cdot \vec{I} \cdot \vec{o}_3 = \sin^2\theta I_j + \cos^2\theta I_k \quad (5.54)$$

Satisfying Eq. 5.45 requires that

$$\left(\cos^2\theta - \sin^2\theta\right)(I_j - I_k) = 0 \quad (5.55)$$

If the gyrostat-satellite has an axis of inerita symmetry, and $\vec{p}_j$ and $\vec{p}_k$ are perpendicular to that axis,

$$I_j = I_k \quad (5.56)$$

then the angle θ is unconstrained. Otherwise, the angle θ must satisfy the following equality.

$$\cos\theta = \pm\sin\theta \quad (5.57)$$

The angle θ is

$$\theta = \frac{\pi}{4} + \kappa\frac{\pi}{2} \quad \kappa \in \mathbf{Z} \quad (5.58)$$

where $\mathbf{Z}$ is the set of integers. Therefore, in order for the magnitude of the first row of $\mathbf{M}$ to be zero, the gyrostat-satellite must be aligned so that one of the principal axes is aligned with $\vec{o}_1$ and the other principal axes are clocked 45° degrees from $\vec{o}_2$ and $\vec{o}_3$.

5.5.2 Magnitude of the Second Row of M is Zero

In order for the magnitude of the second row of the $\mathbf{M}$ matrix to be zero, the following equalities must be satisfied.

$$J_{12} = 0 \quad (5.59)$$
$$J_{23} = 0 \quad (5.60)$$
$$\Delta_{13} = 0 \quad (5.61)$$

The first and second equalities and the necessary condition for a relative equilibrium require that $\vec{o}_i$ must be an eigenvector of $\vec{I}$ so that

$$\vec{o}_i = \pm\vec{p}_j \quad i, j \in 1, 2, 3 \quad (5.62)$$

This means that the principal reference frame is co-aligned with the orbital reference frame. The other requirement means that

$$I_i = I_k \tag{5.63}$$

so that the gyrostat-satellite must have an axis of inertial symmetry. Therefore, in order for the magnitude of the second row of **M** to be zero, the gyrostat-satellite must be co-aligned with the orbital reference frame and have an axis of inertial symmetry.

5.5.3 Magnitude of Both Rows of M is Zero

In order for the magnitude of both rows of the **M** matrix to be zero, the following equalities must be satisfied.

$$J_{12} = 0 \tag{5.64}$$
$$J_{23} = 0 \tag{5.65}$$
$$\Delta_{13} = 0 \tag{5.66}$$
$$\Delta_{23} = 0 \tag{5.67}$$

In Section 5.5.2, it was determined that to satisfy the first three equalities the gyrostat-satellite must be co-aligned with the orbital reference frame and have an axis of inertial symmetry. The addition of the fourth equality requires that the gyrostat-satellite have a second axis of inertial symmetry, which only occurs for spherically symmetric mass distributions.

5.5.4 Rows of M are Linearly Dependent

In order for the rows of the **M** matrix to be linearly dependent, the following equality must be satisfied.

$$\begin{bmatrix} J_{22} - J_{33} & -J_{12} & 0.0 \end{bmatrix} = \lambda \begin{bmatrix} J_{12} & J_{33} - J_{11} & -J_{23} \end{bmatrix} \tag{5.68}$$

Equation 5.68 is satisfied if the following equalities are satisfied.

$$J_{23} = 0 \tag{5.69}$$
$$J_{12}^2 - \Delta_{13}\Delta_{23} = 0 \tag{5.70}$$

Equation 5.69 and the necessary condition for a relative equilibrium are

$$J_{23} = \vec{o}_2 \cdot \vec{I} \cdot \vec{o}_3 = 0 \tag{5.71}$$
$$J_{13} = \vec{o}_1 \cdot \vec{I} \cdot \vec{o}_3 = 0 \tag{5.72}$$

which requires that

$$\rho\vec{o}_1 \times \vec{o}_2 = \vec{I}\cdot\vec{o}_3 \quad (5.73)$$
$$\rho\vec{o}_3 = \vec{I}\cdot\vec{o}_3 \quad (5.74)$$

Therefore, $\vec{o}_3$ must be an eigenvector of $\vec{I}$ so that

$$\vec{o}_3 = \pm\vec{p}_i \quad i \in 1,2,3 \quad (5.75)$$

To solve for the orientation about $\vec{o}_3$, $\vec{o}_1$ and $\vec{o}_2$ are parameterized as function of the angle between $\vec{p}_j$ and $\vec{o}_2$, θ.

$$\vec{o}_1 = \pm\cos\theta\vec{p}_j \pm \sin\theta\vec{p}_k \quad (5.76)$$
$$\vec{o}_2 = \pm\sin\theta\vec{p}_j \mp \cos\theta\vec{p}_k \quad (5.77)$$

The angle θ is solved for by satisfying Eq. 5.70. The values of J_{11}, J_{22}, and J_{33} as a function of θ are

$$J_{11} = \vec{o}_1\cdot\vec{I}\cdot\vec{o}_1 = \sin^2\theta I_j + \cos^2\theta I_k \quad (5.78)$$
$$J_{22} = \vec{o}_2\cdot\vec{I}\cdot\vec{o}_2 = \cos^2\theta I_j + \sin^2\theta I_k \quad (5.79)$$
$$J_{33} = I_i \quad (5.80)$$

Satisfying Eq. 5.70 requires that

$$J_{23}^2 - \Delta_{13}\Delta_{23} = -(I_i - I_j)(I_i - I_k) = 0 \quad (5.81)$$

Equation 5.81 is independent of the angle θ. Therefore, the gyrostat-satellite must have an axis of inerita symmetry that is perpendicular to either $\vec{p}_i$ and $\vec{p}_j$ so that,

$$I_i = I_j \quad (5.82)$$

or $\vec{p}_i$ and $\vec{p}_k$ so that,

$$I_i = I_k \quad (5.83)$$

Therefore, in order for the rows of $\mathbf{M}$ to be linearly dependent, the gyrostat-satellite must be aligned so that one of the principal axes are aligned with $\vec{o}_3$ and have an axis of inertial symmetry.

5.5.5 Summary

The four possible cases for the null space of $\mathbf{M}$ are summarized below:

1. The rows of $\mathbf{M}$ are linearly independent and have magnitudes greater than zero, so that the null space of $\mathbf{M}$ is one-dimensional and is aligned with the cross product of the rows.
2. The magnitude of one row of $\mathbf{M}$ is zero and the magnitude of the other row is greater than zero, so that the null space of $\mathbf{M}$ is two-dimensional and resides in the plane perpendicular to the row with a magnitude greater than zero.
3. The rows of $\mathbf{M}$ are linearly dependent, so that the null space of $\mathbf{M}$ is two-dimensional and resides in the plane perpendicular to the rows.
4. The magnitude of both rows of $\mathbf{M}$ is zero, so that the null space of $\mathbf{M}$ is three-dimensional and occupies the whole of $\mathbf{R}^3$.

Cases 3 and 4 only occur for gyrostat-satellites with inertial symmetries. The qualitative results presented in Sections 5.3 and 5.4 indicate that Case 1 occurs over the majority of COMETs, and therefore COMETs are generally one-dimensional curves in SO(3).

The visualizations presented in Section 5.4 indicated that for a small subset of COMETs there are critical points that represent either isolated relative equilibrium attitudes or furcations of the COMET. Assuming a tri-inertial gyrostat-satellite, these points correspond to Case 2. The results of Sections 5.5.1 indicate that critical points only occur (for a tri-inertial gyrostat-satellite) when one of the principal axes is aligned with $\vec{o}_1$ and the other principal axes are clocked 45° degrees from $\vec{o}_2$ and $\vec{o}_3$. This result matches the locations of the critical points observed in Section 5.4.

5.6 Example Simulations

The purpose of this section is to present the results of numeric simulations of a gyrostat-satellite traveling on two COMETs to verify the analytic and qualitative analysis presented in prior sections. An example gyrosat-satellite is simulated. The principal moments of inertia of the gyrostat-satellite are provided as Gyrostat-Satellite I in Table 5.3. A numeric simulator (presented in Appendix A) simulates the rotational dynamics of the gyrostat-satellite.

Table 5.5 summarizes the key parameters of the simulations. The first four parameters (θ_1, θ_2, θ_3, and h_2^o) are independent input values defining the initial conditions of the simulations. The parameters θ_1, θ_2, and θ_3 define the initial attitude of the gyrostat-satellite through the use of Algorithm 4.1. The parameter h_2^o does not affect the COMET but does impact dynamic quantities such as the relative angular momentum vector. The last two parameters (J_{23} and h_3^o) are derived values that remain constant throughout the simulation and are included for informational purposes.

Figures 5.23 through 5.40 present the results of Simulation I and II. The first set of figures (Figures 5.23 through 5.31) show the results for Simulation I; and, the second set of figures

Table 5.5: Key parameters used to simulate a gyrostat-satellite traversing two COMETs

Parameter	Simulation I	Simulation II
θ_1	-5^o	-40^o
θ_2	-25^o	0^o
θ_3	1.0	1.0
h_2^o	-0.2627	-0.2455
J_{23}	-11.0802 kg-m^2	-6.5490 kg-m^2
h_3^o	-0.0363 Nms	72.7952 Nms

(Figures 5.32 through 5.40) show the results for Simulation II. Each set consists of nine figures. The first two figures of each set (Figures 5.23, 5.24, 5.32, and 5.33) depict the path of the principal basis vectors on the unit sphere fixed in the orbital reference frame. Each figure consists of four sub-figures that each give a three-dimensional view of the unit sphere from a particular vantage point defined by the azimuth α and elevation ϵ angle noted above each view. The first figure (Figures 5.23 and 5.32) shows the views from the $+\vec{o}_3$ hemisphere, and the second figure (Figures 5.24 and 5.33) shows the views from the $-\vec{o}_3$ hemisphere. The paths of $\vec{p}_1$, $\vec{p}_2$, and $\vec{p}_3$ are shown as solid red, blue, and green curves on the surface of the unit sphere, respectively. The third figure of each set (Figures 5.25 and 5.34) shows the path of the vector part of the attitude quaternion throughout the transition maneuver. The fourth figure of each set (Figures 5.26 and 5.35) is a plot of the time history of the components of the attitude quaterion representing the rotation from the orbital reference frame to the principal reference frame on the abscissa and the elapsed simulation time on the ordinate. The vector components of the attitude quaternion (q_1, q_2, and q_3) are shown as blue, green, and red curves, respectively, and the scalar component (q_4) is shown as a cyan curve. The fifth figure of each set (Figures 5.27 and 5.36) is a plot of the time history of the components of the angular velocity of the principal reference frame with respect to the orbital reference frame expressed in the principal reference frame on the abscissa and the elapsed simulation time on the ordinate. The components along $\vec{p}_1$, $\vec{p}_2$, and $\vec{p}_3$ are shown as blue, green, and red curves, respectively. The values of the products of inertia expressed in the orbital reference frame during the simulation are shown in the sixth figure of each set (Figures 5.28 and 5.37). The seventh figure of each set (Figures 5.29 and 5.38) shows the time history of the system angular momentum expressed in the orbital reference frame ($\mathbf{h}^o$). The time history of components of the relative angular momentum vector expressed in the principal reference frame ($\mathbf{h}_s$) are shown in the eighth figure of each set (Figures 5.30 and 5.39). The ninth figure of each set (Figures 5.31 and 5.40) shows the time history of the internal torque vector expressed in the principal reference frame ($\mathbf{g}_s$).

The three-dimensional figures (Figures 5.23, 5.24, 5.32, and 5.33) show that the COMET is a closed-curve in SO(3), and that the gyrostat-satellite is traveling along the COMET. As would be expected while traversing a COMET, J_{13} is zero, J_{23} is constant, and the

components of the system angular momentum vector expressed in the orbital frame are constant throughout the simulation.

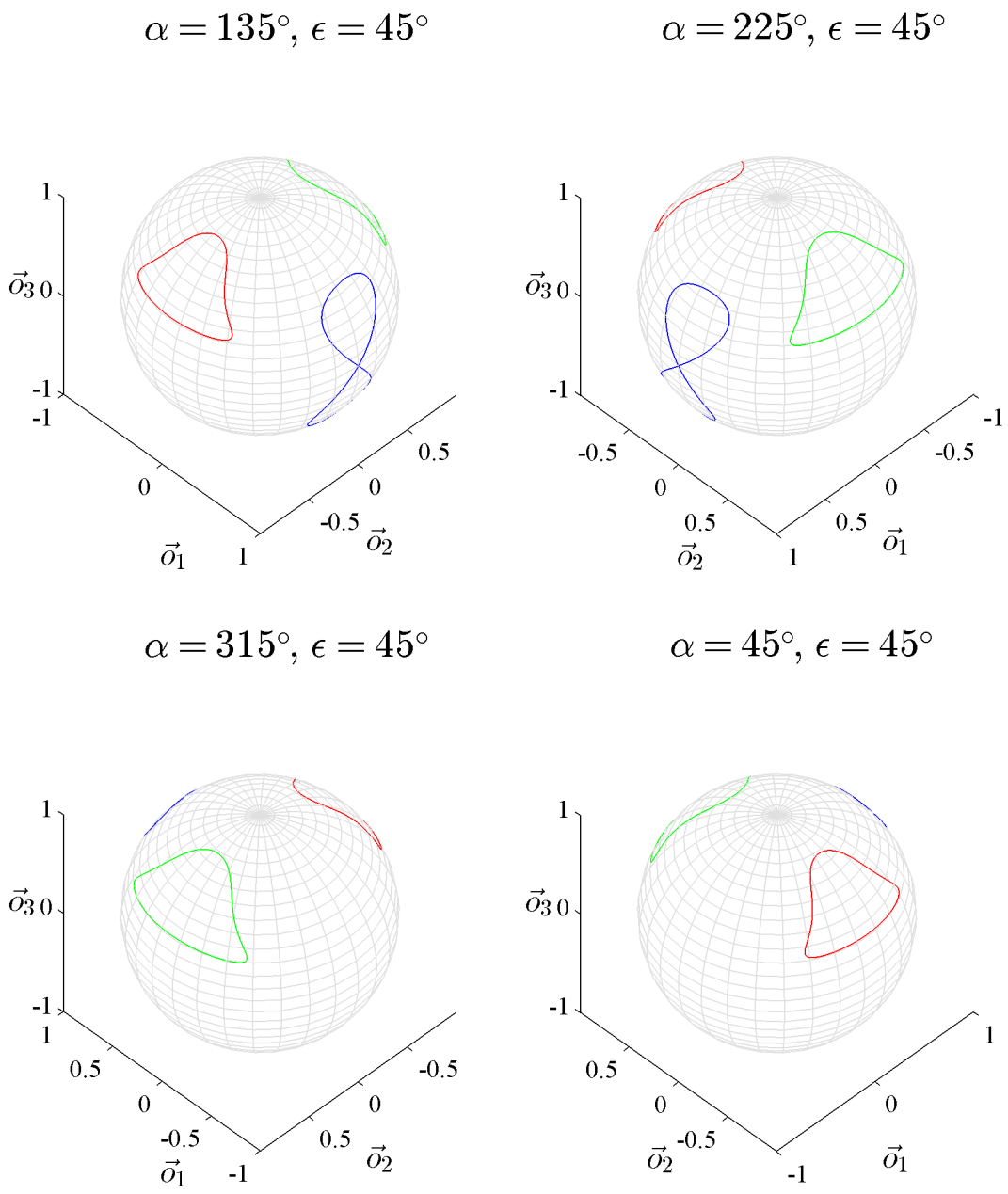

Figure 5.23: Four isometric views from the $+\vec{o}_3$ hemisphere of the paths of the principal frame basis axes on the unit sphere fixed in the orbital reference frame during Simulation I of a gyrostat-satellite traveling along a COMET

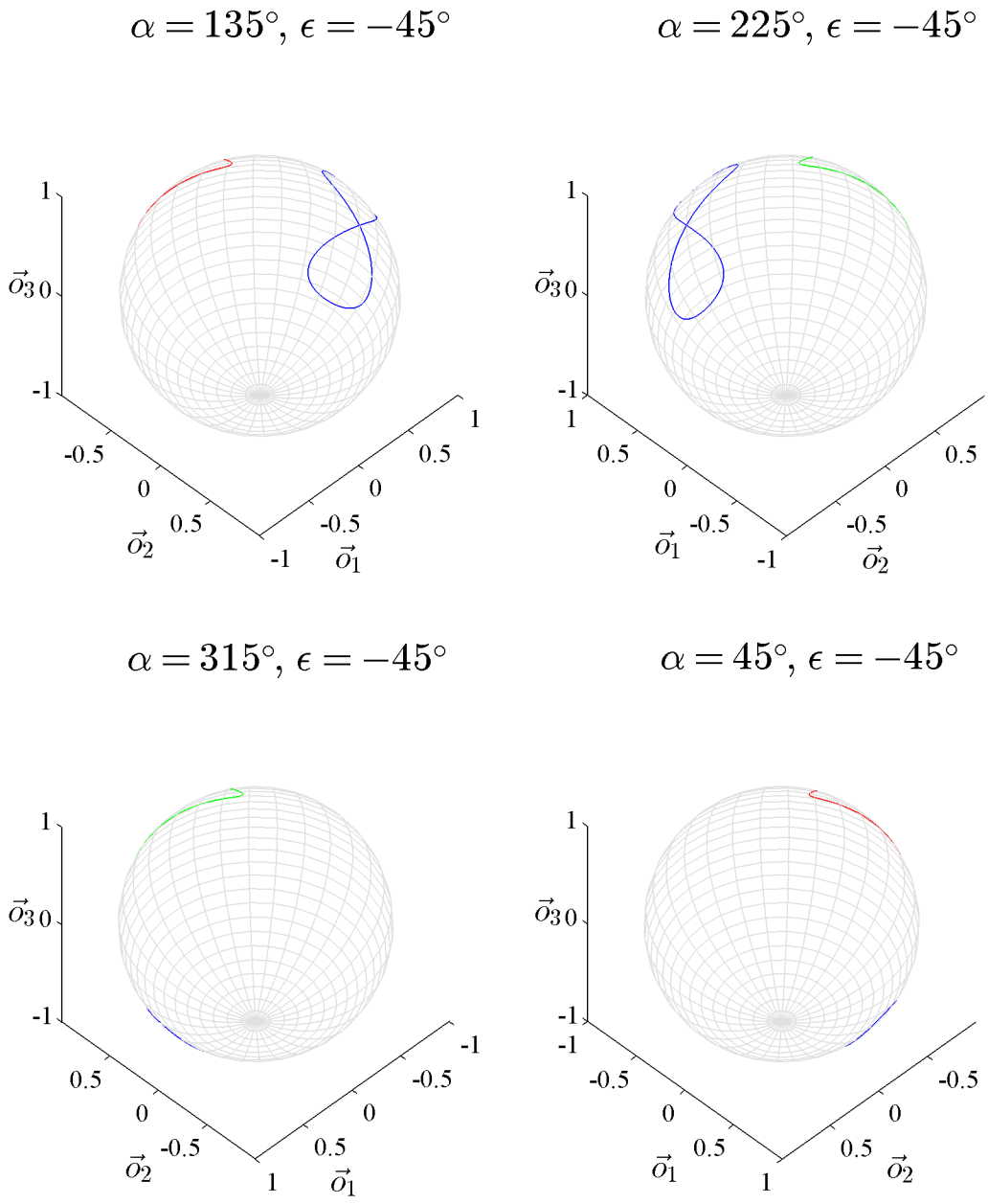

Figure 5.24: Four isometric views from the -$\vec{o}_3$ hemisphere of the paths of the principal frame basis axes on the unit sphere fixed in the orbital reference frame during Simulation I of a gyrostat-satellite traveling along a COMET

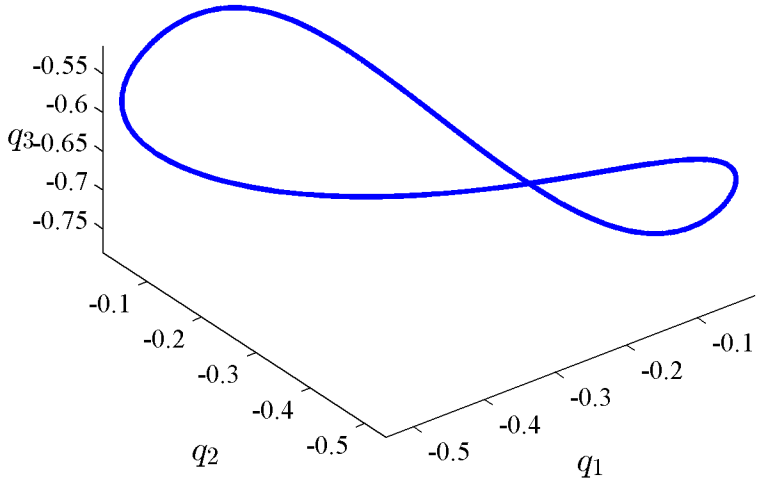

Figure 5.25: Path in the configuration space of the vector part of the attitude quaternion ($\vec{q}^{po}$) during Simulation I of a gyrostat-satellite traveling along a COMET

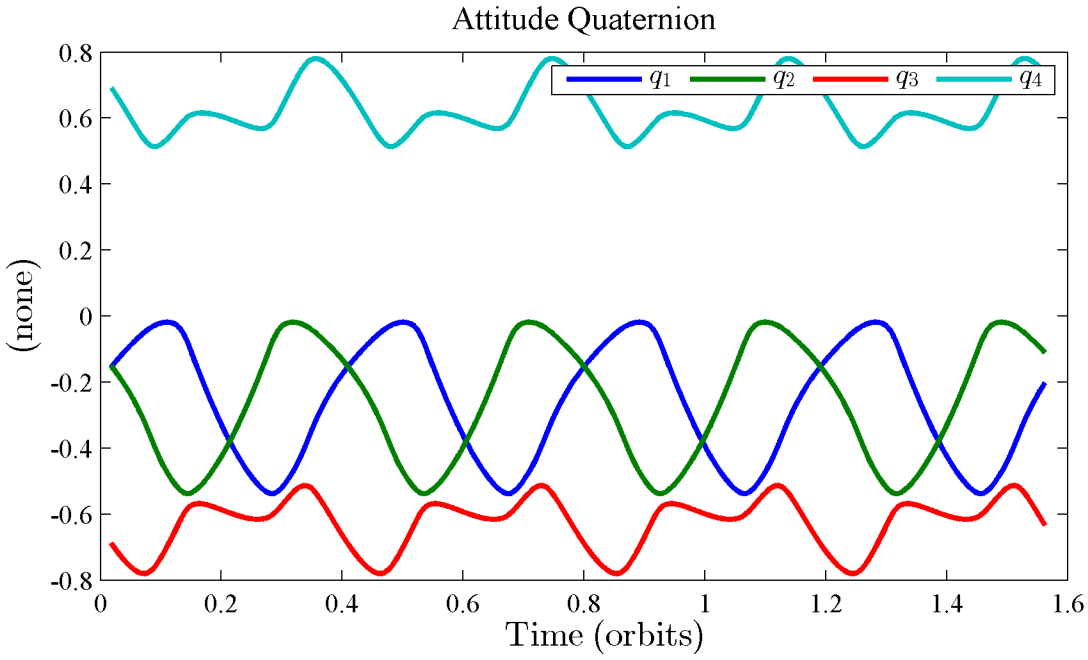

Figure 5.26: Components of the attitude quaternion ($\bar{q}^{po}$) during Simulation I of a gyrostat-satellite traveling along a COMET

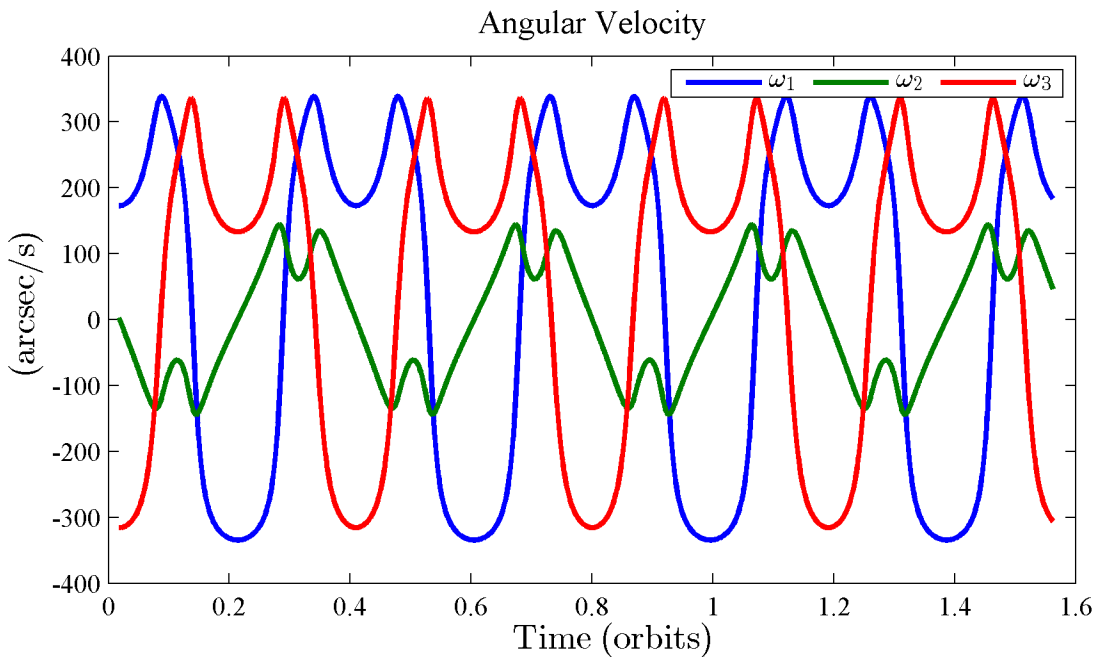

Figure 5.27: Components of the angular velocity of the princpal reference frame with respect to the orbital reference frame expressed in the principal reference frame ($\boldsymbol{\omega}^{po}$) during Simulation I of a gyrostat-satellite traveling along a COMET

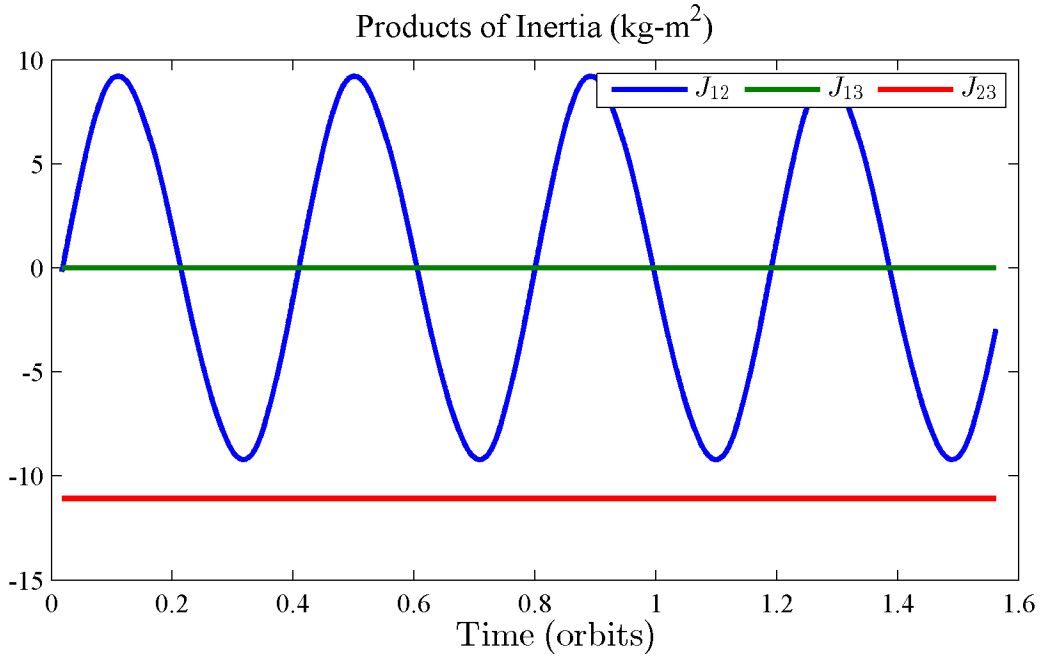

Figure 5.28: Products of inertia expressed in the orbital reference frame (J_{12}, J_{13}, and J_{23}) during Simulation I of a gyrostat-satellite traveling along a COMET

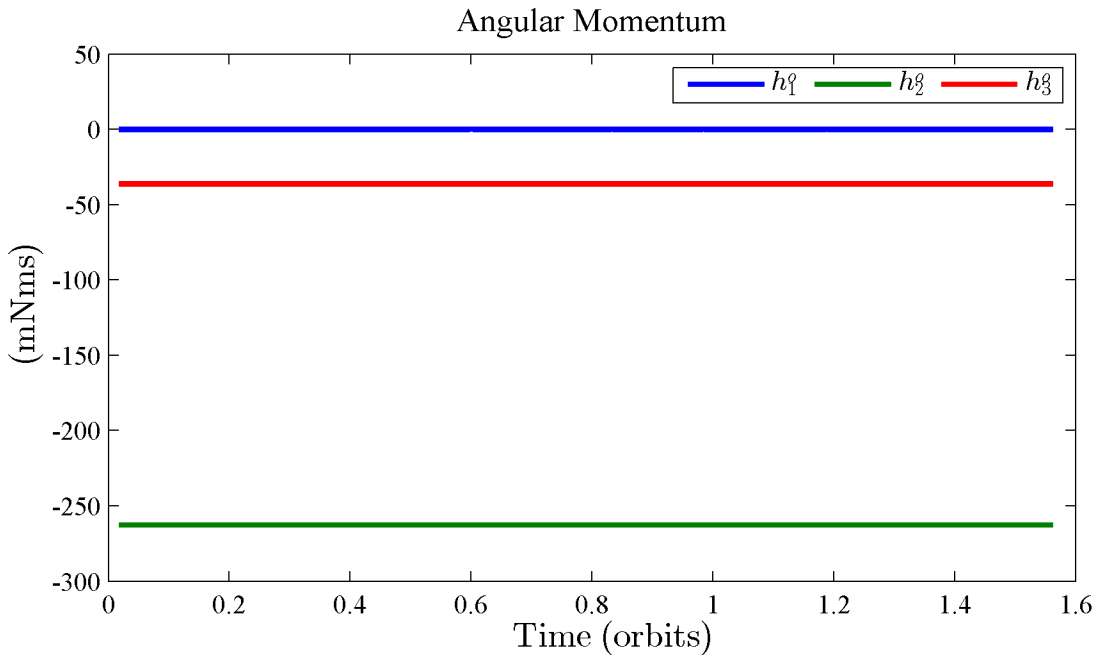

Figure 5.29: Components of the system angular momentum vector expressed in the orbital reference frame ($\mathbf{h}^o$) during Simulation I of a gyrostat-satellite traveling along a COMET

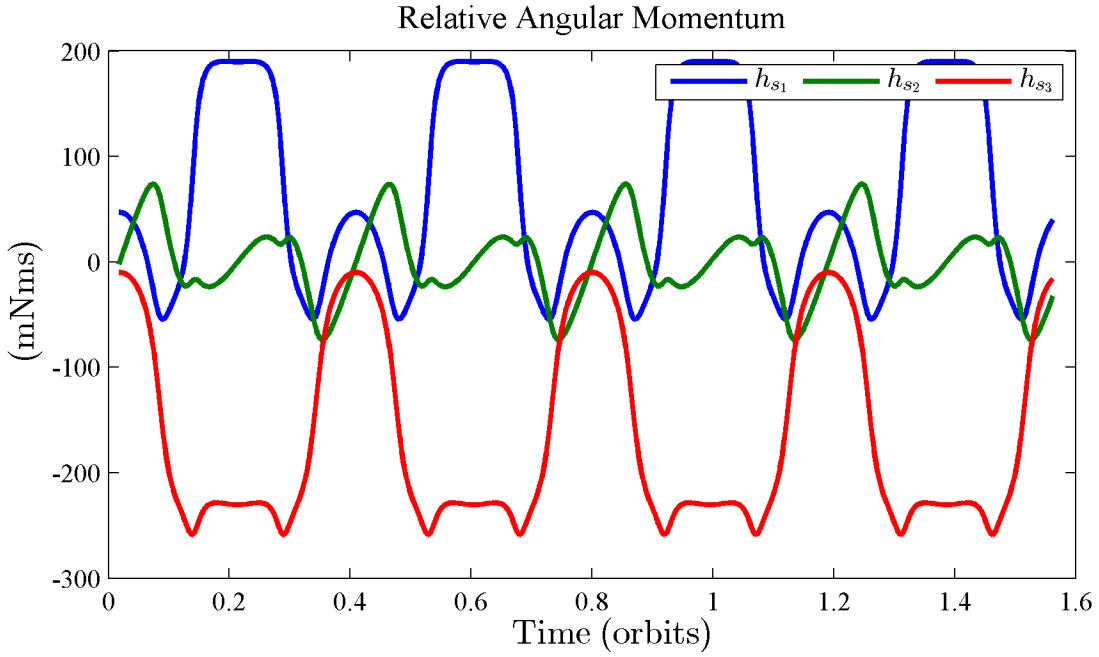

Figure 5.30: Components of the relative angular momentum vector expressed in the principal reference frame ($\mathbf{h}_s$) during Simulation I of a gyrostat-satellite traveling along a COMET

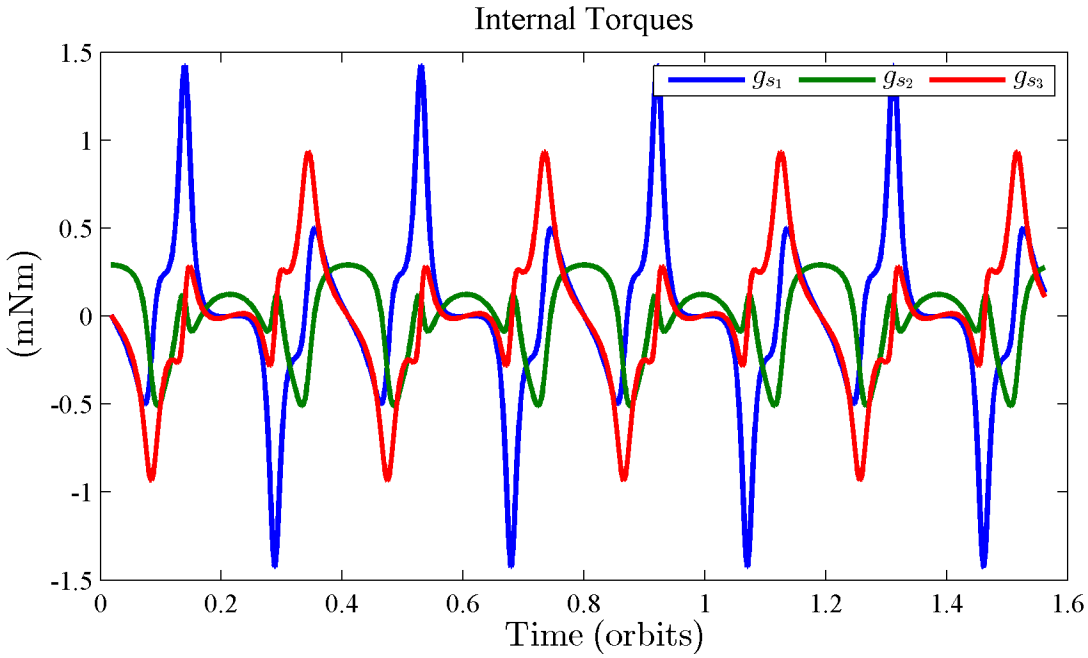

Figure 5.31: Components of the internal torque vector expressed in the principal reference frame ($\mathbf{g}_s$) during Simulation I of a gyrostat-satellite traveling along a COMET

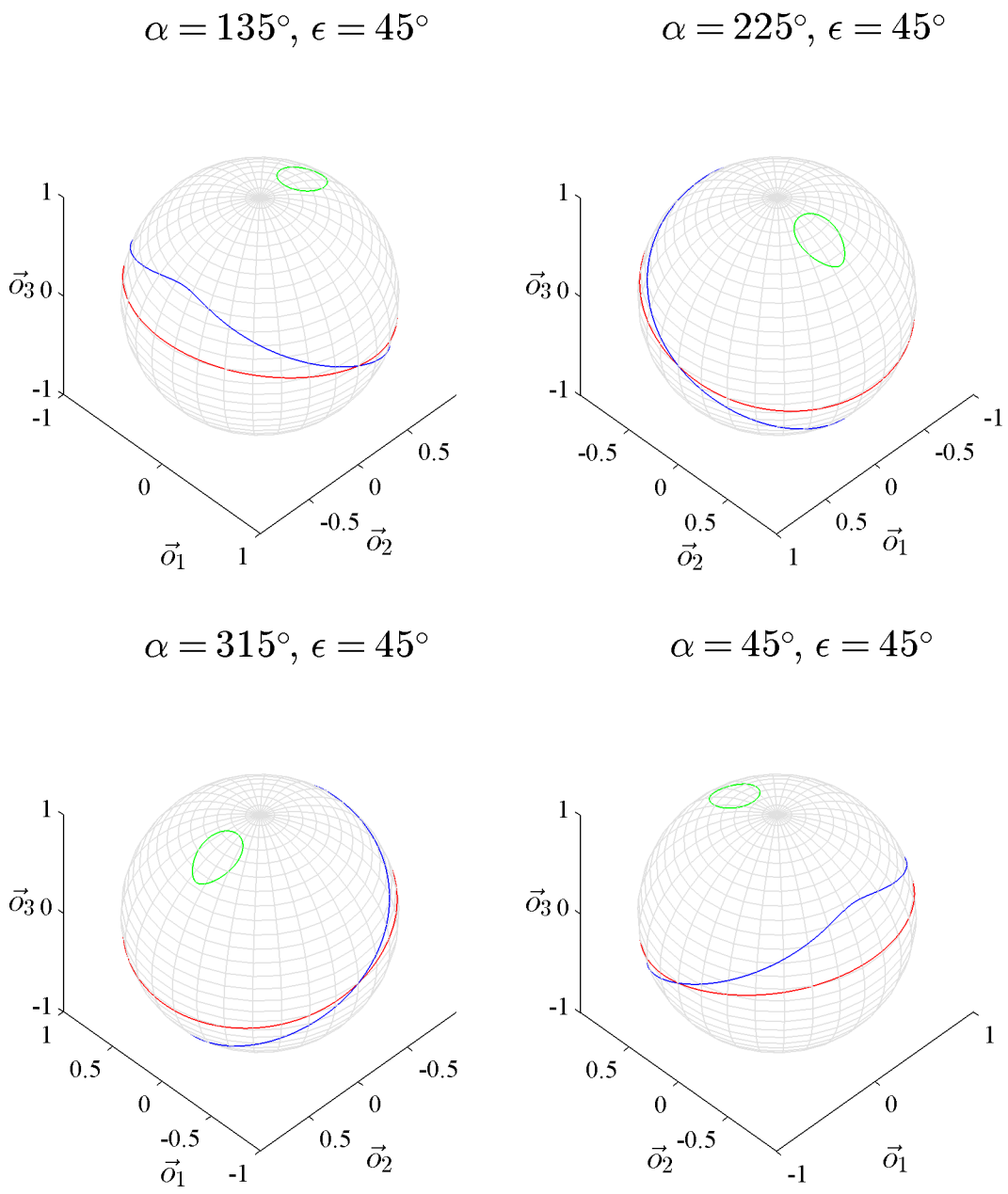

Figure 5.32: Four isometric views from the $+\vec{o}_3$ hemisphere of the paths of the principal frame basis axes on the unit sphere fixed in the orbital reference frame during Simulation II of a gyrostat-satellite traveling along a COMET

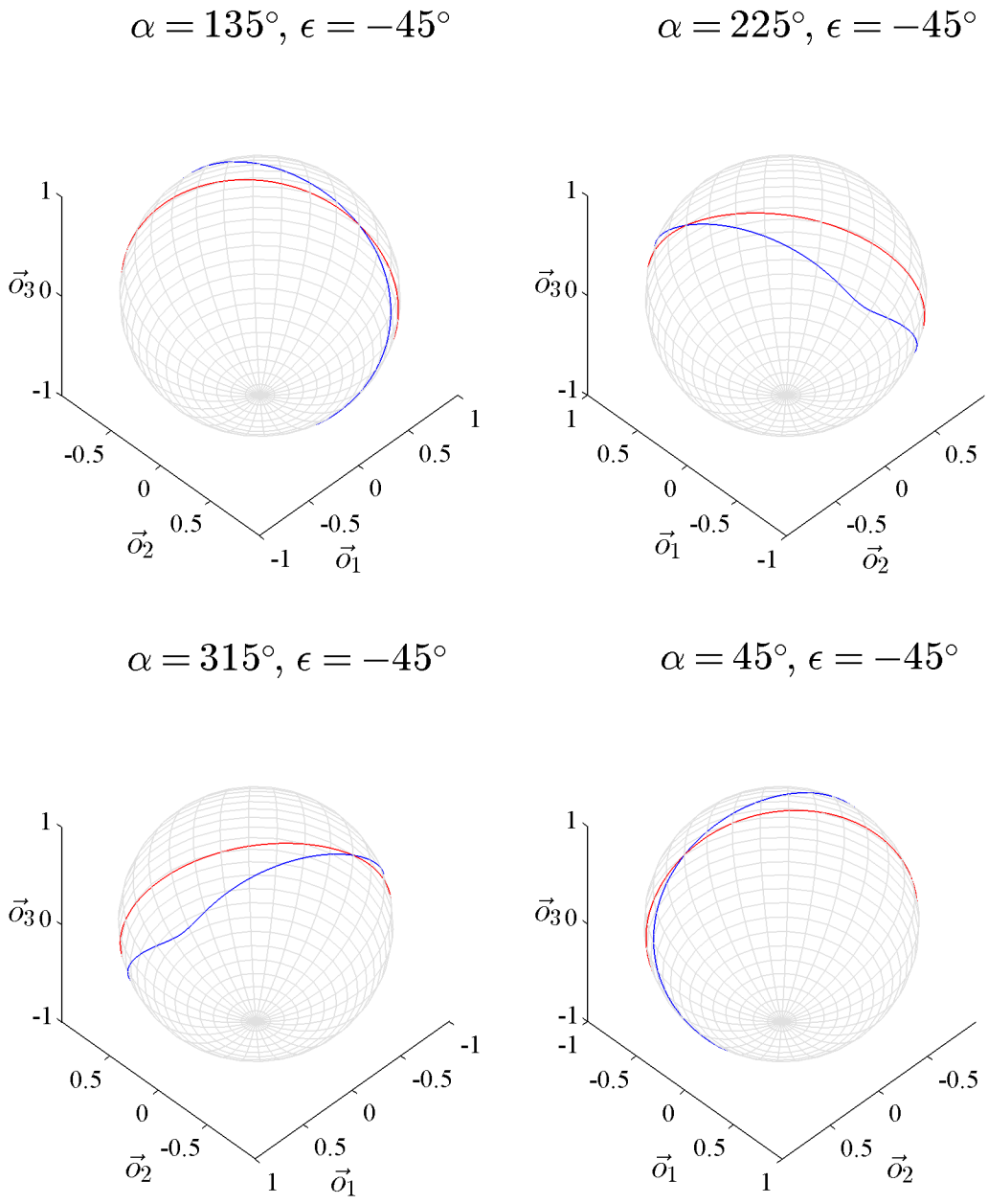

Figure 5.33: Four isometric views from the -$\vec{o}_3$ hemisphere of the paths of the principal frame basis axes on the unit sphere fixed in the orbital reference frame during Simulation II of a gyrostat-satellite traveling along a COMET

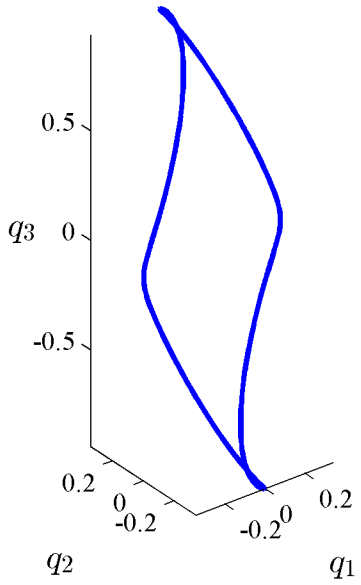

Figure 5.34: Path in the configuration space of the vector part of the attitude quaternion ($\vec{q}^{po}$) during Simulation II of a gyrostat-satellite traveling along a COMET

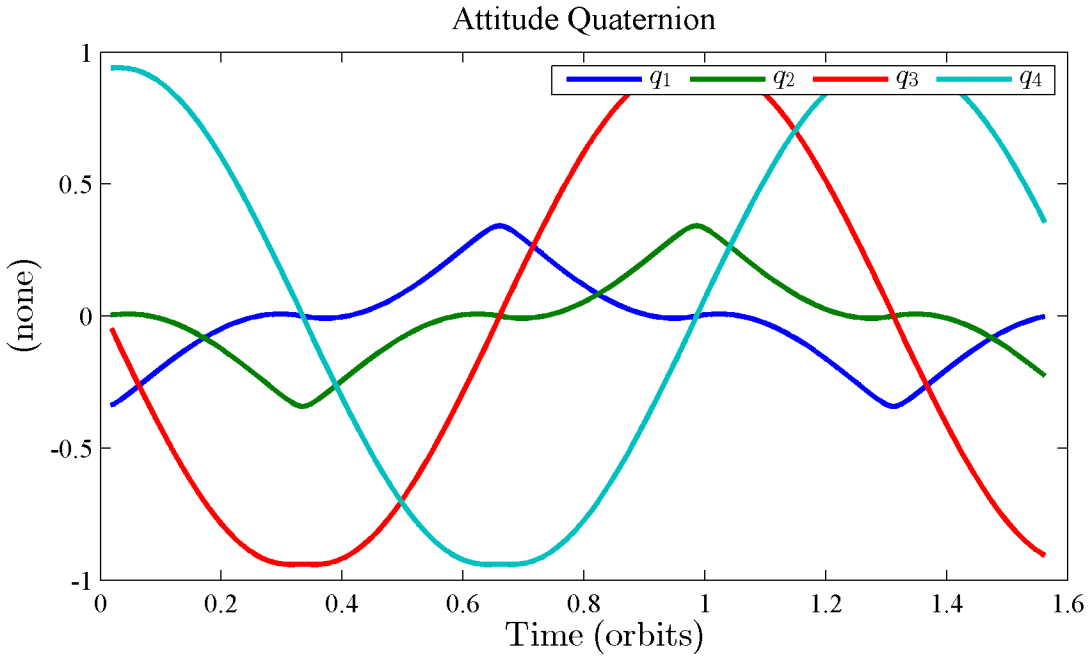

Figure 5.35: Components of the attitude quaternion ($\bar{q}^{po}$) during Simulation II of a gyrostat-satellite traveling along a COMET

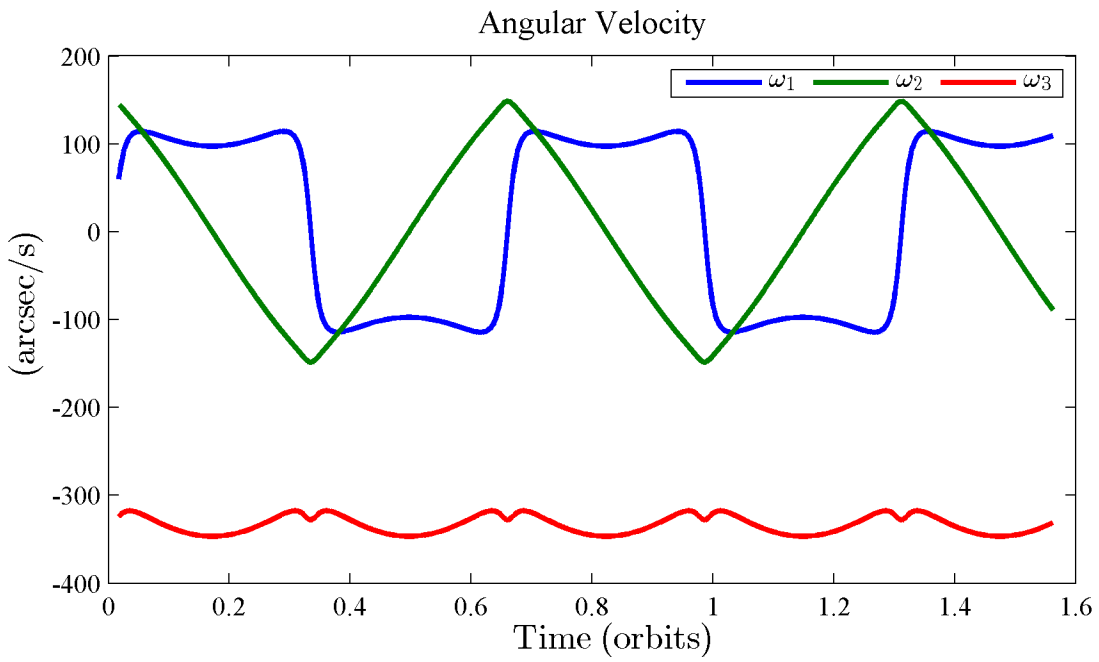

Figure 5.36: Components of the angular velocity of the princpal reference frame with respect to the orbital reference frame expressed in the principal reference frame ($\boldsymbol{\omega}^{po}$) during Simulation II of a gyrostat-satellite traveling along a COMET

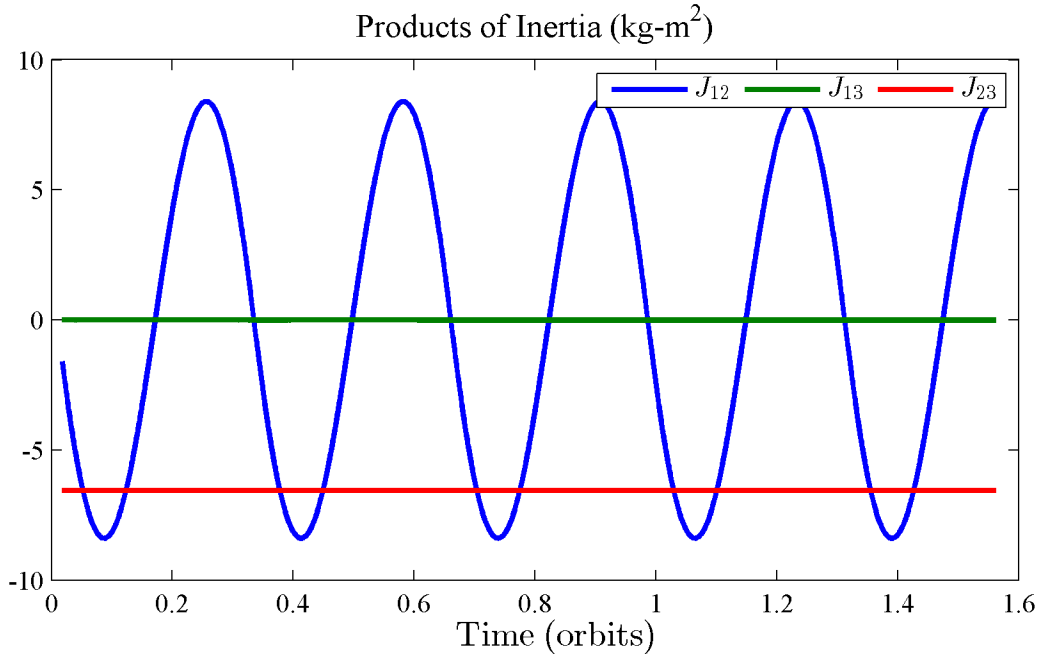

Figure 5.37: Products of inertia expressed in the orbital reference frame (J_{12}, J_{13}, and J_{23}) during Simulation II of a gyrostat-satellite traveling along a COMET

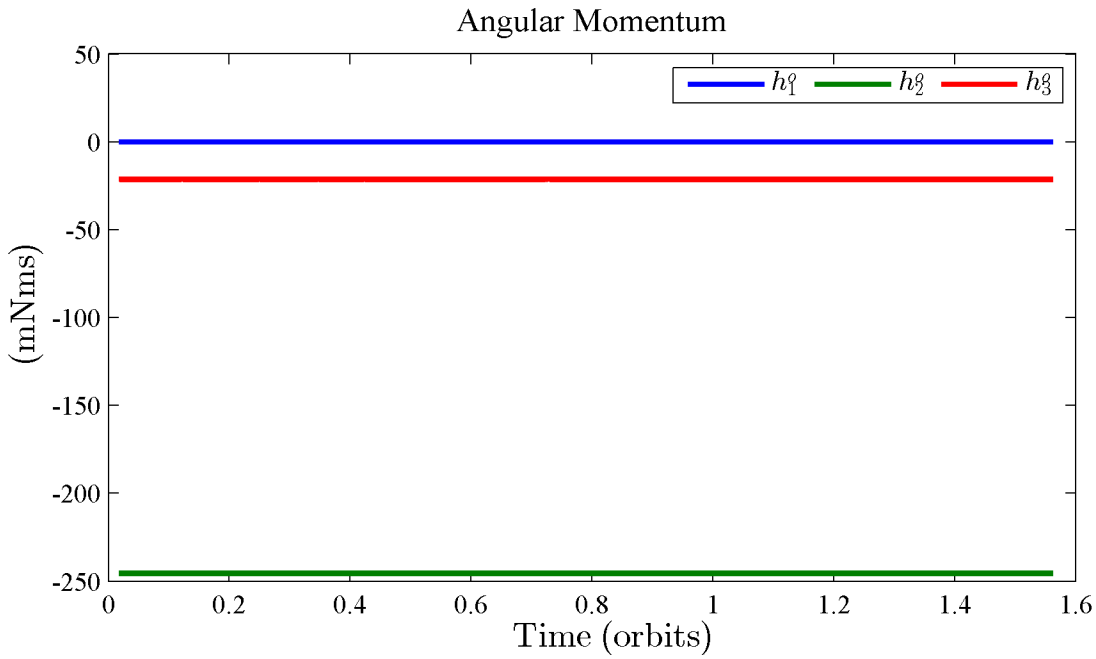

Figure 5.38: Components of the system angular momentum vector expressed in the orbital reference frame ($\mathbf{h}^o$) during Simulation II of a gyrostat-satellite traveling along a COMET

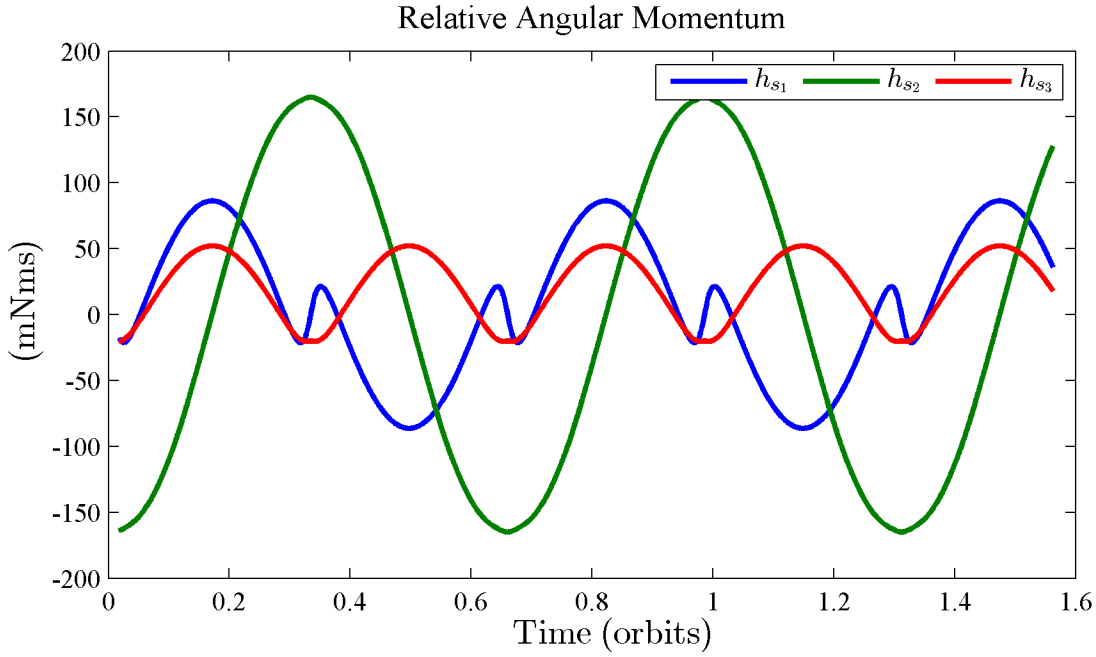

Figure 5.39: Components of the relative angular momentum vector expressed in the principal reference frame ($\mathbf{h}_s$) during Simulation II of a gyrostat-satellite traveling along a COMET

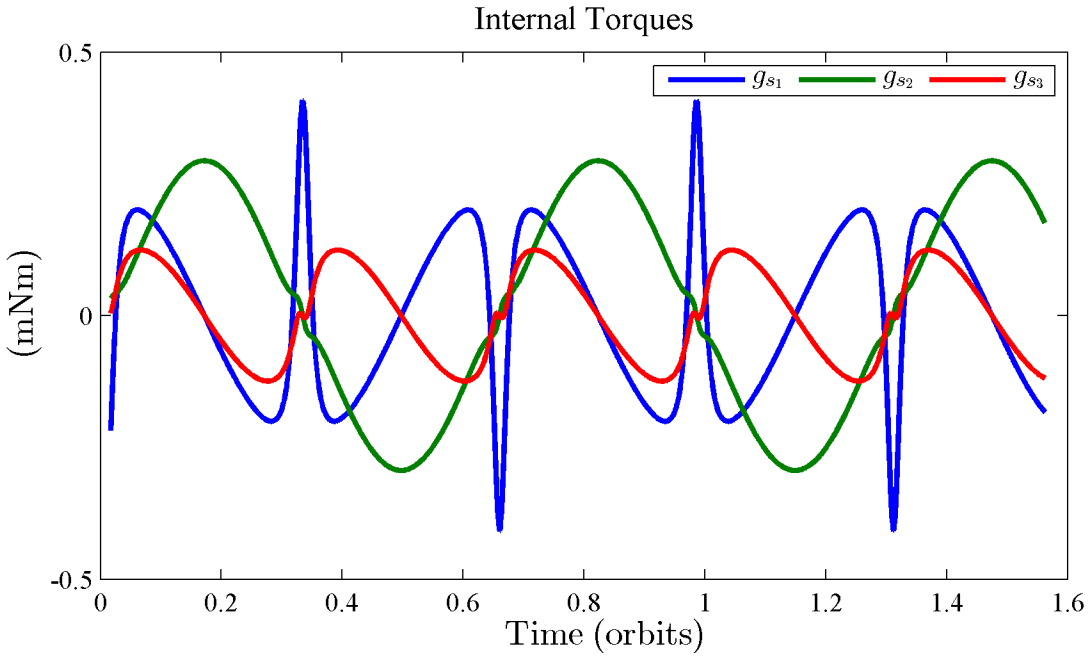

Figure 5.40: Components of the internal torque vector expressed in the principal reference frame ($\mathbf{g}_s$) during Simulation II of a gyrostat-satellite traveling along a COMET

5.7 Summary

Chapter 4 introduced the concept relative equilibrium of a gyrostat-satellite, and it was shown it was a generalization of dynamic equilibrium. In this chapter, a new concept, the COMET, was introduced. The COMET was shown to be a further generalization that relaxes the condition that the gyrostat-satellite is at rest when viewed by an observer embedded in the orbital reference frame. COMETs are equilibrium solutions to the system angular momentum expressed in the orbital reference frame. A mathematical definition for COMETs was derived that included a nonholonomic constraint. A method to map a COMET was presented. Maps generated for several example COMETs were used to show that COMETs are (generally) continuous, one-dimensional, closed curves in SO(3). Visualizations of families of COMETs were presented for two example gyrostat-satellites. The visualizations indicated the existence of critical points on a small subset of COMETs that represent either isolated relative equilibrium attitudes or points furcation of the COMET. It was shown that the critical points correspond to points in SO(3) where the dimensionality of the null space of the $\mathbf{M}$ matrix increases from one to two. Two numeric simulations of a gyrostat-satellite traversing a COMET were presented, and were shown to agree with the analytic and qualitative results presented earlier in the chapter.

Chapter 6

Attitude Transitions Between Relative Equilibria

As discussed in Chapter 2, the literature on equilbria of gyrostat-satellites extensively investigates the determination of relative equilibrium attitudes and the stability characteristics of relative equilibria. However, little work has investigated using internal torque actuation to transition between relative equilibria. The purpose of this chapter is to begin addressing this gap in the literature by investigating open-loop control laws that transition a gyrostat-satellite from an initial relative equilibrium to a desired target relative equilibrium.

The problem of transitioning a gyrostat-satellite from an initial relative equilibrium to a desired target relative equilibrium is broken into two sub-problems. The first sub-problem, presented in Section 6.1, is transitioning between two relative equilibria that reside on the same COMET. The second sub-problem, presented in Section 6.2, is transitioning between two relative equilibria that reside on different COMETs.

6.1 Relative Equilibria on the same COMET

The purpose of this section is to solve the problem of transitioning a gyrostat-satellite from an initial relative equilibrium to a desired target relative equilibrium where both the initial and target relative equilibrium reside on the same COMET. As discussed in Chapter 5, a COMET is a continuous, closed curve in SO(3). Transitions between relative equilibria on the same COMET may be straight-forwardly accomplished by traversing along the COMET until the desired target relative equilibrium is reached.

Section 6.1.1 develops an open-loop control law that transitions a gyrostat-satellite from an initial relative equilibrium to a target relative equilibrium. The open-loop control law is a function of the coordinate s of the coordinate chart developed in Section 5.3. The results

of a numeric simulation of a gyrostat-satellite using the open-loop control law to execute a transition maneuever between two relative equilibria on the same COMET are presented in Section 6.1.2

6.1.1 Open-Loop Control Law

The open-loop control torques to be commanded to the rotors are defined by Eq. B.1 developed in Appendix B, and repeated here for convenience.

$$\mathbf{g}_s = -\mathbf{I}\dot{\boldsymbol{\omega}}^{po} - \omega_o \mathbf{I}\left(\boldsymbol{\omega}^{po}\right)^{\times}\mathbf{o}_2 - \left(\boldsymbol{\omega}^{pi}\right)^{\times}\mathbf{h} + 3\omega_o^2\mathbf{o}_3^{\times}\mathbf{I}\mathbf{o}_3$$

The open-loop control law (Eq. B.1) is fully defined over a transition maneuver given an initial system state and the time history of the angular acceleration of the principal reference frame with respect to the orbital reference frame ($\dot{\boldsymbol{\omega}}^{po}$). The initial system state is the relative equilibrium of the gyrostat-satellite prior to the transition maneuver. The time history of $\dot{\boldsymbol{\omega}}^{po}$ is calculated based on a desired slew profile defined in s-$\dot{s}$ configuration space.

A simple "ramp-coast-ramp" profile is selected as the desired slew profile. Figure 6.1 depicts the two possible slew profiles. Longer s distances will result in a slew profile like that depicted in sub-figure A of Figure 6.1. Shorter s distances will result in a slew profile like that depicted in sub-figure B of Figure 6.1. The quantities labeled in Figure 6.1 are defined below.

$$t_{ramp} = \begin{cases} \sqrt{\frac{\|s_{cmd}\|}{\ddot{s}_{max}}} & \text{if } \dot{s}_{max} \leq \frac{\|s_{cmd}\|}{\ddot{s}_{max}} \\ \frac{\dot{s}_{max}}{\ddot{s}_{max}} & \text{if } \dot{s}_{max} > \frac{\|s_{cmd}\|}{\ddot{s}_{max}} \end{cases} \tag{6.1}$$

$$s_{ramp} = \frac{1}{2}\ddot{s}_{max}t_{ramp}^2 \tag{6.2}$$

$$s_{coast} = s_{cmd} - 2s_{ramp} \tag{6.3}$$

$$t_{coast} = \frac{s_{coast}}{\dot{s}_{max}} \tag{6.4}$$

The s acceleration necessary to follow the slew profile is calculated using the following piecewise continuous function.

$$\ddot{s}(t) = \begin{cases} \ddot{s}_{max} & \text{if } 0 \leq t < t_{ramp} \\ 0 & \text{if } t_{ramp} \leq t < t_{ramp} + t_{coast} \\ -\ddot{s}_{max} & \text{if } t \geq t_{ramp} + t_{coast} \end{cases} \tag{6.5}$$

Equations 6.1 through 6.5 are used by Algorithm 6.1 to calculate the s acceleration command throughout the transition maneuver. The inputs to the algorithm are the targeted s coordinate (s_{cmd}), the maximum s rate ($\dot{s}_{max}$), the maximum s acceleration ($\ddot{s}_{max}$), and the time since the start of the maneuver (t).

It was shown in Chapter 5 that the angular velocity of a gyrostat-satellite traversing a COMET is restricted to satisfy Eq. 5.26, which is repeated below for convenience.

$$\boldsymbol{\omega}^{po} = \sigma\mathbf{R}^{po}\mathbf{v}$$

Input : s_{cmd}, $\dot{s}_{max}$, $\ddot{s}_{max}$, t
Output: $\ddot{s}$

$t_{ramp} \leftarrow \sqrt{\frac{\|s_{cmd}\|}{\ddot{s}_{max}}}$;
if $\ddot{s}_{max} t_{ramp} > \dot{s}_{max}$ **then**
  $t_{ramp} \leftarrow \frac{\dot{s}_{max}}{\ddot{s}_{max}}$;
end
$s_{ramp} \leftarrow \frac{1}{2} \ddot{s}_{max} t_{ramp}^2$;
$s_{coast} \leftarrow s_{cmd} - 2 s_{ramp}$;
$t_{coast} \leftarrow \frac{s_{coast}}{\dot{s}_{max}}$;
if $0 \leq t < t_{ramp}$ **then**
  $\ddot{s} \leftarrow \text{sgn}\left(s_{cmd}\right) \ddot{s}_{max}$;
else if $t_{ramp} \leq t < t_{ramp} + t_{coast}$ **then**
  $\ddot{s} \leftarrow 0$;
else if $t_{ramp} + t_{coast} \leq t \leq t_{max}$ **then**
  $\ddot{s} \leftarrow -\text{sgn}\left(s_{cmd}\right) \ddot{s}_{max}$;
else
  $\ddot{s} \leftarrow 0$;
end

Algorithm 6.1: Algorithm to calculate the acceleration command ($\ddot{s}$) for a simple "ramp-coast-ramp" slew profile

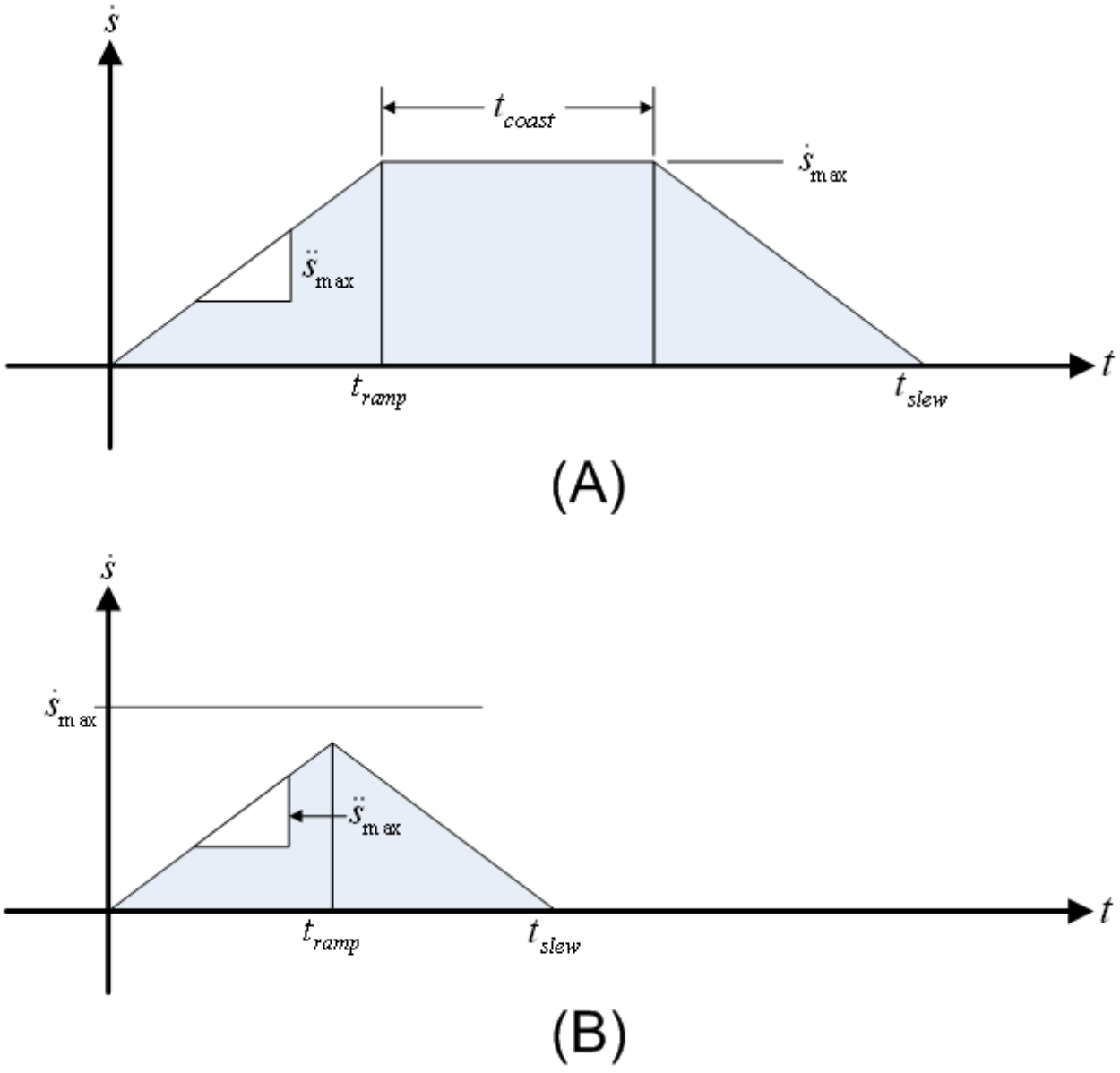

Figure 6.1: The time history of the first time derivative of the coordinate s during a transition between relative equilibria residing on the same COMET using a (A) "ramp-coast-ramp" and a (B) "ramp-ramp" profile.

The first time derivative of the angular velocity vector $\boldsymbol{\omega}_{po}$ is

$$\dot{\boldsymbol{\omega}}^{po} = \dot{\sigma}\mathbf{R}^{po}\mathbf{v} - \sigma\left(\boldsymbol{\omega}^{po}\right)^{\times}\mathbf{R}^{po}\mathbf{v} + \sigma\mathbf{R}^{po}\dot{\mathbf{v}} \tag{6.6}$$

The first time derivative σ is

$$\dot{\sigma} = \frac{\ddot{s} - \sigma\frac{\mathbf{v}^{\mathsf{T}}\dot{\mathbf{v}}}{\sqrt{\mathbf{v}^{\mathsf{T}}\mathbf{v}}}}{\sqrt{\mathbf{v}^{\mathsf{T}}\mathbf{v}}} \tag{6.7}$$

Plugging Eqs. 5.30 and 6.7 into Eqs. 5.26 and 6.6 results in

$$\boldsymbol{\omega}^{po} = \frac{\dot{s}}{\sqrt{\mathbf{v}^{\mathsf{T}}\mathbf{v}}}\mathbf{R}^{po}\mathbf{v} \tag{6.8}$$

$$\dot{\boldsymbol{\omega}}^{po} = \frac{\ddot{s} - \sigma\frac{\mathbf{v}^{\mathsf{T}}\dot{\mathbf{v}}}{\sqrt{\mathbf{v}^{\mathsf{T}}\mathbf{v}}}}{\sqrt{\mathbf{v}^{\mathsf{T}}\mathbf{v}}}\mathbf{R}^{po}\mathbf{v} + \frac{\dot{s}}{\sqrt{\mathbf{v}^{\mathsf{T}}\mathbf{v}}}\left(\mathbf{R}^{po}\dot{\mathbf{v}} - \left(\boldsymbol{\omega}^{po}\right)^{\times}\mathbf{R}^{po}\mathbf{v}\right) \tag{6.9}$$

Equation 6.8 represents the explicit functional relationship between the kinematics of the coordinate s and the kinematics of the principal reference frame with respect to the orbital reference frame. Equation 6.9 is necessary to calculate internal control torques to be applied to the rotors to execute an attitude transition.

In summary, the steps executed at each time step during the transition maneuver are listed below:

1. Algorithm 6.1 is used to calculate the s acceleration command.
2. Equation 6.9 is used to calculate the $\dot{\boldsymbol{\omega}}^{po}$ command.
3. Equation B.1 is used to calculate the internal torques to apply to the rotors.

6.1.2 Example Simulation

The purpose of this section is to present the results of a numeric simulation of a gyrostat-satellite executing a transition maneuver between relative equilibria on the same COMET using the open-loop control developed in Section 6.1.1.

An example gyrosat-satellite is simulated. The principal moments of inertia of the gyrostat-satellite are provided as Gyrostat-Satellite I in Table 5.3. A numeric simulator (presented in Appendix A) simulates the rotational dynamics of the gyrostat-satellite. Table 5.5 summarizes the key parameters for the simulation. The first four parameters (θ_1, θ_2, θ_3, and h_2^o) are independent input values defining the initial conditions of the simulations. The parameters θ_1, θ_2, and θ_3 define the initial attitude of the gyrostat-satellite using Algorithm 4.1. The parameter h_2^o does not affect the COMET but does impact dynamic quantities such as the relative angular momentum vector. The next two parameters (J_{23} and h_3^o) are derived

Table 6.1: Key parameters used in the example simulation of a gyrostat-satellite transitioning between two relative equilibria on the same COMET

Parameter	Value
θ_1	-5°
θ_2	-25°
θ_3	1.0
h_2^o	-0.2627 Nms
J_{23}	-11.0802 kg-m^2
h_3^o	-0.0363 Nms
s_{cmd}	90°
$\dot{s}_{max}$	0.1°/s
$\ddot{s}_{max}$	0.001°/s

values that remain constant throughout the simulation and are included for informational purposes. The final three parameters (s_{cmd}, $\dot{s}_{max}$, and $\ddot{s}_{max}$) define the slew "profile" used to transition from the initial to the target relative equilibrium. The parameter s_{cmd} defines the location of the target relative equilibrium on the COMET. The parameters $\dot{s}_{max}$ and $\ddot{s}_{max}$ define the maximum s velocity and the maximum s acceleration along the COMET during the transition maneuver, respectively.

Figures 6.2 through 6.10 present the results of the simulation. Figures 6.2 and 6.3 depict the path of the principal reference frame basis vectors on the unit sphere fixed in the orbital reference frame. Each figure consists of four sub-figures that each give a three-dimensional view of the unit sphere from a particular vantage point defined by the azimuth α and elevation ϵ angle noted above each view. Figure 6.2 shows the views from the $+\vec{o}_3$ hemisphere, and Figure 6.3 shows the views from the $-\vec{o}_3$ hemisphere. The paths of $\vec{p}_1$, $\vec{p}_2$, and $\vec{p}_3$ are shown as solid red, blue, and green curves on the surface of the unit sphere, respectively. The paths of $\vec{p}_1$, $\vec{p}_2$, and $\vec{p}_3$ throughout the complete COMET are shown as "dash-dot"-ed red, blue, and green curves on the surface of the unit sphere, respectively. Figure 6.4 shows the path of the vector part of the attitude quaternion throughout the transition maneuver. The red curve represents the path over the complete COMET. The green and red circles mark the initial and final attitudes of the gyrostat-satellite, respectively. The blue curve represents the path taken by the gyrostat-satellite to transition from the initial relative equilibrium to the target relative equilibrium. Figure 6.5 is a plot of the time history of the components of the attitude quaterion representing the rotation from the orbital reference frame to the principal reference frame on the abscissa and the elapsed simulation time on the ordinate. The vector components of the attitude quaternion (q_1, q_2, and q_3) are shown as blue, green, and red curves, respectively, and the scalar component (q_4) is shown as a cyan curve. Figure 6.6 is a plot of the time history of the components of the angular velocity of the principal reference frame with respect to the orbital reference frame expressed in the principal reference frame

on the abscissa and the elapsed simulation time on the ordinate. The components along $\vec{p}_1$, $\vec{p}_2$, and $\vec{p}_3$ are shown as blue, green, and red curves, respectively. The values of the products of inertia expressed in the orbital reference frame during the simulation are shown in Figure 6.7. Figure 6.8 shows the time history of the system angular momentum expressed in the orbital reference frame ($\mathbf{h}^o$). The time history of components of the relative angular momentum vector expressed in the principal reference frame ($\mathbf{h}_s$) are shown in Figure 6.9. Figure 6.10 shows the time history of the internal torque vector expressed in the principal reference frame ($\mathbf{g}_s$).

The three-dimensional figures (Figures 6.2 through 6.4) show that the COMET is a closed-curve in SO(3), and that the gyrostat-satellite is traveling along the COMET. The time histories of the system parameters (Figures 6.5 through 6.10) show that the gyrostat-satellite reaches a relative equilibrium because all of the curves are constant over the last 0.02 orbits of the simulation with the internal torques dropping to zero. As would be expected while traversing a COMET, J_{13} is zero, J_{23} is constant, and the components of the system angular momentum vector expressed in the orbital frame are constant throughout the simulation. The time history of the internal torques (Figure 6.10) clearly shows the transitions between the "ramp-up," "coast," and "ramp-down" phases of the transition maneuver, which appear as discontinuities in the curves.

6.2 Transitions Between COMATs

The purpose of this section is to investigate the problem of transitioning a gyrostat-satellite from an initial relative equilibrium to a desired target relative equilibrium that resides on a different COMET.

Section 6.2.1 gives an overview of the method proposed to execute the transition maneuver. Sections 6.2.2 and 6.2.3 describe the component steps of the method in detail. Section 6.2.4 presents the results of an example simulation of a gyrostat-satellite executing the transition maneuver. Section 6.2.5 provides a discussion of the limitations the proposed method.

6.2.1 Overview of Proposed Method

The path taken by a gyrostat-satellite during transitions between relative equilibria on the same COMET may be accomplished independent of duration of the transition. Whereas, the path and duration of transitions between relative equilibria on different COMETs are coupled. The reason for the coupling is that the system angular momentum must be adjusted so that upon reaching the target relative equilibrium attitude the system angular momentum is at the equilibrium value corresponding to the relative equilibrium attitude.

Gravitational torques experienced during the transition maneuver are used to adjust the

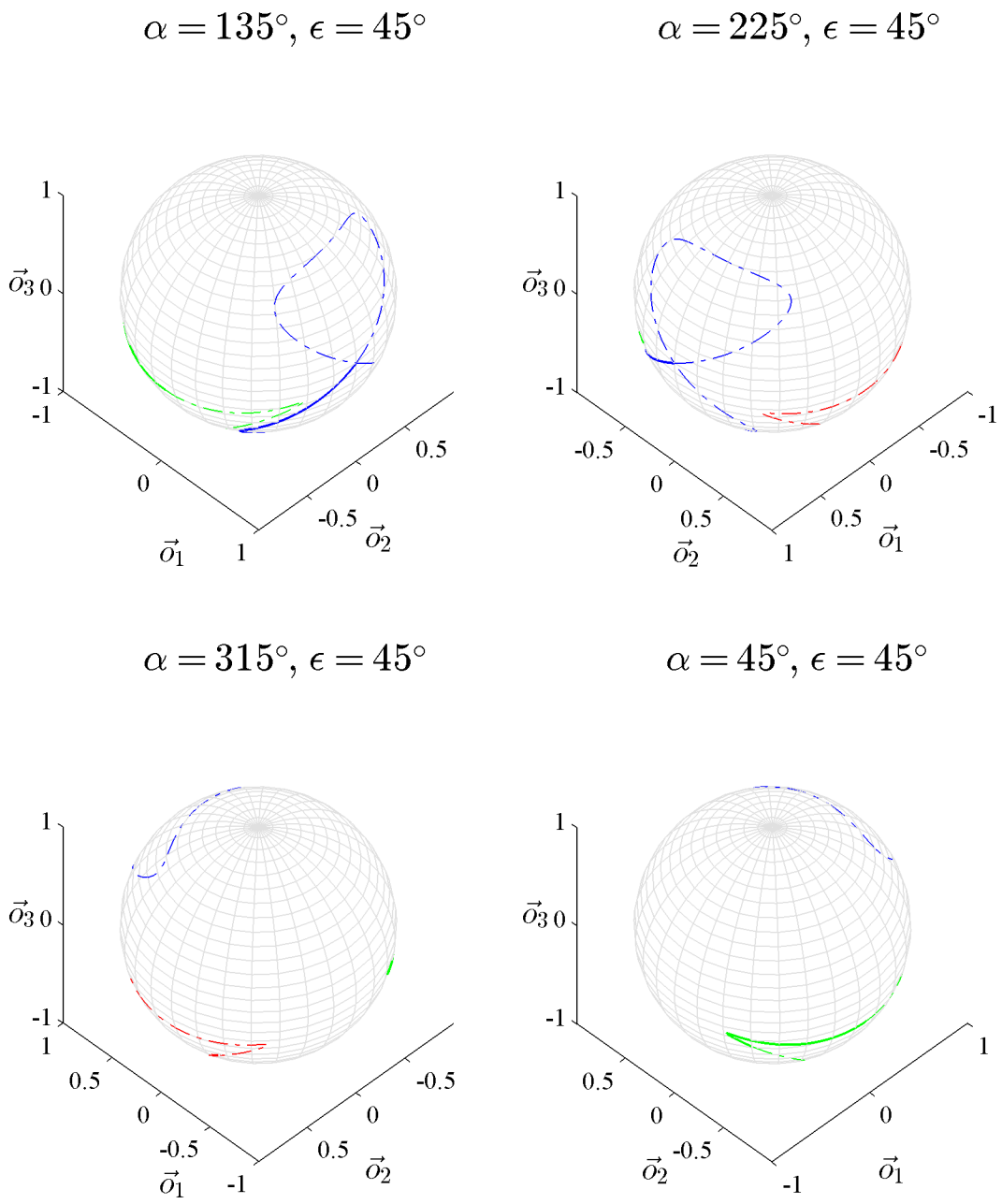

Figure 6.2: Four isometric views from the $+\vec{o}_3$ hemisphere of the paths of the principal frame basis axes on the unit sphere fixed in the orbital reference frame during a transition between two relative equilibria on the same COMET

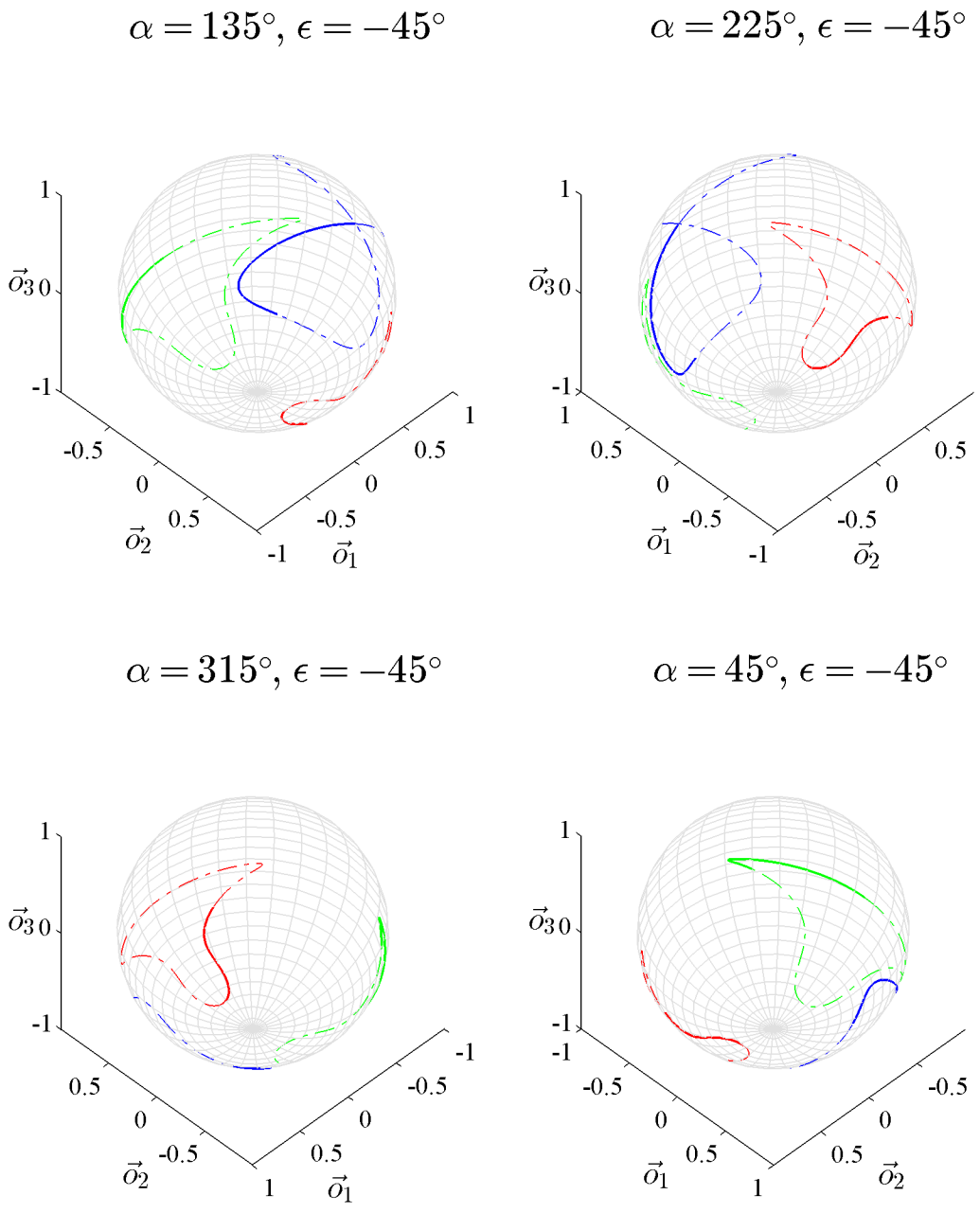

Figure 6.3: Four isometric views from the -$\vec{o}_3$ hemisphere of the paths of the principal frame basis axes on the unit sphere fixed in the orbital reference frame during a transition between two relative equilibria on the same COMET

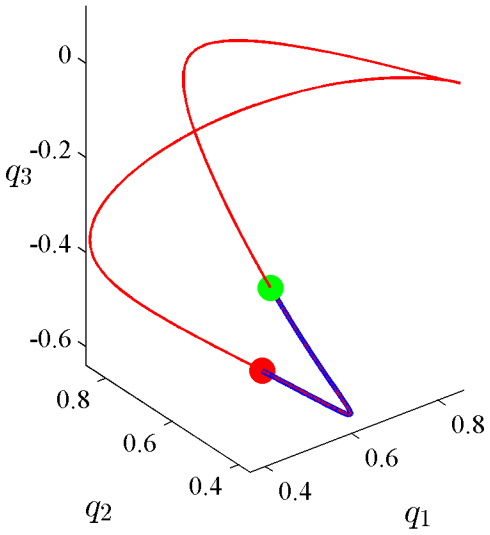

Figure 6.4: Path in the configuration space of the vector part of the attitude quaternion ($\vec{q}^{po}$) of a transition between two relative equilibria on the same COMET overlaid on the COMET path

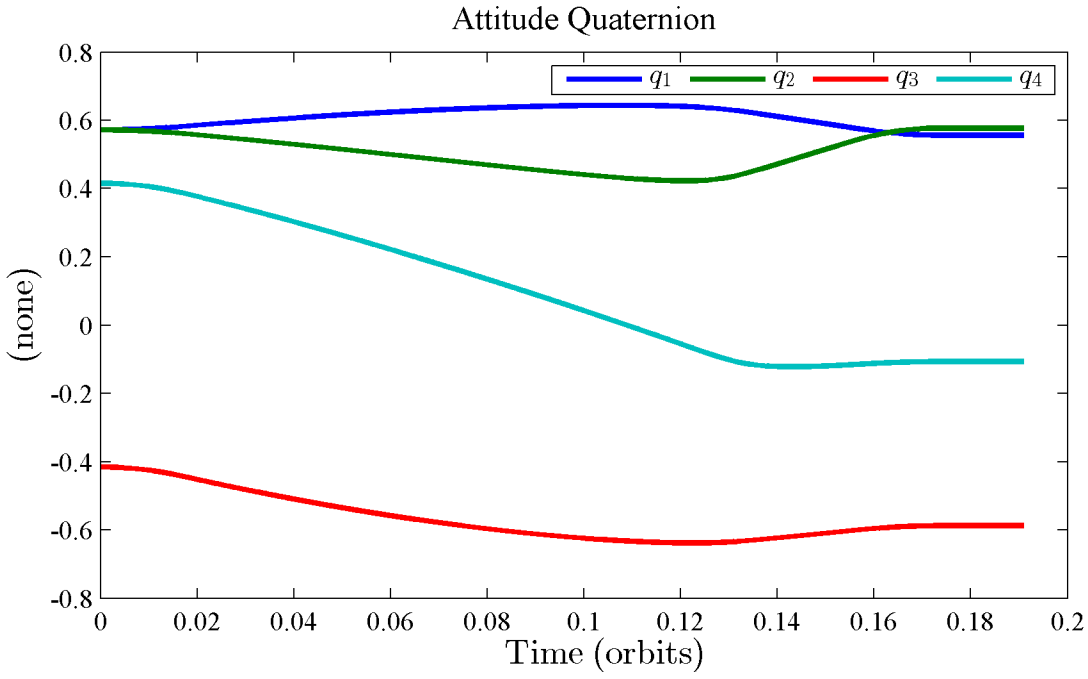

Figure 6.5: Components of the attitude quaternion ($\bar{q}^{po}$) during a transition between two relative equilibria on the same COMET

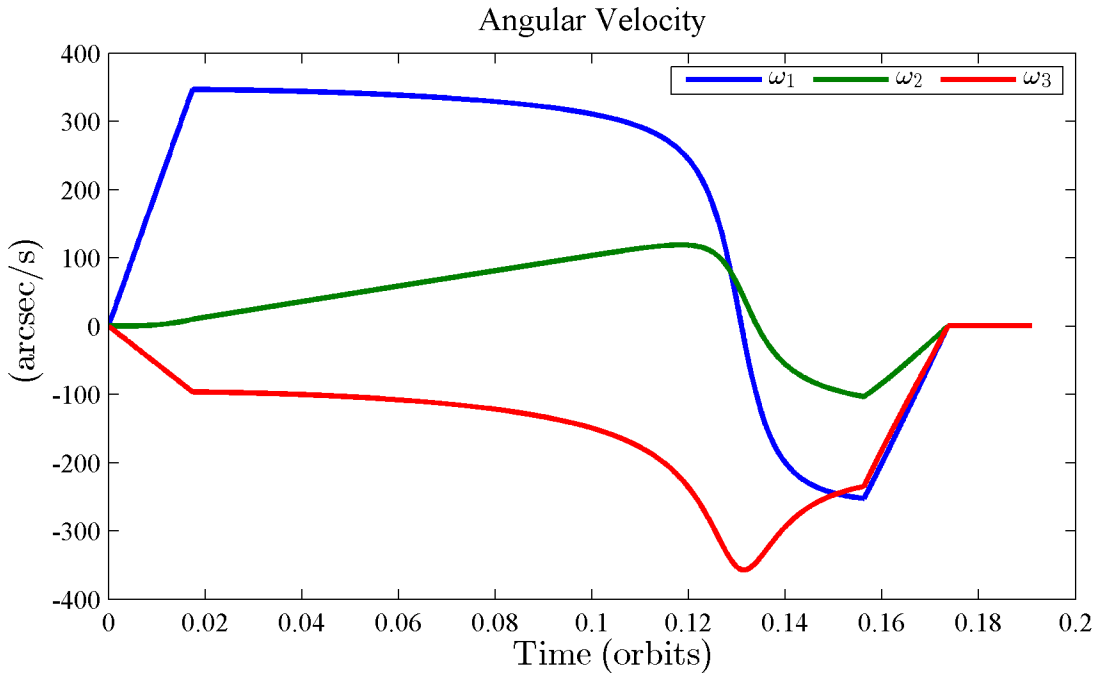

Figure 6.6: Components of the angular velocity of the princpal reference frame with respect to the orbital reference frame expressed in the principal reference frame ($\boldsymbol{\omega}^{po}$) during a transition between two relative equilibria on the same COMET

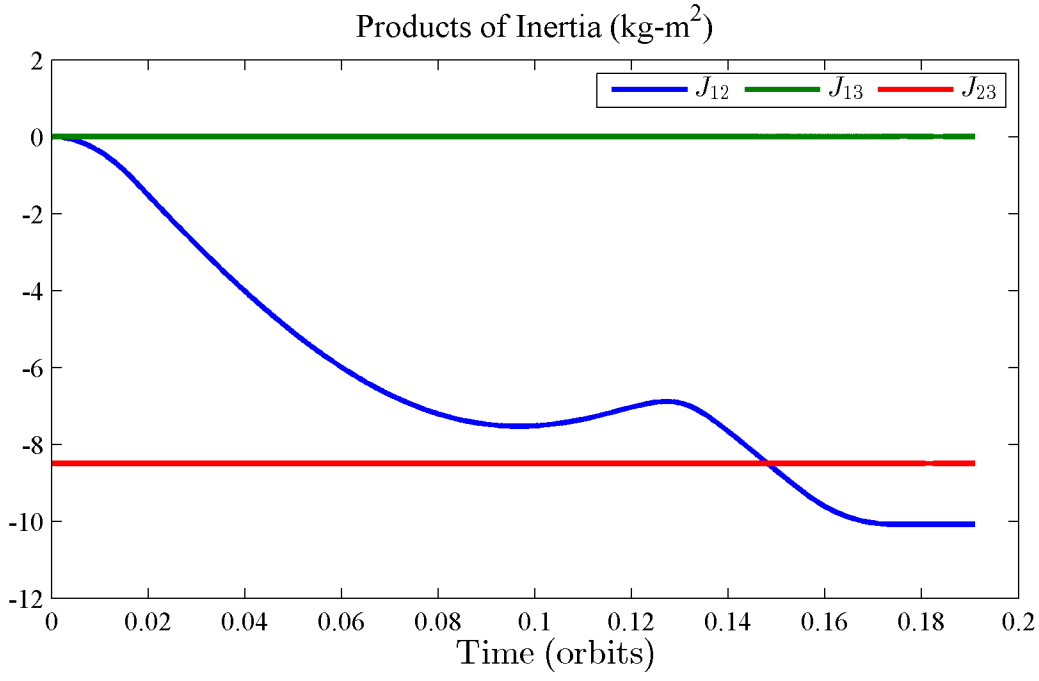

Figure 6.7: Products of inertia expressed in the orbital reference frame (J_{12}, J_{13}, and J_{23}) during a transition between two relative equilibria on the same COMET

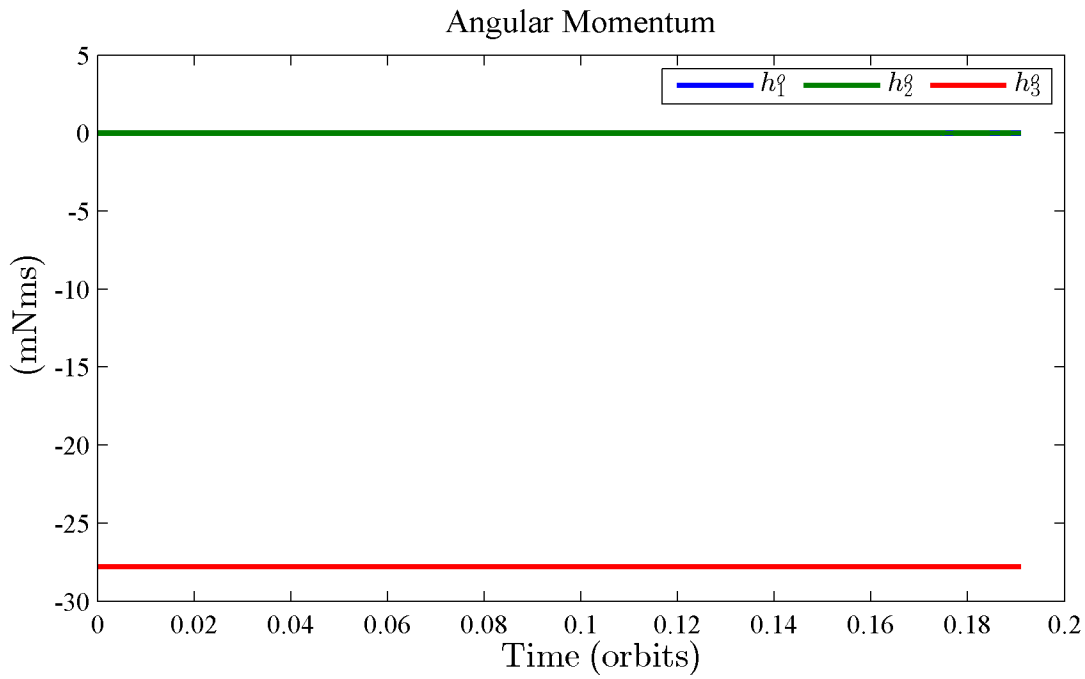

Figure 6.8: Components of the system angular momentum vector expressed in the orbital reference frame ($\mathbf{h}^o$) during a transition between two relative equilibria on the same COMET

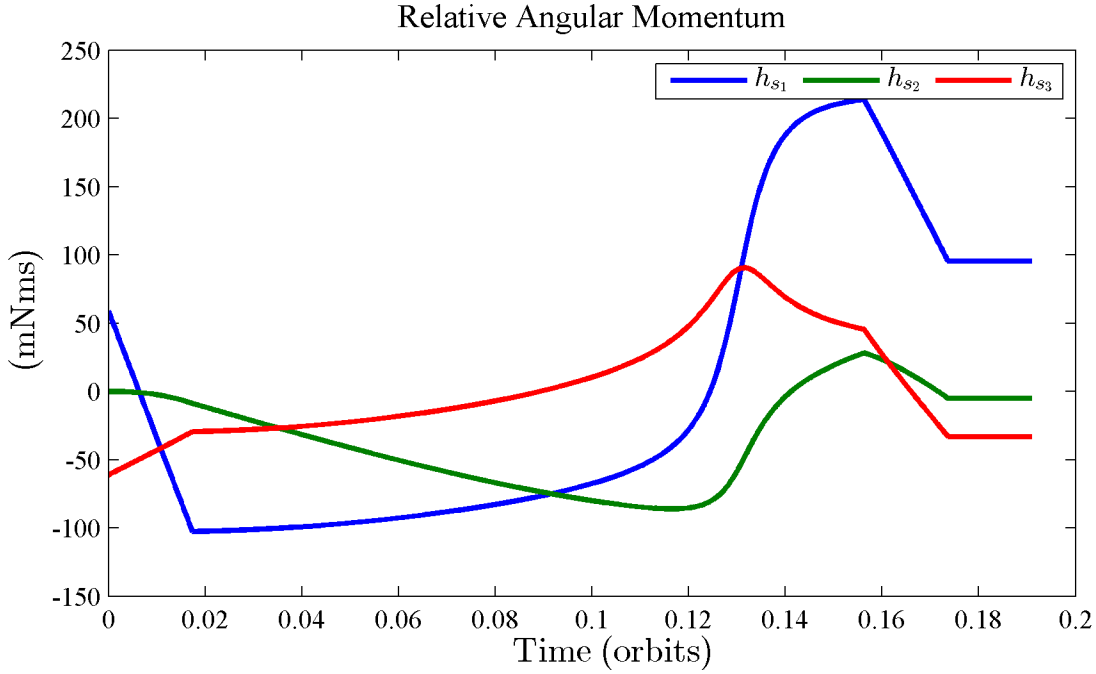

Figure 6.9: Components of the relative angular momentum vector expressed in the principal reference frame ($\mathbf{h}_s$) during a transition between two relative equilibria on the same COMET

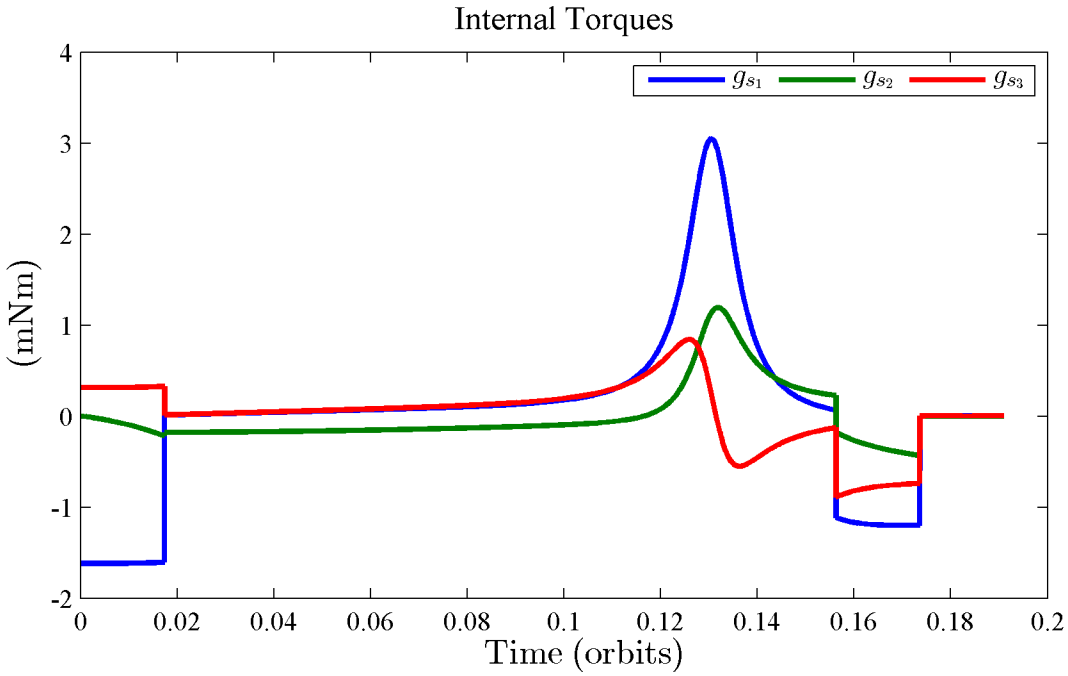

Figure 6.10: Components of the internal torque vector expressed in the principal reference frame ($\mathbf{g}_s$) during a transition between two relative equilibria on the same COMET

system angular momentum of the gyrostat-satellite. As shown in Chapter 3, gravitational torque is a function of gyrostat-satellite's interia matrix expressed in the principal reference frame and the attitude of the gyrostat-satellite relative to the orbital reference frame. Therefore, the attitude trajectory used to accomplished the transition maneuver must be designed such that

1. the terminal attitude is a relative equilibrium attitude,
2. the terminal angular velocity with respect to the orbital reference frame is $\vec{0}$, and
3. the terminal system angular momentum is equal to the equilibrium value of the target relative equilibrium.

In Chapter 5, it was shown that the dynamics of the system angular momentum expressed in the orbital reference frame are a function of the products of inertia expressed in the orbital reference frame (specifically J_{13} and J_{23}). Therefore, the correct adjustment of the system angular momentum may be accomplished by designing a time history of the products of inertia expressed in the orbital reference frame. The time histories of the products of inertia are parameterized as polynomial functions of the quantity $\omega_o t$. The attitude trajectory requirements (enumerated above) are mapped to a set of boundary conditions on the system angular momentum and products of inertia. The coefficients of the polynomials are calculated so that the boundary conditions are satisfied. Section 6.2.2 derives and describes the

set of equations and algorithms used to calculate the coefficients of the polynomials. The time history of the products of inertia is mapped to a continuous attitude trajectory that begins at the initial relative equilibrium attitude, takes a path that correctly adjusts the system angular momentum, and ends at the target relative equilibrium attitude. Section 6.2.3 derives the equations necessary to map the time history of the products of inertia to an attitude trajectory.

6.2.2 Product of Inertia Trajectories

The first step in determining an attitude trajectory that successfully transitions a gyrostat-satellite from an initial relative equilibrium to a desired target relative equilibrium is determining the time histories of the 1-3 and 2-3 product of inertia expressed in the orbital reference frame. The equations and algorithms required to determine the time histories of the products of inertia are derived and discussed in this section. First, the time history of J_{13} is addressed, and then the time history of J_{23}.

Time History of J_{13}

The functional relationship of the dynamics of the pitch system angular momentum to the 1-3 component of the inertia matrix expressed in the orbital reference frame (J_{13}) is defined by Eq. 5.5, and is repeated below for convenience.

$$\dot{h}_2^o = 3\omega_o^2 J_{13}$$

The Laplace transform of Eq. 5.5 is

$$sH_2^o - h_2^o(0) = 3\omega_o^2 \mathcal{L}\left[J_{13}\right] \tag{6.10}$$

Solving for the Laplace transform of h_2^o (H_2^o) results in

$$H_2^o = \frac{h_2^o(0) + 3\omega_o^2 \mathcal{L}\left[J_{13}\right]}{s} \tag{6.11}$$

The inverse Laplace transform is applied Eq. 6.11 to determine the time domain solution to Eq. 5.5.

$$h_2^o(t) = h_2^o(0) + 3\omega_o^2 \int_0^t J_{13}(\tau) d\tau \tag{6.12}$$

As discussed in Section 6.2.1, the 1-3 product of inertia (J_{13}) is parameterized as a polynomial function of the quantity $\omega_o t$.

$$J_{13}(t) = J_{13}(0) + \sum_{k=2}^{n} a_k \omega_o^k t^k \tag{6.13}$$

The variable a_k is the coefficient of the k-th order term of the polynomial. The first time derivative of Eq. 6.13 is

$$\dot{J}_{13}(t) = \sum_{k=2}^{n} k a_k \omega_o^k t^{k-1} \tag{6.14}$$

The definite integral of Eq. 6.13 from 0 to t is

$$\int_0^t J_{13}(\tau) d\tau = J_{13}(0)t + \sum_{k=2}^{n} a_k \omega_o^k \frac{t^{k+1}}{k+1} \tag{6.15}$$

Plugging Eq. 6.15 into Eq. 6.12 results in

$$h_2^o(t) = h_2^o(0) + 3\omega_o^2 J_{13}(0)t + \sum_{k=2}^{n} a_k \omega_o^k \frac{t^{k+1}}{k+1} \tag{6.16}$$

The attitude trajectory requirements (enumerated in Section 6.2.1) are mapped to a set of boundary conditions on the system angular momentum and products of inertia. It is assumed that the initial state of the gyrostat-satellite is a relative equilibrium so that the following boundary conditions are satisfied.

$$\dot{J}_{13}(0) = 0 \tag{6.17}$$
$$J_{13}(0) = 0 \tag{6.18}$$
$$\dot{h}_2^o(0) = 0 \tag{6.19}$$
$$h_2^o(0) = h_{2_0}^o \tag{6.20}$$

The starting boundary conditions on J_{13} and $\dot{h}_2^o$ (Eqs. 6.17 through 6.20) are satisfied for any values selected for a_k due to the exclusion of the 1st order term from the polynomial parameterization of the time history of J_{13}. The terminal boundary conditions of the transition maneuver are

$$\dot{J}_{13}(T) = 0 \tag{6.21}$$
$$J_{13}(T) = 0 \tag{6.22}$$
$$\dot{h}_2^o(T) = 0 \tag{6.23}$$
$$h_2^o(T) = h_{2_T}^o \tag{6.24}$$

The terminal boundary conditions on J_{13} and $\dot{h}_2^o$ are redundant due to their functional relationship (Eq. 5.5). Therefore, the independent terminal boundary conditions that must be satisfied are Eqs. 6.23, 6.22, and 6.24. Equations 6.23 and 6.22 require that the gyrostat-satellite is at a relative equilibrium, whereas, Eq. 6.24 ensures that the pitch system angular momentum is at its target value at the end of the transition maneuver.

The independent set of terminal boundary conditions form a system of three equations that consist of linear terms of the J_{13} polynomial coefficients. The system of equations may be written as

$$\mathbf{C}_a\mathbf{a} = \mathbf{c}_a \tag{6.25}$$

where

$$\mathbf{C}_a = \begin{bmatrix} \omega_o^2T^2 & \cdots & \omega_o^iT^i & \cdots & \omega_o^nT^n \\ 2\omega_o^2T & \cdots & i\omega_o^iT^{i-1} & \cdots & n\omega_o^nT^{n-1} \\ \omega_o^4T^3 & \cdots & 3/(i+1)\omega_o^{2+i}T^{i+1} & \cdots & 3/(n+1)\omega_o^{2+n}T^{n+1} \end{bmatrix} \tag{6.26}$$

$$\mathbf{a} = \begin{bmatrix} a_2 & \cdots & a_i & \cdots & a_n \end{bmatrix}^\mathsf{T} \tag{6.27}$$

$$\mathbf{c}_a = \begin{bmatrix} 0 & 0 & h^o_{2_T} - h^o_{2_0} \end{bmatrix}^\mathsf{T} \tag{6.28}$$

If the parameter n in Eq. 6.13 is selected to be greater than four, the system is underdetermined and there are (in general) an infinite number of solutions for $\mathbf{a}$ that satisfy the system of equations. The selected solution for $\mathbf{a}$ is chosen as the solution that minimizes the magnitude of $\mathbf{a}$. The selected solution for $\mathbf{a}$ is calculated using

$$\mathbf{a} = \mathbf{C}_a^+\mathbf{c}_a \tag{6.29}$$

The operation $(\cdot)^+$ is the Moore-Penrose pseudoinverse.

Time History of J_{23}

The dynamics of the "roll" and yaw system angular momenta form a second order coupled system defined by Eqs. 5.4 and 5.6.

$$\begin{aligned} \dot{h}^o_1 - \omega_o h^o_3 &= -3\omega_o^2 J_{23} \\ \dot{h}^o_3 + \omega_o h^o_1 &= 0 \end{aligned}$$

Solving Eq. 5.4 for $\dot{h}^o_1$ results in

$$\dot{h}^o_1 = -\frac{\ddot{h}^o_3}{\omega_o} \tag{6.30}$$

Plugging Eq. 6.30 into Eq. 5.6 results in

$$\ddot{h}^o_3 + \omega_o^2 h^o_3 = 3\omega_o^3 J_{23} \tag{6.31}$$

Equation 6.31 defines the functional relationship of the dynamics of the yaw system angular momentum to the 2-3 component of the inertia matrix expressed in the orbital reference frame (J_{23}). The Laplace transform of Eq. 6.31 is

$$s^2H^o_3 - sh^o_3(0) - \dot{h}^o_3(0) + \omega_o^2 H^o_3 = 3\omega_o^3\mathcal{L}\left[J_{23}\right] \tag{6.32}$$

Solving for the Laplace transform of h_3^o (H_3^o) results in

$$H_3^o = \frac{sh_3^o(0) + \dot{h}_3^o(0) + 3\omega_o^3 \mathcal{L}\left[J_{23}\right]}{s^2 + \omega_o^2} \tag{6.33}$$

The inverse Laplace transform is applied Eq. 6.33 to determine the time domain solution.

$$h_3^o(t) = h_3^o(0)\cos\left(\omega_o t\right) + \frac{\dot{h}_3^o(0)}{\omega_o}\sin\left(\omega_o t\right) + 3\omega_o^3 \mathcal{L}^{-1}\left[\frac{\mathcal{L}\left[J_{23}\right]}{s^2 + \omega_o^2}\right] \tag{6.34}$$

As discussed in Section 6.2.1, the 2-3 product of inertia (J_{23}) is parameterized as a polynomial function of the quantity $\omega_o t$.

$$J_{23}(t) = J_{23}(0) + \sum_{k=2}^{n} b_k \omega_o^k t^k \tag{6.35}$$

The variable b_k is the coefficient of the k-th order term of the polynomial. The first time derivative of Eq. 6.35 is

$$\dot{J}_{23}(t) = \sum_{k=2}^{n} k b_k \omega_o^k t^{k-1} \tag{6.36}$$

The Laplace transform of Eq. 6.35 is

$$\mathcal{L}\left[J_{23}(t)\right] = \frac{J_{23}(0)}{s} + \sum_{k=2}^{n} b_k \omega_o^k \frac{k!}{s^{k+1}} \tag{6.37}$$

Plugging Eq. 6.37 into the inverse Laplace transform portion of the last term in Eq. 6.34 gives

$$\mathcal{L}^{-1}\left[\frac{\mathcal{L}\left[J_{23}(t)\right]}{s^2 + \omega_o^2}\right] = J_{23}(0)\cos\omega_o t + \sum_{k=2}^{n} b_k \omega_o^k k! \mathcal{L}^{-1}\left[\frac{1}{s^{k+1}(s^2 + \omega_o^2)}\right] \tag{6.38}$$

The inverse Laplace transform remaining in Eq. 6.38 for even values of $k+1$ is

$$\mathcal{L}^{-1}\left[\frac{1}{s^i(s^2 + \omega_o^2)}\right] = \varsigma(i)\left(-\frac{\sin\omega_o t}{\omega_o^{i+1}} + \sum_{j=0}^{i/2-1}(-1)^j \frac{t^{2j+1}}{(2j+1)!\omega_o^{i-2j}}\right) \tag{6.39}$$
$$\{i | i \in 2\mathbf{Z},\ i > 0\}$$

The inverse Laplace transform remaining in Eq. 6.38 for odd values of $k+1$ is

$$\mathcal{L}^{-1}\left[\frac{1}{s^i(s^2 + \omega_o^2)}\right] = \varsigma(i)\left(-\frac{\cos\omega_o t}{\omega_o^{i+1}} + \sum_{j=0}^{(i-1)/2}(-1)^j \frac{t^{2j}}{(2j)!\omega_o^{i-2j+1}}\right) \tag{6.40}$$
$$\{i | i \in 2\mathbf{Z}+1,\ i > 0\}$$

The function $\varsigma(k)$ is defined

$$\varsigma(i) = \begin{cases} +1, & (i-1 \bmod 4) \leq 1 \\ -1, & (i-1 \bmod 4) \geq 2 \end{cases} \tag{6.41}$$

The attitude trajectory requirements (enumerated in Section 6.2.1) are mapped to a set of boundary conditions on the yaw system angular momentum and the 2-3 product of inertia. It is assumed that the initial state of the gyrostat-satellite is a relative equilibrium so that the following boundary conditions are satisfied.

$$\dot{J}_{23}(0) = 0 \tag{6.42}$$
$$J_{23}(0) = J_{23_0} \tag{6.43}$$
$$\dot{h}_3^o(0) = 0 \tag{6.44}$$
$$h_3^o(0) = h_{3_0}^o \tag{6.45}$$

The starting boundary conditions on J_{23} (Eqs. 6.42 through 6.43) are satisfied for any values selected for b_k due to the exclusion of the 1st order term from the polynomial parameterization of the time history of J_{23}. The terminal boundary conditions of the transition maneuver are

$$\dot{J}_{23}(T) = 0 \tag{6.46}$$
$$J_{23}(T) = J_{23_T} \tag{6.47}$$
$$\dot{h}_3^o(T) = 0 \tag{6.48}$$
$$h_3^o(T) = h_{3_T}^o \tag{6.49}$$

Equations 6.48 and 6.46 require that the gyrostat-satellite is at a relative equilibrium. Equations 6.47 and 6.49 ensure that the yaw system angular momentum is at its target equilibrium value at the end of the transition maneuver.

The terminal boundary conditions form a system of four equations that consist of linear terms of the J_{23} polynomial coefficients. The system of equations may be written as

$$\mathbf{C}_b\mathbf{b} = \mathbf{c}_b \tag{6.50}$$

where

$$\mathbf{C}_b = \begin{bmatrix} \omega_o^2 T^2 & \cdots & \omega_o^i T^i & \cdots & \omega_o^n T^n \\ \omega_o^2 T & \cdots & \omega_o^i T^{i-1} & \cdots & \omega_o^n T^{n-1} \\ f(2,\omega_o,T) & \cdots & f(i,\omega_o,T) & \cdots & f(n,\omega_o,T) \\ d(2,\omega_o,T) & \cdots & d(i,\omega_o,T) & \cdots & d(n,\omega_o,T) \end{bmatrix} \tag{6.51}$$

$$\mathbf{b} = \begin{bmatrix} b_2 & \cdots & b_i & \cdots & b_n \end{bmatrix}^\mathsf{T} \tag{6.52}$$

$$\mathbf{c}_b = \begin{bmatrix} J_{23_T} - J_{23_0} & 0 & h_{3_T}^o - h_{3_0}^o & 0 \end{bmatrix}^\mathsf{T} \tag{6.53}$$

The functions f and d are calculated using Algorithms 6.2 and 6.3, which make use of Equations 6.38 through 6.41.

Input : i, t, ω_o
Output: f

if $(i \bmod 4) \leq 1$ **then**
  $\varsigma \leftarrow +1$;
else if $(i \bmod 4) \geq 2$ **then**
  $\varsigma \leftarrow -1$;
end
$i \leftarrow i + 1$;
if $(i \bmod 2) == 0$ **then**
  $x \leftarrow -\frac{\sin \omega_o t}{\omega_o^{i+1}} + \sum_{j=0}^{i/2-1} (-1)^j \frac{t^{2j+1}}{(2j+1)! \omega_o^{i-2j}}$;
else if $(i \bmod 2) == 1$ **then**
  $x \leftarrow -\frac{\cos \omega_o t}{\omega_o^{i+1}} + \sum_{j=0}^{(i-1)/2} (-1)^j \frac{t^{2j}}{(2j)! \omega_o^{i-2j+1}}$;
end
$f \leftarrow 3\omega_o^{3+i-1}(i-1)! \varsigma x$;

Algorithm 6.2: Algorithm to calculate the i-th entry in the third row of $\mathbf{C}_{23}$ coefficient matrix

Input : i, t, ω_o
Output: d

if $(i \bmod 4) \leq 1$ **then**
  $\varsigma \leftarrow +1$;
else if $(i \bmod 4) \geq 2$ **then**
  $\varsigma \leftarrow -1$;
end
$i \leftarrow i + 1$;
if $(i \bmod 2) == 0$ **then**
  $x \leftarrow -\frac{\cos \omega_o t}{\omega_o^{i}} + \sum_{j=0}^{i/2-1} (2j+1)(-1)^j \frac{t^{2j}}{(2j+1)! \omega_o^{i-2j}}$;
else if $(i \bmod 2) == 1$ **then**
  $x \leftarrow \frac{\sin \omega_o t}{\omega_o^{i}} + \sum_{j=0}^{(i-1)/2} (2j)(-1)^j \frac{t^{2j-1}}{(2j)! \omega_o^{i-2j+1}}$;
end
$d \leftarrow 3\omega_o^{3+i-1}(i-1)! \varsigma x$;

Algorithm 6.3: Algorithm to calculate the i-th entry in the fourth row of $\mathbf{C}_{23}$ coefficient matrix

If the parameter n in Eq. 6.35 is selected to be greater than four, the system is underdetermined and there are (in general) an infinite number of solutions for $\mathbf{b}$ that satisfy the system of equations. The selected solution for $\mathbf{b}$ is chosen as the solution that minimizes the magnitude of $\mathbf{b}$. The selected solution for $\mathbf{b}$ is calculated using

$$\mathbf{b} = \mathbf{C}_b^+ \mathbf{c}_b \tag{6.54}$$

The operation $(\cdot)^+$ is the Moore-Penrose pseudoinverse.

6.2.3 Open-Loop Control Law

The open-loop control torques to be commanded to the rotors are defined by Eq. B.1 developed in Appendix B, and are repeated here for convenience.

$$\mathbf{g}_s = -\mathbf{I}\left(\dot{\boldsymbol{\omega}}^{po} + \omega_o \left(\boldsymbol{\omega}^{po}\right)^{\times} \mathbf{o}_2\right) - \left(\boldsymbol{\omega}^{pi}\right)^{\times} \mathbf{h} + 3\omega_o^2 \mathbf{o}_3^{\times} \mathbf{I}\mathbf{o}_3$$

The open-loop control law (Eq. B.1) is fully defined over a transition maneuver given an initial system state and the time history of the angular acceleration of the principal reference frame with respect to the orbital reference frame ($\dot{\boldsymbol{\omega}}^{po}$). The initial system state is the relative equilibrium of the gyrostat-satellite prior to the transition maneuver. The time history of $\dot{\boldsymbol{\omega}}^{po}$ is calculated based on the time history of J_{13} and J_{23} calculated in the previous section.

The time histories of J_{13} and J_{23} are related to the kinematics of the principal reference frame with respect to the orbital reference frame through Eq. 5.23. Equation 5.23 is rewritten as

$$\dot{\mathbf{p}}_{cmd} = \mathbf{M}\mathbf{R}^{op}\boldsymbol{\omega}_{po} \tag{6.55}$$

where

$$\dot{\mathbf{p}}_{cmd} = \begin{bmatrix} j_{23}^{cmd} & j_{13}^{cmd} \end{bmatrix}^{\mathsf{T}} \tag{6.56}$$

and

$$\mathbf{M} = \begin{bmatrix} J_{22} - J_{33} & -J_{12} & J_{13} \\ J_{12} & J_{33} - J_{11} & -J_{23} \end{bmatrix} \tag{6.57}$$

The angular velocity ($\boldsymbol{\omega}^{po}$) required to follow a commanded time history of the products of inertia is calculated using

$$\boldsymbol{\omega}^{po} = \mathbf{R}^{po}\mathbf{P}\dot{\mathbf{p}}_{cmd} \tag{6.58}$$

where $\mathbf{P}$ is the Moore-Penrose pseudoinverse of the matrix $\mathbf{M}$. The corresponding angular acceleration ($\dot{\boldsymbol{\omega}}^{po}$) is calculated using

$$\dot{\boldsymbol{\omega}}^{po} = -(\boldsymbol{\omega}^{po})^{\times}\mathbf{R}^{po}\mathbf{P}\dot{\mathbf{p}}_{cmd} + \mathbf{R}^{po}\dot{\mathbf{P}}\dot{\mathbf{p}}_{cmd} + \mathbf{R}^{po}\mathbf{P}\ddot{\mathbf{p}}_{cmd} \tag{6.59}$$

The vectors $\dot{\mathbf{p}}_{cmd}$ and $\ddot{\mathbf{p}}_{cmd}$ are the first and second time derivatives of polynomial functions. The Moore-Penrose pseudoinverse of $\mathbf{M}$ ($\mathbf{P}$) can be written as

$$\mathbf{P} = \mathbf{M}^{+} = \mathbf{M}^{\mathsf{T}}\mathbf{N}^{-1} \tag{6.60}$$

where

$$\mathbf{N} = \mathbf{M}\mathbf{M}^{\mathsf{T}} \tag{6.61}$$

$$= \begin{bmatrix} (J_{22}-J_{33})^2+J_{12}^2+J_{13}^2 & J_{12}(J_{11}+J_{22}-2J_{33})-J_{13}J_{23} \\ J_{12}(J_{11}+J_{22}-2J_{33})-J_{13}J_{23} & J_{12}^2+(J_{11}-J_{33})^2+J_{23}^2 \end{bmatrix} \tag{6.62}$$

The first time derivative of the $\mathbf{P}$ matrix is

$$\dot{\mathbf{P}} = \dot{\mathbf{M}}^{\mathsf{T}}\mathbf{N}^{-1} - \mathbf{M}^{\mathsf{T}}\mathbf{N}^{-1}\dot{\mathbf{N}}\mathbf{N}^{-1} \tag{6.63}$$

where

$$\dot{\mathbf{M}} = \begin{bmatrix} \dot{J}_{22}-\dot{J}_{33} & -\dot{J}_{12} & \dot{J}_{13} \\ \dot{J}_{12} & \dot{J}_{33}-\dot{J}_{11} & -\dot{J}_{23} \end{bmatrix} \tag{6.64}$$

and

$$\dot{\mathbf{N}} = \begin{bmatrix} \dot{N}_{11} & \dot{N}_{12} \\ \dot{N}_{21} & \dot{N}_{22} \end{bmatrix} \tag{6.65}$$

$$\dot{N}_{11} = 2(J_{22}-J_{33})(\dot{J}_{22}-\dot{J}_{33}) + 2J_{12}\dot{J}_{12} + 2J_{13}\dot{J}_{13} \tag{6.66}$$

$$\dot{N}_{12} = \dot{J}_{12}(J_{11}+J_{22}-2J_{33}) + J_{12}(\dot{J}_{11}+\dot{J}_{22}-2\dot{J}_{33}) - \dot{J}_{13}J_{23} - J_{13}\dot{J}_{23} \tag{6.67}$$

$$\dot{N}_{21} = \dot{N}_{12} \tag{6.68}$$

$$\dot{N}_{22} = 2J_{12}\dot{J}_{12} + 2(J_{11}-J_{33})(\dot{J}_{11}-\dot{J}_{33}) + 2J_{23}\dot{J}_{23} \tag{6.69}$$

Equations 6.58 and 6.59 combined with the initial relative equilibrium of the gyrostat-satellite fully define the transition from the initial relative equilibrium to a relative equilibrium on the target COMET.

In summary, the steps executed to accomplish the transition maneuver are listed below:

1. Prior to the start of the maneuver, Eqs. 6.29 and 6.54 are used to calculate the polynomial coefficients defining the values of $\mathbf{p}_{cmd}$, $\dot{\mathbf{p}}_{cmd}$, and $\ddot{\mathbf{p}}_{cmd}$ to command throughout the maneuver.
2. At each time step during the maneuver,
   (a) The values of $\mathbf{p}_{cmd}$, $\dot{\mathbf{p}}_{cmd}$, and $\ddot{\mathbf{p}}_{cmd}$ are calculated based on the polynomial coefficients.
   (b) Equation 6.59 is used to calculate the $\dot{\boldsymbol{\omega}}^{po}$ command.
   (c) Equation B.1 is used to calculate the internal torques to apply to the rotors.

Table 6.2: Key parameters used in the example simulation of a gyrostat-satellite transitioning between two relative equilibria on different COMETs

Parameter	Value
$\theta_1(0)$	-36°
$\theta_2(0)$	-36°
$\theta_3(0)$	1.0
$h_2^o(0)$	0 Nms
$\theta_1(T)$	-54°
$\theta_2(T)$	-54°
$\theta_3(T)$	1.0
$h_2^o(T)$	0 Nms
T	1.2 orbits
$\dot{s}_{max}$	0.1°/s
$\ddot{s}_{max}$	0.001°/s

6.2.4 Example Simulation

The purpose of this section is to present the results of the numeric simulation of a gyrostat-satellite executing a transition maneuver between relative equilibria on different COMETs. An example gyrosat-satellite is simulated. The principal moments of inertia of the gyrostat-satellite are provided as Gyrostat-Satellite I in Table 5.3. A numeric simulator (presented in Appendix A) simulates the rotational dynamics of the gyrostat-satellite.

Table 6.2 summarizes the key parameters for the example simulation. The first four parameters ($\theta_1(0)$, $\theta_2(0)$, $\theta_3(0)$, and $h_2^o(0)$) define the initial conditions of the simulations, and thus the initial relative equilibrium. The fifth through eighth parameters ($\theta_1(T)$, $\theta_2(T)$, $\theta_3(T)$, and $h_2^o(T)$) define the target relative equilibrium. The parameters θ_1, θ_2, and θ_3 define the relative equilibrium attitude of the gyrostat-satellite using Algorithm 4.1. The parameter h_2^o affects dynamic quantities such as the relative angular momentum vector. The parameter T defines the duration of the transition from the initial to the target COMET. The final two parameters ($\dot{s}_{max}$ and $\ddot{s}_{max}$) define the slew profile used to transition to the target relative equilibrium once the target COMET has been reached. The parameters $\dot{s}_{max}$ and $\ddot{s}_{max}$ define the maximum s velocity and the maximum s acceleration along the COMET during the transition maneuver, respectively.

Figures 6.11 through 6.19 present the results of the simulation. Figures 6.11 and 6.12 depict the paths of the principal reference frame basis vectors on the unit sphere fixed in the orbital reference frame. Each figure consists of four sub-figures that each give a three-dimensional view of the unit sphere from a particular vantage point defined by the azimuth α and elevation ϵ angle noted above each view. Figure 6.11 shows the views from the $+\vec{o}_3$ hemisphere, and

Figure 6.12 shows the views from the $-\vec{o}_3$ hemisphere. The paths of $\vec{p}_1$, $\vec{p}_2$, and $\vec{p}_3$ are shown as solid red, blue, and green curves on the surface of the unit sphere, respectively. The paths of $\vec{p}_1$, $\vec{p}_2$, and $\vec{p}_3$ through the complete initial COMET are shown as dotted red, blue, and green curves on the surface of the unit sphere, respectively. The paths of $\vec{p}_1$, $\vec{p}_2$, and $\vec{p}_3$ through the complete target COMET are shown as "dash-dot"-ed red, blue, and green curves on the surface of the unit sphere, respectively. Figure 6.13 shows the path of the vector part of the attitude quaternion throughout the transition maneuver. The green curve represents the path over the complete initial COMET. The red curve represents the path over the complete target COMET. The green and red circles mark the initial and final attitudes of the gyrostat-satellite, respectively. The blue curve represents the path taken by the gyrostat-satellite to transition from the initial relative equilibrium to the target relative equilibrium. Figure 6.14 is a plot of the time history of the components of the attitude quaternion representing the rotation from the orbital reference frame to the principal reference frame on the abscissa and the elapsed simulation time on the ordinate. The vector components of the attitude quaternion (q_1, q_2, and q_3) are shown as blue, green, and red curves, respectively, and the scalar component (q_4) is shown as a cyan curve. Figure 6.15 is a plot of the time history of the components of the angular velocity of the principal reference frame with respect to the orbital reference frame in the principal reference frame on the abscissa and the elapsed simulation time on the ordinate. The components along $\vec{p}_1$, $\vec{p}_2$, and $\vec{p}_3$ are shown as blue, green, and red curves, respectively. The values of the products of inertia expressed in the orbital reference frame during the simulation are shown in Figure 6.16. Figure 6.17 shows the time history of the total system angular momentum expressed in the orbital reference frame ($\mathbf{h}^o$). The time history of components of the relative angular momentum vector expressed in the principal reference frame ($\mathbf{h}_s$) are shown in Figure 6.18. Figure 6.19 shows the time history of the internal torque vector expressed in the principal reference frame ($\mathbf{g}_s$).

The three-dimensional figures (Figures 6.11 through 6.13) show that both the initial and target COMETs are closed-curves in SO(3). These figures also distinctly show the two phases of the transition maneuver. The gyrostat-satellite first transfers from the initial COMET to the target COMET, and then travels along the target COMET to reach the target relative equilibrium attitude. The time histories of the system parameters (Figures 6.14 through 6.19) show that the gyrostat-satellite reaches a relative equilibrium because all of the curves are constant over the last 0.02 orbits of the simulation with the internal torques dropping to zero. During the transition to the target COMET, J_{13} is zero, J_{23} varies, and the components of the system angular momentum vector expressed in the orbital frame vary. The value of J_{13} remains zero because the chosen boundary conditions required no pitch system momentum adjustment. The profile of J_{23} during the transition to the target COMET adjusts the yaw system angular momentum from its intitial value to the targeted final value. As would be expected while traversing the target COMET, J_{13} is zero, J_{23} is constant, and the components of the system angular momentum vector expressed in the orbital frame are constant. The time history of the internal torques (Figure 6.19) clearly shows the transitions between the "ramp-up," "coast," and "ramp-down" phases of the transition maneuver along the target COMET as discontinuities in the curves.

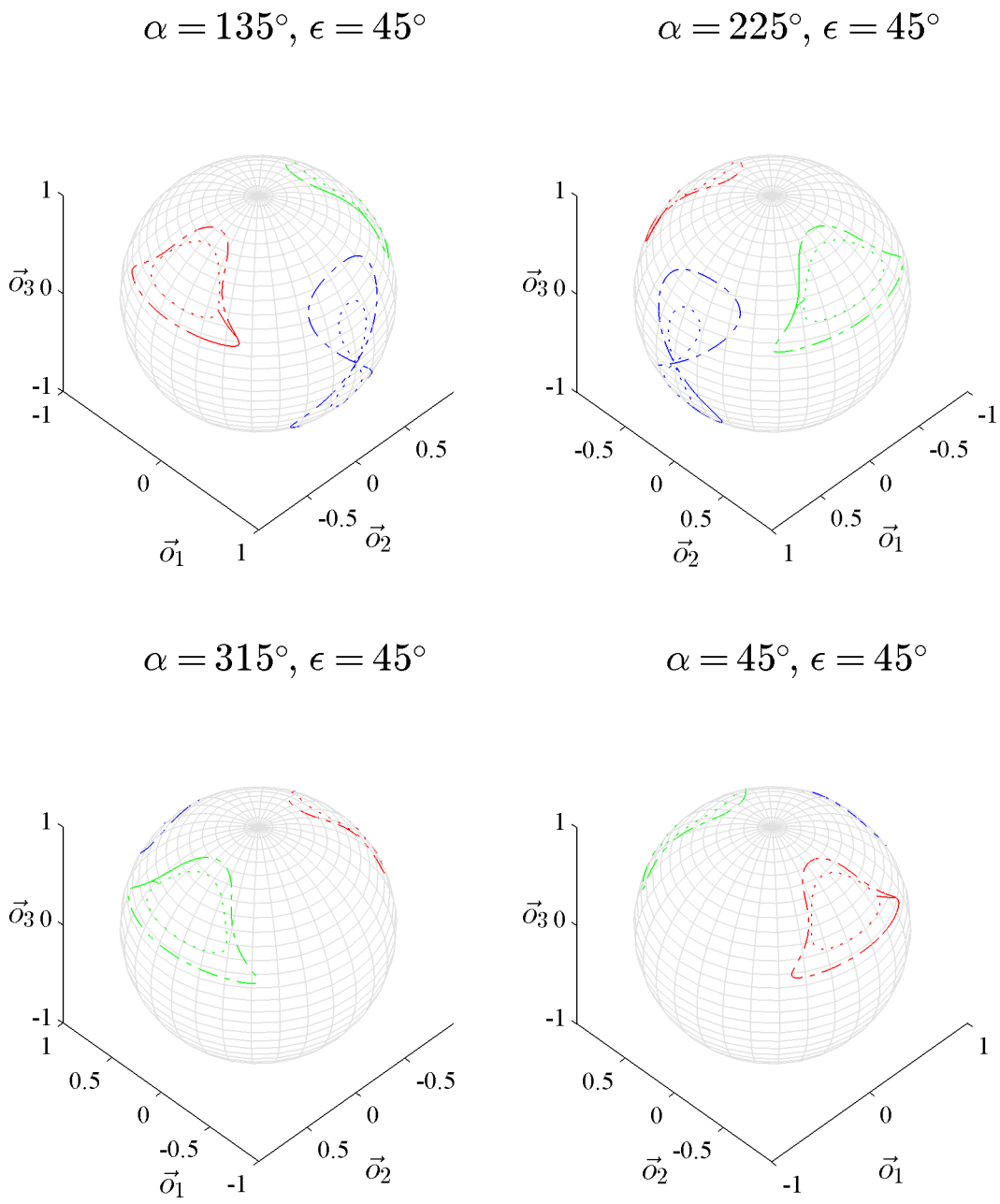

Figure 6.11: Four isometric views from the $+\vec{o}_3$ hemisphere of the paths of the principal frame basis axes on the unit sphere fixed in the orbital reference frame during a transition between two relative equilibria on different COMETs

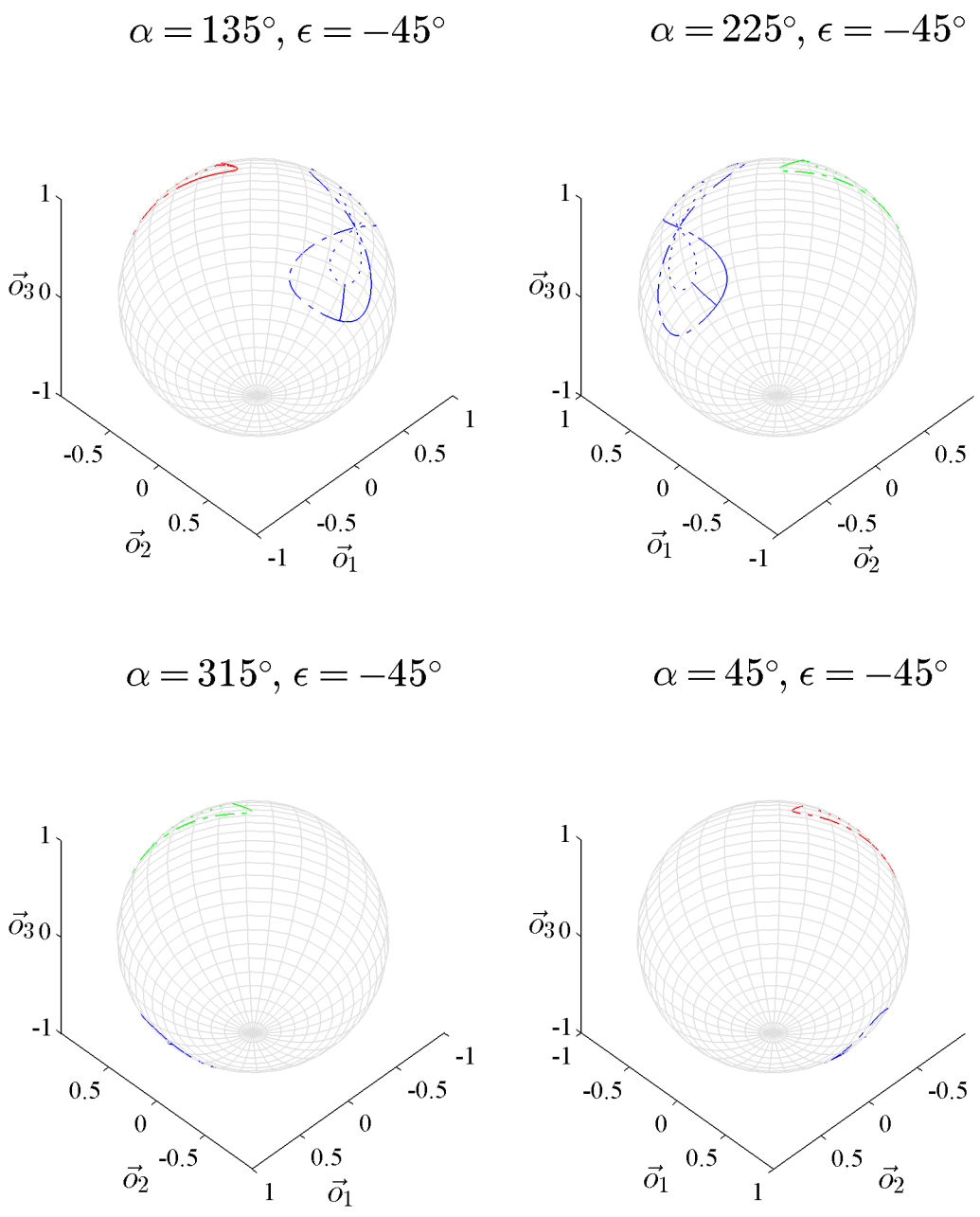

Figure 6.12: Four isometric views from the -$\vec{o}_3$ hemisphere of the paths of the principal frame basis axes on the unit sphere fixed in the orbital reference frame during a transition between two relative equilibria on different COMETs

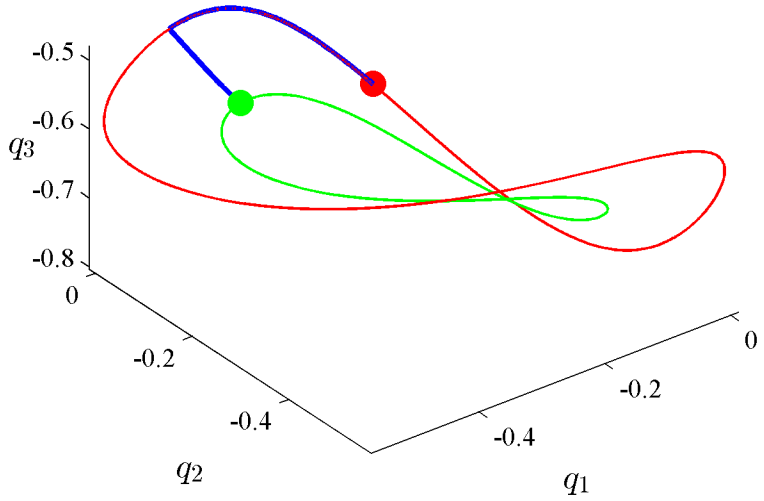

Figure 6.13: Path in the configuration space of the vector part of the attitude quaternion ($\vec{q}^{po}$) of a transition between two relative equilibria on different COMETs overlaid on the COMET path

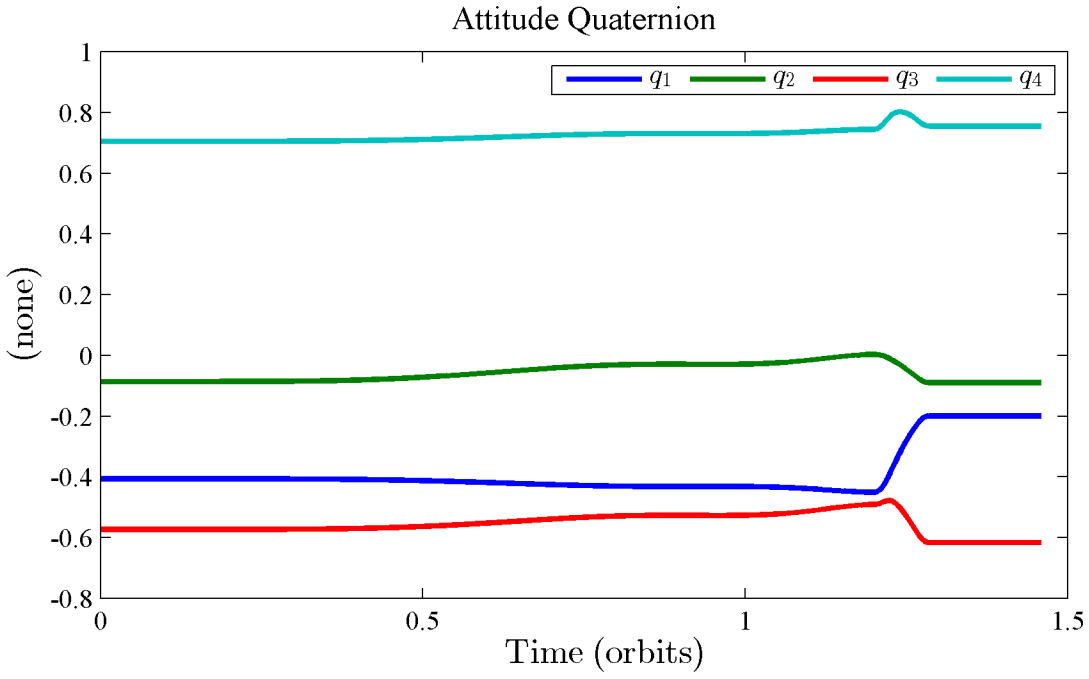

Figure 6.14: Components of the attitude quaternion ($\bar{q}^{po}$) during a transition between two relative equilibria on different COMETs

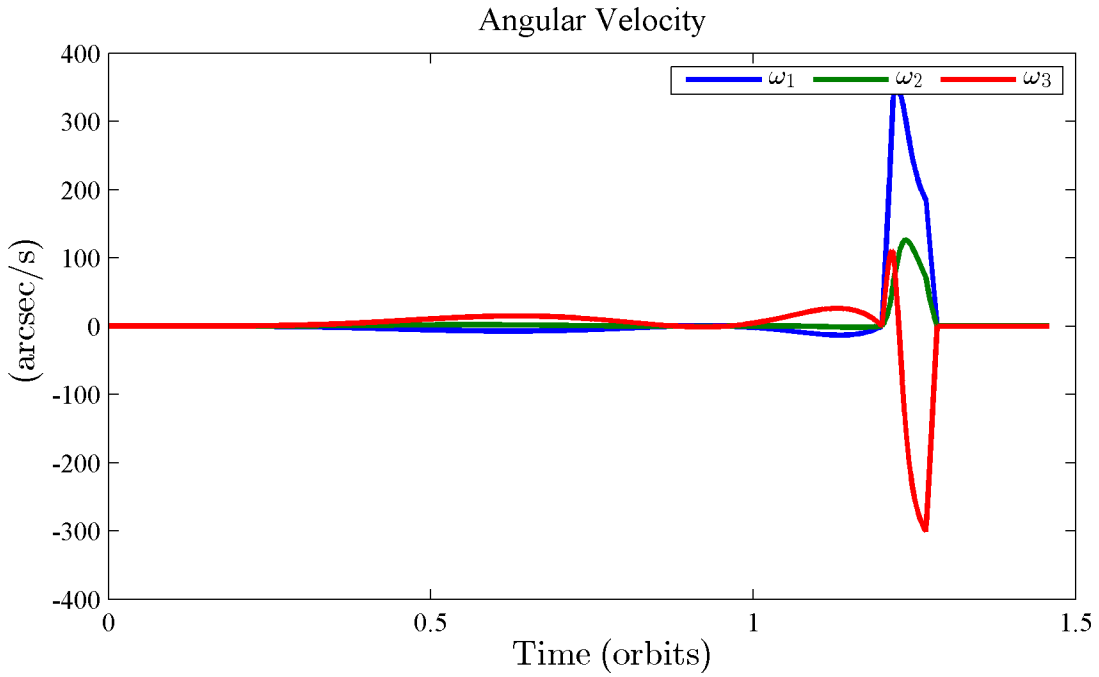

Figure 6.15: Components of the angular velocity of the princpal reference frame with respect to the orbital reference frame expressed in the principal reference frame ($\boldsymbol{\omega}^{po}$) during a transition between two relative equilibria on different COMETs

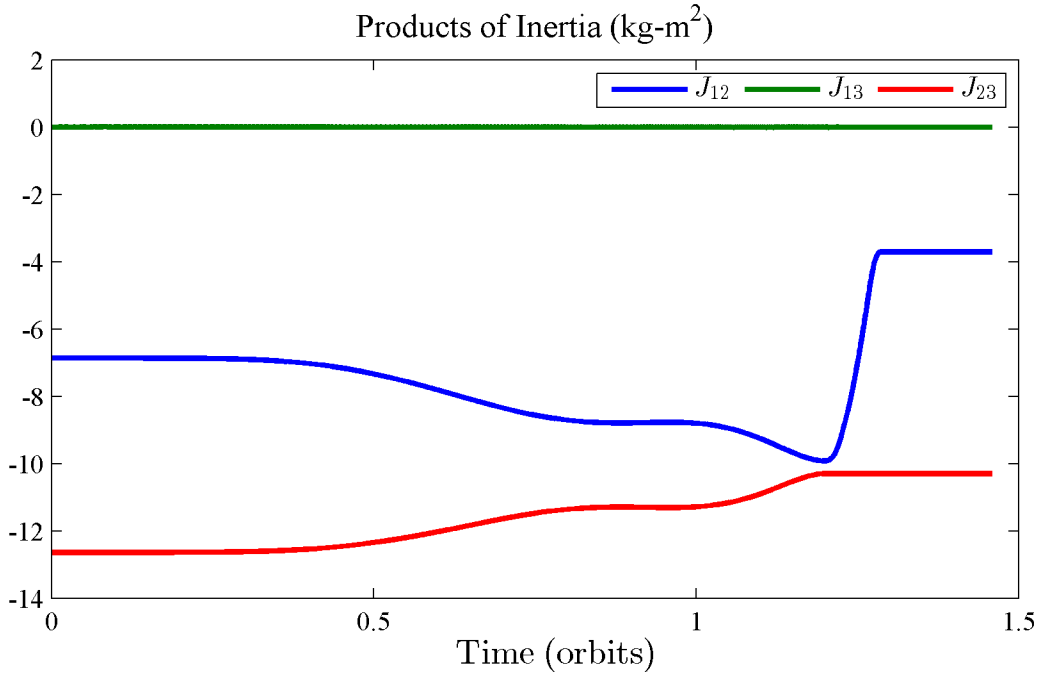

Figure 6.16: Products of inertia expressed in the orbital reference frame (J_{12}, J_{13}, and J_{23}) during a transition between two relative equilibria on different COMETs

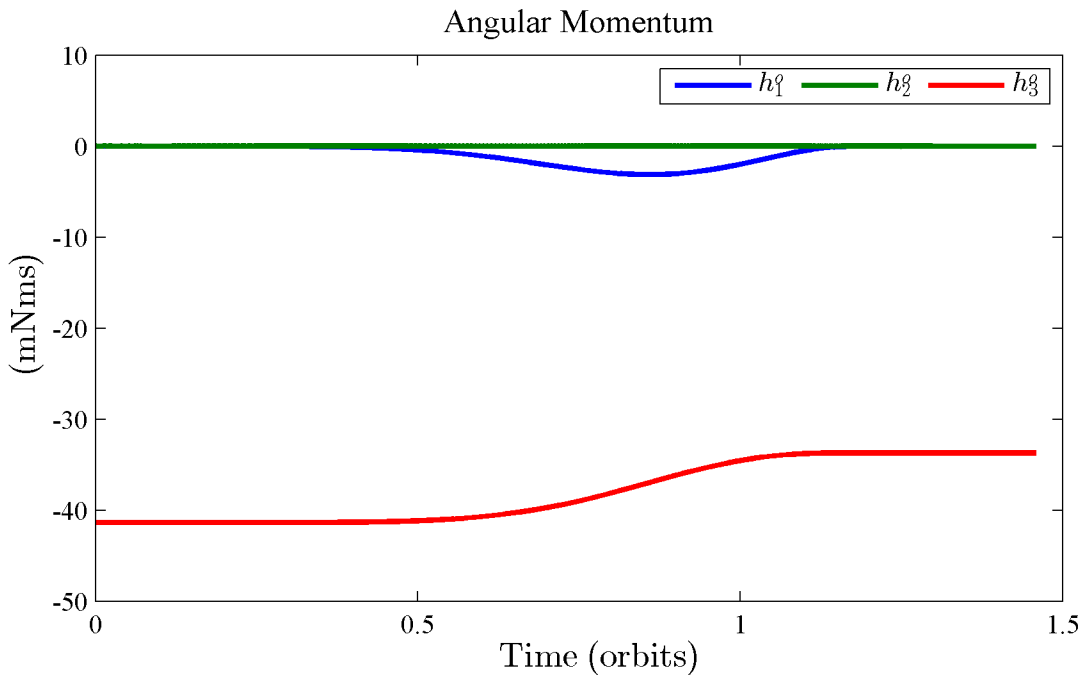

Figure 6.17: Components of the system angular momentum vector expressed in the orbital reference frame ($\mathbf{h}^o$) during a transition between two relative equilibria on different COMETs

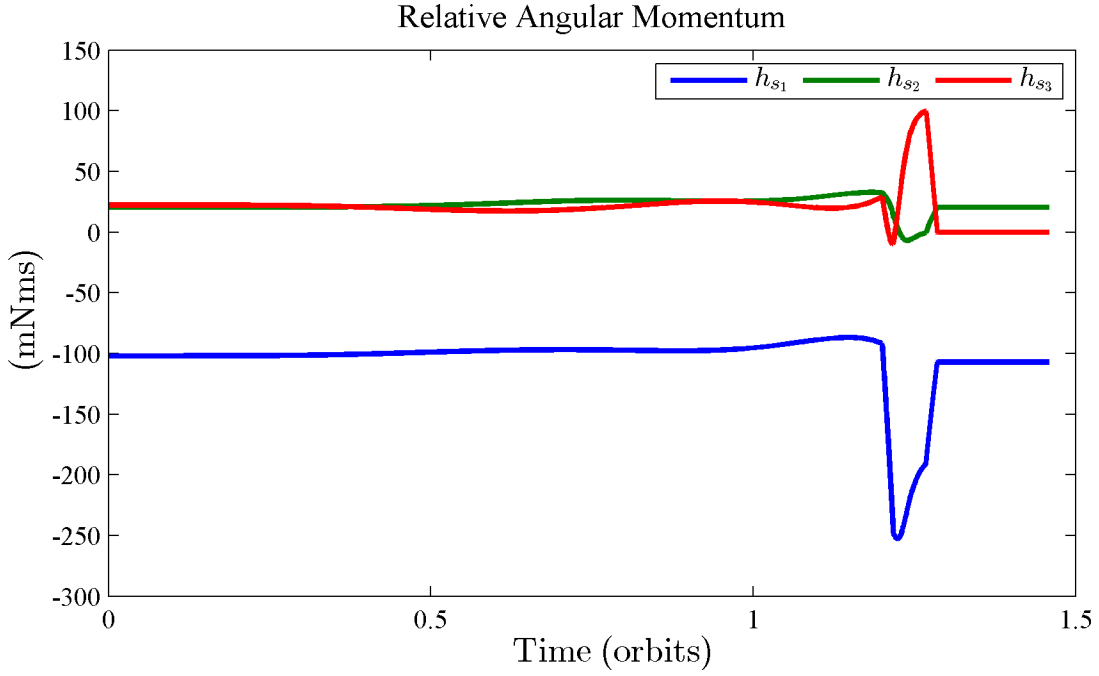

Figure 6.18: Components of the relative angular momentum vector expressed in the principal reference frame ($\mathbf{h}_s$) during a transition between two relative equilibria on different COMETs

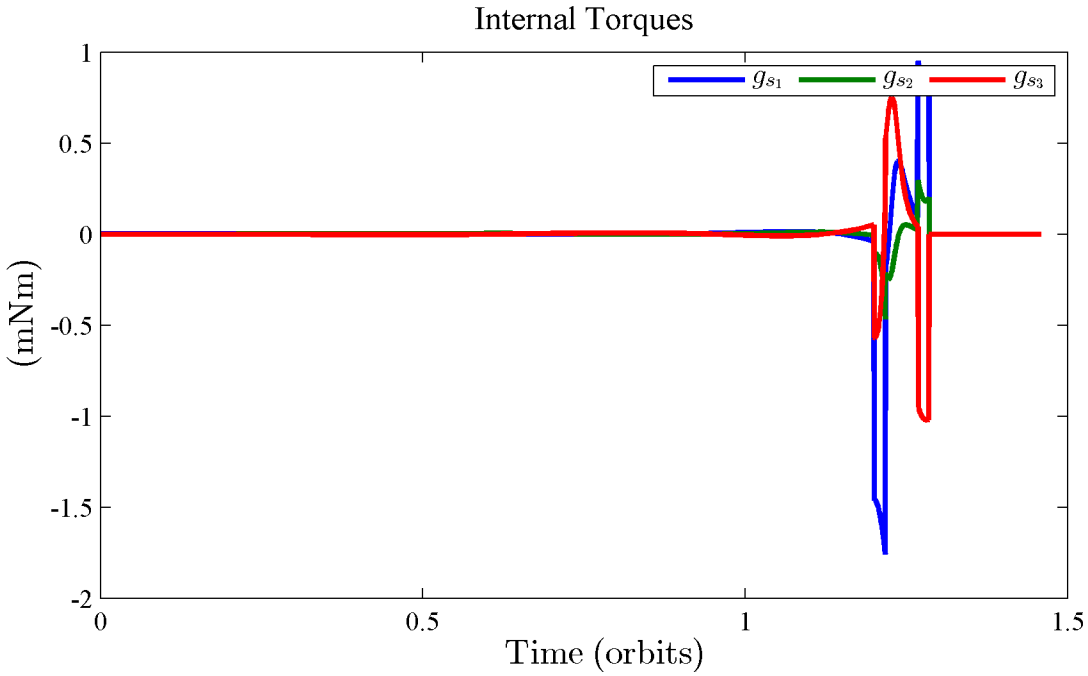

Figure 6.19: Components of the internal torque vector expressed in the principal reference frame ($\mathbf{g}_s$) during a transition between two relative equilibria on different COMETs

6.2.5 Limitations of the Proposed Method

The proposed method to transition between relative equilibria residing on different COMETs has been shown to be viable for slow transitions between "neighboring" non-extrema relative equilibria. The computational complexity of the method is sufficiently low to allow "on-board" implementation on standard radiation-hardened flight computers.

However, the proposed method is not a global solution to the problem of transitioning between relative equilibrium attitudes. It also requires careful selection of inputs to ensure a physically realizable transition is determined. The boundary conditions used in the calculation of the product of inertia time histories guarantee that target products of inertia and system momentum are reached, but do not guarantee that a particular relative equilibrium attitude is reached. Analysis of many simulation results show that the proposed method generally works for slow transitions between "neighboring" relative equilibrium that are not at extrema points of the physically realizable products of inertia.

A simple example of transition on which the proposed method would fail is when the initial and target relative equilbria have the same product of inertia values. The calculation of the time histories of the products of inertia via the proposed method would result in a trivial solution where the values are constant throughout the transition time, which would have the gyrostat-satellite remain at the initial relative equilibrium.

Another limitation of the proposed method is that the process used to solve for the polynomial coefficients provides no explicit guarantee that the time histories of the products of inertia are physically realizable. The values in the time histories may exceed the physical minimum and maximum values for products of inertia especially when either the initial or target product of inertia values are near those limits or when the commanded transition time is relatively short.

6.3 Summary

This chapter investigated transitions between relative equilibria using internal torque actuation, which is a topic that has received little attention in the literature. The problem of transitioning a gyrostat-satellite from an initial relative equilibrium to a desired target relative equilibrium was broken into two sub-problems:

1. Transitions between two relative equilibria that reside on the same COMET, and
2. Transitions between relative equilibria that reside on different COMETs.

It was shown that transitions between relative equilibria on the same COMET may be straight-forwardly accomplished by traversing along the COMET. An open-loop control law was presented that transitions a gyrostat-satellite from an initial relative equilibrium to a target relative equilibrium on the same COMET. Results from a numeric simulation of a gyrostat-satellite executing a transition maneuver verified the efficacy of using the COMET to execute the transition.

A method to transition a gyrostat-satellite from an initial relative equilibrium to a desired target relative equilibrium that resides on a different COMET was developed. The proposed method broke up the maneuver into two phases. During the first phase, the gyrostat-satellite transitions from the initial relative equilibrium to a relative equilibrium residing on the same COMET as the target relative equilibrium. The transition to the target COMET is accomplished by first determining a time history for the products of inertia that correctly adjust the system angular momentum. The time histories of the products of inertia are mapped to a continuous attitude trajectory that begins at the initial relative equilibrium attitude, takes a path that correctly adjusts the system angular momentum, and ends at a relative equilibrium attitude on the target COMET. The second phase of the maneuver transitions the gyrostat-satellite along the COMET to the target relative equilibrium. The second phase is executed using the open-loop control law developed to transition between relative equilibria on the same COMET. Results from a numeric simulation of a gyrostat-satellite executing a transition maneuver were presented, and verified the efficacy of the proposed method. Finally, some limitations of the transition method were discussed.

Chapter 7

Summary

This dissertation investigated the dynamics and control of a gyrostat-satellite. A thorough and targeted review of the literature on the topic identified a significant gap in the published work. The majority of the published work investigated the determination of relative equilibrium attitudes and the stability characteristics of relative equilibria. The literature review only identified one published work that investigated transitions between relative equilibria (Anchev[1]).

7.1 Summary

The focus of this dissertation was the investigation of attitude transition maneuvers of a gyrosat-satellite between relative equilibria. First, the equations of motion for a gyrostat-satellite were derived, and served as foundation upon which the rest of the presented work was built. Next, the concept of relative equilibria was introduced. A significant portion of the presentation on relative equilibria largely followed that of already published work. This included the definition of relative equilibrium, the determination of relative equilibrium attitudes, and the determination of sufficient conditions for the stability of a relative equilibrium. A detailed investigation into the basis vector directions (principal and orbital) that admit relative equilibrium attitudes was performed and represents a new contribution to the literature. Algorithms were developed to determine admissible relative equilibrium attitudes when the set is limited to those attitudes with a single basis vector constraint. The investigation led to six insights:

- For each possible $\vec{o}_1$ on the unit sphere fixed in the principal reference frame there are two possible relative equilibrium attitude separated by rotations of 180^o about $\vec{o}_1$.
- For each possible $\vec{o}_2$ on the unit sphere fixed in the principal reference frame there are four possible relative equilibrium attitude separated by rotations of 90^o about $\vec{o}_2$.

- For each possible $\vec{o}_3$ on the unit sphere fixed in the principal reference frame there are two possible relative equilibrium attitude separated by rotations of 180^o about $\vec{o}_3$.
- The value of β (Eq. 4.57) defines the regions on the unit sphere fixed in the orbital reference frame in which a principal basis vector direction admits at least one relative equilibrium attitude.
- If values the moments of inertia of the gyrostat-satellite and the direction of the principal basis vector are such that $\|\beta\gamma\| \leq 1$, then there exist two admissible relative equilibrium attitudes.
- The requirement $\|\beta\gamma\| \leq 1$ is always satisfied if $\vec{p}_i$ is aligned with an intermediate axis of inertia of the gyrostat-satellite.

The remainder of the dissertation was dedicated to the investigation of a new concept termed the constant orbital momentum equilibrium trajectory or COMET, which is a new contribution to the literature. The primary challenge in transitioning between relative equilibria is the adjustment of the system angular momentum so that upon reaching the target relative equilibrium attitude the gyrostat-satellite will satisfy all the requirements for a relative equilibrium. The terminal system angular momentum is a function of the attitude trajectory taken during the transition maneuver. The COMET represents (somewhat literally) a "loop"-hole that may be exploited for a subset of possible transition maneuvers. COMETs are trajectories along which a gyrostat-satellite may travel and maintain a constant system angular momentum vector expressed in the orbital reference frame. The requirements for an attitude trajectory to be a COMET were formally defined. A method to map a COMET was developed and presented. Maps generated for several example COMETs were used to show that COMETs are (generally) continuous, one-dimensional, closed curves in SO(3). Visualizations of "families" of COMETs were presented and discussed in detail. The visualizations indicated the existence of critical points on a small subset of COMETs that represent either isolated relative equilibrium attitudes or points furcation of the COMET. It was shown that the critical points correspond to points in SO(3) where the dimensionality of the nonholonomic constraint increases from one to two.

Finally, the impetus for this dissertation, the significant gap in the literature, was addressed through the development and validation of open-loop control laws that transition a gyrostat-satellite from an initial relative equilibrium to a target relative equilibrium. The transitions were split into two categories: transitions between relative equilibria on the same COMET and transitions between relative equilibria on different COMETs. For transitions between relative equilibria on the same COMET, the open-loop control law commands internal torques that result in the gyrostat-satellite traversing the COMET in the direction of the target relative equilibrium until the target relative equilibrium is reached. For transitions between relative equilibria on different COMETs, a two-phase method was developed. During the first phase, the gyrostat-satellite transfers from the initial relative equilibrium to a relative equilibrium that resides on the same COMET as the target relative equilibrium. For this

transition, the open-loop control law commands internal torques that result in the gyrostat-satellite following an attitude trajectory that adjusts the system angular momentum to match the target relative equilibrium value. During the second phase, the gyrostat-satellite travels along the COMET to reach the target relative equilibrium attitude using the open-loop control law designed to transition between relative equilibria on the same COMET. The results of numeric simulations of a gyrostat-satellite executing both categories of transitions were presented to validate the efficacy of the control laws.

The following is a list of the new and significant contributions to the field of research put forward by this dissertation.

1. Detailed investigation into the basis vector directions (principal and orbital) that admit relative equilibrium attitudes
2. Identification and definition of the concept of a COMET
3. Development of a method to map the extent of a COMET
4. Presentation of visualizations of "families" of COMETs
5. Identification, definition, and determination of critical points that occur on a small subset of COMETs
6. Development and validation (via numeric simulation) of an open-loop control law to transition between relative equilibrium residing on the same COMET
7. Development and validation (via numeric simulation) of an open-loop control law to transition between "neighboring" relative equilibrium residing on different COMETs with non-extrema J_{23} values

7.2 Recomendations for Further Study

Investigations into transitions between relative equilibria represent a potentially large area for new and significant contributions related to the dynamics and control of gyrostat-satellites. This dissertation started to address this area, however there is still significant work yet to be done.

The open-loop control law developed to transition between relative equilibria on different COMETs is not a global solution. The development of a global solution would represent a significant contribution to the literature. There are several avenues of investigation which may lead to a global solution. These include using other parameterizations for the time history of the products of inertia, more sophisticated methods for parameter selection, and nonlinear feedback control methods similar to those developed by Vadali.[34] Time and energy

optimal solutions to transitions between relative equilibria would also represent a significant contribution.

It was surmised via numerous examples that COMETs are one-dimensional, continuous, closed curves in SO(3), however it has not been proven analytically. An analytic proof that COMETs are always closed-curves in SO(3) would be a significant contribution to the literature.

There is a possibly significant body of work associated with the practical application of methods and theories developed in this dissertation to active three-axis control of a satellite. This would include investigations determining the types of satellites and regimes of orbits for which these results are applicable. Case studies into concepts of operation that utilize relative equilibria and COMETs to extend mission life via fuel expenditure minimization would be useful in determining the most practically fruitful areas for further investigation. It is possible that extensions to the gyrostat-satellite model to include other dynamic effects such as flexible dynamics, environmental disturbances, and liquid slosh may be necessary. Additionally, in real engineering systems parameter values are uncertain. The effects of these uncertainties on the performance of the open-loop control laws needs to be fully investigated.

Bibliography

[1] A. A. Anchev, *Equilibrium attitude transitions of a three-rotor gyrostat in a circular orbit*, AIAA Journal **11** (1973), no. 4, 46717472.

[2] Roger R. Bate, Donald D. Mueller, and Jerry E. White, *Fundamentals of astrodynamics*, Dover Publications, Inc., New York, 1971.

[3] M.R.M. Crespo da Silva, *Attitude stability of a gravity-stabilized gyrostat satellite*, Celestial Mechanics **2** (1970), 14717165.

[4] ———, *Non-linear resonance attitude motions in gravity-stabilized gyrostat satellites*, International Journal of Non-Linear Mechanics **7** (1972), 62117641.

[5] Z. Ge and Hsien-Keng Chen, *Improved stability of a dual-spin satellite in circular orbit*, Japanese Journal of Applied Physics **36** (1997), no. 2, 948–956.

[6] C.D. Hall, *Attitude dynamics of orbiting gyrostats*, US 17 European Celestial Mechanics Workshop (Adam Mickiewicz University in Poznan, Poland), July 2000.

[7] Christopher D. Hall, *Class notes - spacecraft attitude dynamics and control*, January 12, 2003.

[8] Christopher D. Hall and Jeffery A. Beck, *Relative equilibria of orbiting gyrostats*, AAS/AIAA Astrodynamics Specialist Conference, AAS 99-459 (Girdwood, AK), August 1999, pp. 319–348.

[9] Christopher D. Hall and Jeffrey A. Beck, *Hamiltonian mechanics and relative equilibria of orbiting gyrostats*, Journal of the Astronautical Sciences **55** (2007), no. 1, 55–65.

[10] P. C. Hughes, *Attitude stability of an orbiting gyrostat in conical equilibrium*, Journal of Guidance, Control, and Dynamics **8** (1985), no. 5, 57317578.

[11] Peter C. Hughes, *Spacecraft attitude dynamics*, Dover Publications, Inc., 31 East 2nd Street, Mineola, New York, 11501, 2004.

[12] T. R. Kane and D.L. Mingori, *Effect of a rotor on the attitude stability of a satellite in a circular orbit*, AIAA Journal **3** (1965), no. 5, 936–940.

[13] V.V. Krementulo, *Optimal stabilization of rotation of a gyrostat in the newtonian force field (gyrostat in circular orbit in newtonian force field, solving for optimal rotational motion stabilization)*, PMM-Journal of Applied Mathematics and Mechanics **34** (1970), no. 5, 925–935.

[14] F.C. Liu, *Coupled librational motions of a gyrostat satellite*, Journal of Spacecraft and Rockets **11** (1974), no. 4, 230–235.

[15] R. W. Longman, *Generalized approach to gravity-gradient stabilization of gyrostat satellites*, Research Memoranda RM-5921-PR, RAND Corporation, 1969.

[16] _____, *Stability analysis of all possible equilibria for gyrostat satellites under gravitational torques*, AIAA Journal **10** (1972), no. 6, 80017806.

[17] _____, *Stable tumbling motions of a dual-spin satellite subject to gravitational torques*, AIAA Journal **11** (1973), no. 7, 91617921.

[18] Richard W. Longman, *Gravity-gradient stabilization of gyrostat satellites with rotor axes in principal planes*, Celestial Mechanics (1970), 169–188.

[19] R.W. Longman, P. Hagedorn, and A. Beck, *Stabilization due to gyroscopic coupling in dual-spin satellites subject to gravitational torques*, Celestial Mechanics **25** (1981).

[20] R.W. Longman and R.E. Roberson, *General solution for the equilibria of orbiting gyrostats subject to gravitational torques*, The Journal of the Astronautical Sciences **XVI** (1969), no. 2, 491758.

[21] R. Molina and F. Mond'ejar, *Equilibria and stability for a gyrostat satellite in circular orbit*, Acta Astronautica **54** (2003), 77–82.

[22] M. Pascal, *Attitude equilibria of dual spin satellites subject to gravitational torques of n bodies*, Celestial Mechanics **36** (1985), 319–347.

[23] M. Pascal and S. Ia. Stepanov, *On a semi-inverse problem in the motion of gyrostat satellites*, Celestial Mechanics and Dynamical Astronomy **50** (1991), 99–108.

[24] B.K. Powell, *Gravity gradient desaturation of a momentum exchange attitude control system*, AIAA Guidance, Control and Flight Mechanics Conference (Hofstra University, Hempstead, New York), no. AIAA Paper No. 71-940, August 16-18 1971.

[25] R.E. Roberson, *Rotors in gravity-stabilized satellites*, Attitude Changes and Stabilization of Satellites (Paris), October 8-11 1968, pp. 319–348.

[26] _____, *Stability of orbiting gyrostats in the elementary cases*, Archive of Applied Mechanics (Ingenieur Archiv) **39** (1970), no. 5, 317–329.

[27] R.E. Roberson and W.W. Hooker, *Gravitational equilibria of a rigid body containing symmetric rotors*, Proceedings of the XVII International Astronautical Congress (Madrid), vol. 4, International Astronautical Federation, October 9-15 1966, pp. 203–210.

[28] L.S. Saakian, *On the optimal stabilization of the positins of a gyrostat-satellite's relative equilibrium*, PMM-Journal of Applied Mathematics and Mechanics **40** (1976), no. 5, 750–758.

[29] V. A. Sarychev and S. A. Mirer, *Relative equilibria of a gyrostat satellite with internal angular momentum along a principal axis*, Acta Astronautica **49** (2001), no. 11, 641–644.

[30] V. A. Sarychev, S. A. Mirer, and A. A. Degtyarev, *The dynamics of a satellite-gyrostat with a single nonzero component of the vector of gyrostatic moment*, Cosmic Research **43** (2005), no. 4, 268–279.

[31] Hanspeter Schaub and John L. Junkins, *Analytical mechanics of space systems*, AIAA Education Series, American Institute of Aeronautics and Astronautics, Reston, Virginia, 2003.

[32] S.I.A. Stepanov, *On the steady motions of a gyrostat satellite (gyrostabilized satellite steady state motions in newtonian force field having displaced satellite center of mass orbital plane relative to center of attraction)*, PMM-Journal of Applied Mathematics and Mechanics **33** (1969), no. 1, 121–126.

[33] Donald Tong, *Spacecraft momentum dumping using gravity gradient*, Journal of Spacecraft and Rockets **35** (1998), no. 5, 714–717.

[34] S.R. Vadali and H.-S. Oh, *Space station attitude control and momentum management: A nonlinear look*, Journal of Guidance, Control, and Dynamics **15** (1992), no. 3.

[35] L. Wang, K. Lian, and P. Chen, *Steady motions of gyrostat satellites and their stability*, IEEE Transactions on Automatic Control **40** (1995), no. 10, 1732–1743.

[36] Katsuhiko Yamada, Shoji Yoshikawa, Toshio Kashiwase, and Toshihisa Matsue, *Wheel unloading by gravity-gradient torque*, The Japan Society of Mechanical Engineers (2001), 79–86.

[37] E.Y. Yu, *Attitude stability of an orbiting vehicle containing a gyrostat*, Journal of Spacecraft and Rockets **6** (1969), no. 8, 948–951.

Appendix A

Gyrostat-Satellite Simulation

A numeric simulation of the rotational dynamics of a gyrostat-satellite was implemented in MATLAB®. The state vector used by the gyrostat-satellite simulator is defined

$$\mathbf{x} = \left[\begin{array}{ccc} (\bar{\mathbf{q}}^{po})^{\mathsf{T}} & (\boldsymbol{\omega}^{po})^{\mathsf{T}} & (\mathbf{h}_s)^{\mathsf{T}} \end{array} \right]^{\mathsf{T}} \tag{A.1}$$

where $\bar{\mathbf{q}}^{po}$ is the attitude quaternion representing the rotation from the orbital reference frame to the principal reference frame, $\boldsymbol{\omega}^{po}$ is the angular velocity of the principal reference frame with respect to the orbital reference frame expressed in the principal reference frame, and $\mathbf{h}_s$ is the relative angular momentum vector expressed in the principal reference frame. The simulation propagates the state vector forward in time using the built-in MATLAB® function `ode45()`. The `odeset()` function is used to set the parameters `'AbsTol'` and `'RelTol'` to a value of 1.0×10^{-12} for all simulations. All other parameters are left at their default values.

The `ode45()` function requires as an input a function to calculate the first time derivative of the state vector. The first time derivative of the state vector is

$$\dot{\mathbf{x}} = \left[\begin{array}{ccc} \left(\dot{\bar{\mathbf{q}}}^{po}\right)^{\mathsf{T}} & (\dot{\boldsymbol{\omega}}^{po})^{\mathsf{T}} & \left(\dot{\mathbf{h}}_s\right)^{\mathsf{T}} \end{array} \right]^{\mathsf{T}} \tag{A.2}$$

Equations used to calculate the first time derivatives of the components of the state vector are now presented. The first time derivative of $\bar{\mathbf{q}}^{po}$ is

$$\dot{\bar{\mathbf{q}}}^{po} = \frac{1}{2}\bar{\boldsymbol{\omega}}^{po} \otimes \bar{\mathbf{q}}^{po} \tag{A.3}$$

where the binary quaternion operator $\otimes$ is defined

$$\bar{\mathbf{a}} \otimes \bar{\mathbf{b}} = \left[\begin{array}{cc} a_4\mathbf{1} - \mathbf{a}^{\times} & \mathbf{a} \\ -\mathbf{a}^{\mathsf{T}} & a_4 \end{array} \right] \bar{\mathbf{b}} \tag{A.4}$$

The angular velocity vector $\boldsymbol{\omega}^{po}$ can be calculated using

$$\boldsymbol{\omega}^{po} = \boldsymbol{\omega}^{pi} - \boldsymbol{\omega}^{oi} = \boldsymbol{\omega}^{pi} + \omega_o \mathbf{o}_2 \tag{A.5}$$

The first time derivative of $\boldsymbol{\omega}^{po}$ is

$$\dot{\boldsymbol{\omega}}^{po} = \dot{\boldsymbol{\omega}}^{pi} + \omega_o \dot{\mathbf{o}}_2 = \dot{\boldsymbol{\omega}}^{pi} - \omega_o \left(\boldsymbol{\omega}^{po}\right)^{\times} \mathbf{o}_2 \tag{A.6}$$

Solving Eq. 3.62 for $\dot{\boldsymbol{\omega}}^{pi}$ results in

$$\dot{\boldsymbol{\omega}}^{pi} = \mathbf{I}^{-1}\left(3\omega_o^2 \mathbf{o}_3^{\times}\mathbf{I}\mathbf{o}_3 - \left(\boldsymbol{\omega}^{pi}\right)^{\times}\left(\mathbf{I}\boldsymbol{\omega}^{pi} + \mathbf{h}_s\right) - \mathbf{g}_s\right) \tag{A.7}$$

Plugging Eq. A.7 into Eq. A.6 results in

$$\dot{\boldsymbol{\omega}}^{po} = \mathbf{I}^{-1}\left(3\omega_o^2 \mathbf{o}_3^{\times}\mathbf{I}\mathbf{o}_3 - \left(\boldsymbol{\omega}^{pi}\right)^{\times}\mathbf{h} - \mathbf{g}_s\right) - \omega_o \left(\boldsymbol{\omega}^{po}\right)^{\times} \mathbf{o}_2 \tag{A.8}$$

The first time derivative of $\mathbf{h}_s$ is

$$\dot{\mathbf{h}}_s = \mathbf{g}_s \tag{A.9}$$

The algorithm used to calculate the first time derivative of the state vector is presented in Algorithm A.1. The first three inputs of the algorithm ($\bar{\mathbf{q}}^{po}$, $\boldsymbol{\omega}^{po}$, $\mathbf{h}_s$) are the components of the state vector. The fourth input $\mathbf{g}_s$ is the output of the open-loop control law presented in Appendix B. The fifth input ω_o is the magnitude of the rate of rotation of the orbital reference frame (or, equivalently the mean motion of the orbit of the gyrostat-satellite).

Input : $\bar{\mathbf{q}}^{po}$, $\boldsymbol{\omega}^{po}$, $\mathbf{h}_s$, $\mathbf{g}_s$, ω_o
Output: $\dot{\bar{\mathbf{q}}}^{po}$, $\dot{\boldsymbol{\omega}}^{po}$, $\dot{\mathbf{h}}_s$

$\mathbf{o}_2^o \leftarrow \begin{bmatrix} 0 & 1 & 0 \end{bmatrix}^{\mathsf{T}}$;
$\mathbf{o}_3^o \leftarrow \begin{bmatrix} 0 & 0 & 1 \end{bmatrix}^{\mathsf{T}}$;
$\mathbf{o}_2 \leftarrow R(\bar{\mathbf{q}}^{po})\mathbf{o}_2^o$;
$\mathbf{o}_3 \leftarrow R(\bar{\mathbf{q}}^{po})\mathbf{o}_3^o$;
$\boldsymbol{\omega}^{pi} \leftarrow \boldsymbol{\omega}^{po} - \omega_o \mathbf{o}_2$;
$\mathbf{h} \leftarrow \mathbf{I}\boldsymbol{\omega}^{pi} + \mathbf{h}_s$;
$\dot{\bar{\mathbf{q}}}^{po} \leftarrow \frac{1}{2}\bar{\boldsymbol{\omega}}^{po} \otimes \bar{\mathbf{q}}^{po}$;
$\dot{\boldsymbol{\omega}}^{po} \leftarrow \mathbf{I}^{-1}\left(3\omega_o^2 \mathbf{o}_3^{\times}\mathbf{I}\mathbf{o}_3 - \left(\boldsymbol{\omega}^{pi}\right)^{\times}\mathbf{h} - \mathbf{g}_s\right) - \omega_o \left(\boldsymbol{\omega}^{po}\right)^{\times} \mathbf{o}_2$;
$\dot{\mathbf{h}}_s \leftarrow \mathbf{g}_s$;

Algorithm A.1: Algorithm to calculate the first time derivative of the state vector

Appendix B

Open-Loop Control Law

The algorithms developed in Chapter 6 calculate attitude trajectories that transition a gyrostat-satellite between relative equilibria. The attitude trajectories are time histories of the attitude, angular velocity, and angular acceleration of the principal reference frame with respect to the orbital reference frame. A gyrostat-satellite executes the transition via the application of internal torques to the rotors. The functional relationship between the internal torque vector and the attitude trajectory is given by Eq. A.8 (repeated below for conviencence).

$$\dot{\boldsymbol{\omega}}^{po} = \mathbf{I}^{-1}\left(3\omega_o^2\mathbf{o}_3^{\times}\mathbf{I}\mathbf{o}_3 - \left(\boldsymbol{\omega}^{pi}\right)^{\times}\mathbf{h} - \mathbf{g}_s\right) - \omega_o\left(\boldsymbol{\omega}^{po}\right)^{\times}\mathbf{o}_2$$

Solving Eq. A.8 for the internal torque vector $\mathbf{g}_s$ results in

$$\mathbf{g}_s = -\mathbf{I}\left(\dot{\boldsymbol{\omega}}^{po} + \omega_o\left(\boldsymbol{\omega}^{po}\right)^{\times}\mathbf{o}_2\right) - \left(\boldsymbol{\omega}^{pi}\right)^{\times}\mathbf{h} + 3\omega_o^2\mathbf{o}_3^{\times}\mathbf{I}\mathbf{o}_3 \tag{B.1}$$

Equation B.1 is an open-loop control law that drives the gyrostat-satellite from the initial state along the attitude trajectory defined by $\dot{\boldsymbol{\omega}}^{po}$ and $\boldsymbol{\omega}^{po}$.